THE ELECTRONIC SPECTRA OF THE CYANOGEN HALIDES

VACUUM ULTRAVIOLET SPECTROSCOPY OF THE CYANOGEN HALIDES

by

ALBERT WILLIAM RICHARDSON, B.Sc.

A Thesis

Submitted to the Faculty of Graduate Studies

in Partial Fulfillment of the Requirements

for the Degree

Doctor of Philosophy

McMaster University

October 1966

DOCTOR OF PHILOSOPHY (1966) MCMASTER UNIVERSITY

Hamilton, Ontario.

TITLE: Vacuum Ultraviolet Spectroscopy of the Cyanogen Halides.

AUTHOR: Albert William Richardson, B.Sc. (McMaster University)

SUPERVISOR: Dr. G. W. King

NUMBER OF PAGES: ix, 189, a.20

SCOPE AND CONTENTS:

In Part I of this thesis, the design, construction, and calibration of a twenty-one foot off-plane Eagle vacuum spectrograph, a Lyman source, and predispersion unit are described.

In Part II, the results of an investigation of the electronic absorption spectra of the cyanogen halides, obtained with the apparatus described in Part I, are given. Several electronic absorption systems have been observed for each of the cyanogen halides. These have been correlated and assigned to electronic transitions. Vibrational analyses have been made and the excited state dimensions have been determined by a quantitative application of the Franck-Condon principle for two absorption systems of each of the cyanogen halides.

ACKNOWLEDGEMENTS

I wish to express my thanks to Dr. G. W. King for his advice and encouragement during the course of my research and the preparation of this thesis.

I would like to thank Dr. A. E. Douglas of the National Research Council, Ottawa, who gave invaluable advice on the design of the Lyman source and predispersion unit, and to Mr. S. Kocsis of the machine shop who was extremely helpful during the construction of the apparatus.

I would also like to thank my colleagues, Mr. W. J. Balfour, Dr. V. A. Job, Dr. E. H. Pinnington, Mr. C. H. Warren, Dr. J. L. Hencher, Mrs. H. E. Lock, Mr. J. D. P. McBride, Dr. D. C. Moule, Mr. S. P. So, and Mr. K. I. Srikameswaran for helpful discussions and experimental assistance.

I am grateful to the Dow Chemical Co. Ltd. for a fellowship 1961-1962, to the National Research Council for studentships 1962-1965, and to the Ontario government for a fellowship 1965-1966.

Finally, I would like to thank my wife for help during my graduate work and for the skillful typing of this thesis.

TABLE OF CONTENTS

	Page
CHAPTER 1	
Introduction.....	2
CHAPTER 2	
Theory of the Concave Diffraction Grating.....	8
CHAPTER 3	
Design of the Spectrograph.....	19
CHAPTER 4	
The Lyman Source and Predispersion Unit.....	27
CHAPTER 5	
Calibration of Apparatus.....	44
CHAPTER 6	
Tests of the Apparatus.....	58
CHAPTER 7	
Introduction to the Spectroscopic Problem.....	64
CHAPTER 8	
Experimental.....	80
CHAPTER 9	
Theory of Electronic Spectra.....	91
CHAPTER 10	
Description and Analysis of the Spectra.....	118
BIBLIOGRAPHY	183
APPENDIX	189

LIST OF TABLES

			Page
Table	4.1	Wavelength Range of the Rare Gas Continua	28
	5.1	Wavelength Range of the Vacuum Spectrograph in Various Orders.....	49
	7.1	Internuclear Distances and Dipole Moments for the Cyanogen Halides (From Reference 36).....	72
	7.2	Fundamental Vibrational Frequencies (cm^{-1}) for the Cyanogen Halides.....	72
	7.3	Fundamental Vibrational Frequencies (cm^{-1}) of the Cyanogen Halides from High Resolution Infrared Measurements.....	75
	7.4	Absorption by the Cyanogen Halide Vapours in the Near Ultraviolet.....	75
	7.5	Absorption by Cyanogen Iodide in the Vacuum Ultraviolet.....	77
	7.6	Appearance Potentials for the Cyanogen Halide Monopositive Molecular Ions.....	79
	9.1	The Irreducible Representations of the $C_{\infty v}$ Point Group.....	92
	9.2	The Irreducible Representations of the C_s Point Group.....	92
	9.3	The Irreducible Representations of Some Atomic Orbitals Under the C_s and $C_{\infty v}$ Point Groups....	116
	10.1	Wavelengths of Maximum Absorption (λ_{max}) and Oscillator Strengths for the Cyanogen Halide A Systems.....	121
	10.2	Long Wavelength Absorption for Some Organic Halides.....	121
	10.3	Absorption of Some 1-Alkynes and 1-Halo-1-Alkynes.....	130
	10.4	Assignment of the Vibrational Bands for the Cyanogen Iodide B System.....	133
	10.5	Assignment of the Vibrational Bands for the Cyanogen Iodide C System.....	133

Page

Table 10.6 Possible Bond Length Changes for the Cyanogen Iodide B System..... 138

10.7 Potential Energy Distribution for the Cyanogen Iodide B System..... 138

10.8 Possible Bond Length Changes for the Cyanogen Iodide C System..... 141

10.9 Potential Energy Distribution for the Cyanogen Iodide C System..... 141

10.10 Vibrational Frequencies and Bond Lengths for the Cyanogen Iodide X, B, and C States..... 141

10.11 Assignment of the Vibrational Bands for the Cyanogen Bromide B System..... 143

10.12 Assignment of the Vibrational Bands for the Cyanogen Bromide C System..... 143

10.13 Possible Bond Length Changes for the Cyanogen Bromide B System..... 150

10.14 Potential Energy Distribution for the Cyanogen Bromide B System..... 150

10.15 Possible Bond Length Changes for the Cyanogen Bromide C System..... 152

10.16 Potential Energy Distribution for the Cyanogen Bromide C System..... 152

10.17 Vibrational Frequencies and Bond Lengths for the Cyanogen Bromide X, B, and C States..... 152

10.18 Assignment of the Vibrational Bands for the Cyanogen Chloride B System..... 154

10.19 Assignment of the Vibrational Bands for the Cyanogen Chloride C System..... 154

10.20 Possible Bond Length Changes for the Cyanogen Chloride B System..... 156

10.21 Potential Energy Distribution for the Cyanogen Chloride B System..... 156

10.22 Possible Bond Length Changes for the Cyanogen Chloride C System..... 158

Page

Table 10.23 Potential Energy Distribution for the Cyanogen Chloride C System..... 158

10.24 Vibrational Frequencies and Bond Lengths for the Cyanogen Chloride X, B, and C States..... 160

10.25 Comparison of Data on the B and C Systems of the Hydrogen Halides, Methyl Halides, and Cyanogen Halides..... 162

10.26 Comparison of Some Term Values of the Halogen Atoms and the Cyanogen Halides..... 164

10.27 Spin-Orbit Coupling Constants of the Halogen Atoms and the Hydrogen Halide and Methyl Halide Monopositive Molecular Ions..... 164

10.28 Shorter Wavelength Absorption of Cyanogen Iodide..... 172

10.29 Some Pairs of Bands of Cyanogen Iodide..... 175

10.30 Shorter Wavelength Absorption of Cyanogen Bromide..... 175

LIST OF FIGURES

			Page
Figure	2.1	Schematic Optical Diagram of a Concave Diffraction Grating Spectrograph.....	10
	2.2	The Rowland Cylinder Mounting used in the Off-Plane Eagle Vacuum Spectrograph.....	16
	3.1	Schematic Diagram of the Vacuum Spectrograph..	20
	3.2	Horizontal Section of Slit and Predispersion Units.....	24
	4.1	Lyman Flash Source.....	31
	4.2	Lyman Source Power Supply.....	33
	4.3	Spark Gap.....	35
	4.4	Lyman Source Vacuum and Flow System.....	36
	4.5	Window Holder.....	38
	4.6	Absorption Cell and Flow System.....	40
	4.7	Overall View of Vacuum Spectrograph and Associated Apparatus.....	43
	5.1	Plate Tilt Calibration Curve.....	47
	5.2	Grating Tilt Calibration Curve.....	47
	5.3	Rowland Circle Projection of the Off-Plane Eagle Vacuum Spectrograph.....	49
	5.4	Grating Focus Calibration Curve.....	52
	5.5	Slit Rotation Angle φ Versus Angle of Incidence α_o.....	52
	5.6	Image Distance p versus Wavelength for Lithium Fluoride Fore-prism.....	59
	6.1	Leak Rate of Vacuum Spectrograph.....	59
	6.2	Lyman Source Circuit Characteristics.....	61
	6.3	Hg 4358 Å Line and O_2 Schumann-Runge Absorption under High Resolution.....	62

			Page
Figure	9.1	Molecular Orbitals for the Linear and Non-Linear Cyanogen Halides.....	94
	9.2	Molecular Orbital Correlation Diagram for the Cyanogen Halides.....	96
	10.1	Schematic Representation of the Electronic Absorption Spectra of the Cyanogen Halides.....	119
	10.2	The B and C Absorption Systems of the Cyanogen Halides.....	132
	10.3	Fermi Resonance in the Cyanogen Bromide B and C Excited States.....	146
	10.4	Correlation Diagram for (Λ,S) and (Ω_c,ω) Coupling of a ... $(\pi)^3(\sigma)$ Electron Configuration.....	146
	10.5	Some Rydberg Levels of Cyanogen Iodide.....	180
	A.3.1	.....	a.14

PART I

CONSTRUCTION OF THE APPARATUS

Scope of Part I

A brief description of the design and construction of a twenty-one foot off-plane Eagle vacuum spectrograph is given. A Lyman source and predispersion unit have been designed and constructed for use with this spectrograph and are described in more detail.

The calibration of the vacuum spectrograph and the predispersion unit is described and techniques for use of the apparatus are given. Some tests to show the performance of the instrument are described.

CHAPTER 1

INTRODUCTION

1.1 Experimental Problems

In the past the majority of the investigations of molecular electronic spectra have been carried out in the visible and near ultraviolet regions; relatively little work has been done in the vacuum ultraviolet. This is especially true in the field of high resolution spectroscopy, the chief reason being the experimental difficulties encountered in this region. A short outline of some of these problems is given in order to show the considerations that must be kept in mind when designing equipment for the vacuum region.

The first problem is that the two major constituents of the atmosphere both have strong electronic absorption systems in this region, molecular oxygen absorbing at wavelengths below about 1950 Å, and molecular nitrogen at wavelengths below about 1450 Å.[1] This requires that the spectrograph either is flushed with a gas which is transparent in the region of interest, or is evacuated to a pressure low enough to make the absorption due to residual oxygen and nitrogen negligible. The technique of flushing has been used in some instances, but in general is not too successful. Thus it is necessary to design the spectrograph so that it can be evacuated. For a high resolution spectrograph of the type to be described, this is a difficult undertaking since the total path length is about forty-four feet, and so

the pressure must be reduced to about 10^{-5} mm Hg.

A second difficulty in vacuum ultraviolet absorption spectroscopy is the source of continuous radiation. There are few sources available commercially, so that it is usually necessary to construct a source. All the light sources that are suitable for the vacuum region have the further drawbacks that they are difficult to operate, have a short lifetime, and have low intensity compared to the continuous sources available for the visible and near ultraviolet regions.

There are few substances that are suitable for use as windows in the vacuum ultraviolet. At wavelengths longer than about 1600 Å, specially purified fused silica windows may be used. Calcium fluoride windows may be used down to about 1250 Å, and lithium fluoride windows down to about 1100 Å, the lower limit depending upon the particular window and its thickness. Below the lithium fluoride limit there are no substances that can be used for windows in optical spectroscopy. It is possible to avoid employing windows by using the spectrograph body itself as the absorption cell, but in high resolution instruments which contain very expensive gratings, this is only possible with non-corrosive compounds. Differential pumping techniques may also be employed, but these are rather complex and difficult to use, and do not completely isolate the absorption cell from the spectrograph.

For dispersion of the light, either a prism or diffraction grating may be used. The former is used only rarely in the vacuum region, since it does not give good dispersion or resolution, and there is considerable light loss due to reflection from the prism

surfaces and absorption by the prism material. For high resolution studies, diffraction gratings must be employed since only by use of higher orders of the grating is it possible to obtain the required dispersion and resolution. Gratings that appear to be quite good in visible light may not be nearly so good in the vacuum ultraviolet because ruling errors which do not impair image formation with the long wavelength light of the visible may be harmful with the shorter wavelength light of the vacuum region. Another problem with diffraction gratings in the vacuum ultraviolet is the low reflectivity of the coating (usually aluminum), although this may be overcome to some extent by overcoating the grating surface with magnesium fluoride.[2]

Another aspect of obtaining spectra in the vacuum region that must be considered, is the problem of recording the spectra. Although photoelectric detection is used to some extent in small spectrometers, either photographic plates or film are normally used on larger instruments. Photographic materials for use in the vacuum ultraviolet must be specially made so that the light sensitive material is at the surface of the emulsion, rather than buried in it as is the case for materials used in the visible and near ultraviolet, since the gelatin absorbs rather strongly in the vacuum ultraviolet. This makes the photographic plates and film very sensitive, and consequently great care must be used in handling them.

1.2 Usefulness of the Vacuum Ultraviolet

The vacuum ultraviolet presents a wide area for spectroscopic investigation. In the wavelength region from 2000 Å to 1000 Å, the

energy range covered is 50,000 cm^{-1} which is greater than that available for the visible and near ultraviolet regions combined (from about 10,000 Å(10,000cm^{-1}) to 2,000 Å(50,000cm^{-1})). For almost all molecules, it is possible to observe transitions to higher electronically excited states in the vacuum region.

There are very many molecules that show no easily observed electronic absorption spectra except in the vacuum ultraviolet. Among these are a large number of the most familiar and simple molecules; for example, oxygen, nitrogen, carbon monoxide, carbon dioxide, and water, to name a few.

In the vacuum ultraviolet, it is quite often possible to find Rydberg series of molecules from which very accurate values of the ionization potentials can be derived. These are important since they give an idea of the binding energy of some of the electrons in the molecule, and it is possible to compare these values with those obtained from various types of molecular orbital calculations to test the methods employed.

Information obtained from the study of simple molecules in the vacuum ultraviolet has extensive astrophysical applications. For many of the molecules expected to exist in planetary atmospheres, the sun, the stars, etc., either the only or the most convenient method of identification is by spectroscopic observations in the vacuum ultraviolet. Some work in this line has been done by sending up spectrometers in rockets.[3]

1.3 Spectrographs for the Vacuum Ultraviolet

Spectrographs for the vacuum ultraviolet have been in use

since before the beginning of this century, the first one having been built in 1893 by V. Schumann.[4] However, these early instruments were very small fluorite spectrographs which gave little dispersion, and with which it was not possible to make very accurate wavelength measurements. Lyman[5] constructed the first grating spectrograph for the vacuum ultraviolet in 1906, and with it not only made the first accurate wavelength measurements in this region, but also extended the accessible region to about 500 Å.

In the 1930's and 1940's, many small grating vacuum spectrographs were constructed for atomic and molecular spectroscopy. Most of these had very limited resolution, and in molecular spectroscopy the work was mainly limited to the identification of Rydberg series. At the present time, there are several small vacuum spectrographs and spectrometers available commercially which are suitable for the analysis of vibrational structure of electronic spectra, and of Rydberg series.

For high resolution work, there are relatively few spectrographs available. One of the first was built in 1929, and later modified, by Harrison.[6] This spectrograph was moved to the University of Chicago, and was then completely modified by Wilkinson[7] in 1957. This spectrograph is a twenty-one foot off-plane Eagle type and is capable of very high resolution in the vacuum ultraviolet. It is essentially the same type of spectrograph as will be described in part I of this thesis. The Jarrell-Ash Company now offers for sale commercially a vacuum spectrograph modelled after the one at the University of Chicago. At the present time there are twenty-one foot Jarrell-Ash vacuum spectrographs at the U. S. Naval Research

Laboratory, Washington, D. C.,[8] and at Vanderbilt University, Nashville, Tennessee.[9]

A thirty-five foot in-plane Eagle spectrograph of a somewhat different design has been in operation for some time at the National Research Council, Ottawa.[10] In the same size range, there is a thirty-five foot echelle spectrograph for use in the vacuum ultraviolet now under construction at Imperial College, London.

CHAPTER 2

THEORY OF THE CONCAVE DIFFRACTION GRATING

2.1 Introduction

The first concave diffraction grating was made by H. A. Rowland in 1882,[11] some sixty years after Fraunhofer made the first plane grating. The advantage of the concave grating lies in the fact that with it the spectrograph consists only of slit, grating, and recording device, thus eliminating the auxilliary focussing optics required by the plane grating. This makes spectra easier to record since there is much less loss of intensity due to reflection and absorption. In the vacuum ultraviolet the low light loss with the concave diffraction grating is especially important.

However, use of a concave grating introduces a new set of problems. It is not possible to obtain concave gratings that are of such high quality as plane gratings since the former are much more difficult to rule. Also, there are a number of inherent defects in the image formed by a concave grating that must be considered if the highest resolution is to be attained.

2.2 Theoretical Considerations

There have been a number of treatments of the theory of the concave diffraction grating in the past.[7,12,13,14,15] The most recent of these is by T. Namioka[15] who has derived the results by

the use of geometrical optics, and checked them in some instances by the use of physical optics.

A schematic optical diagram of a spectrograph employing a concave diffraction grating is given in Figure 2.1. The origin of the Cartesian coordinate system is taken at O(0,0,0), the centre of the grating, and the axes are oriented so that Ox is normal to the centre of the grating and Oz is parallel to the grating rulings. The grating spacing is d, thus restricting the coordinate w on the grating in the y direction such that w/d is an integer. The radius of curvature of the grating is R.

A point light source at A(x,y,z) on the slit illuminates the grating at any point P(u,w,ℓ) and is diffracted to an image at B(x',y',z'). The angle of incidence α, and the angle of diffraction β are measured in the xy plane. In order for an image to be formed, the condition for constructive interference must be obeyed, i.e. the path difference between adjacent grooves must be an integral number of wavelengths. Thus, for monochromatic radiation of wavelength λ the path difference for two grooves separated by w in the y direction must be $(w/d)m\lambda$, where m is an integer known as the order number and is equal to the number of wavelengths in the path difference between adjacent grooves.

For any light ray APB, a light path function F may be defined by

$$F = AP + BP + \frac{w}{d}m\lambda \qquad (2.1)$$

In a cylindrical coordinate system, also with origin at O(0,0,0), A and B have the coordinates (r,α,z) and (r',β,z'), respectively, as indicated in Figure 2.1. By transforming to cylindrical

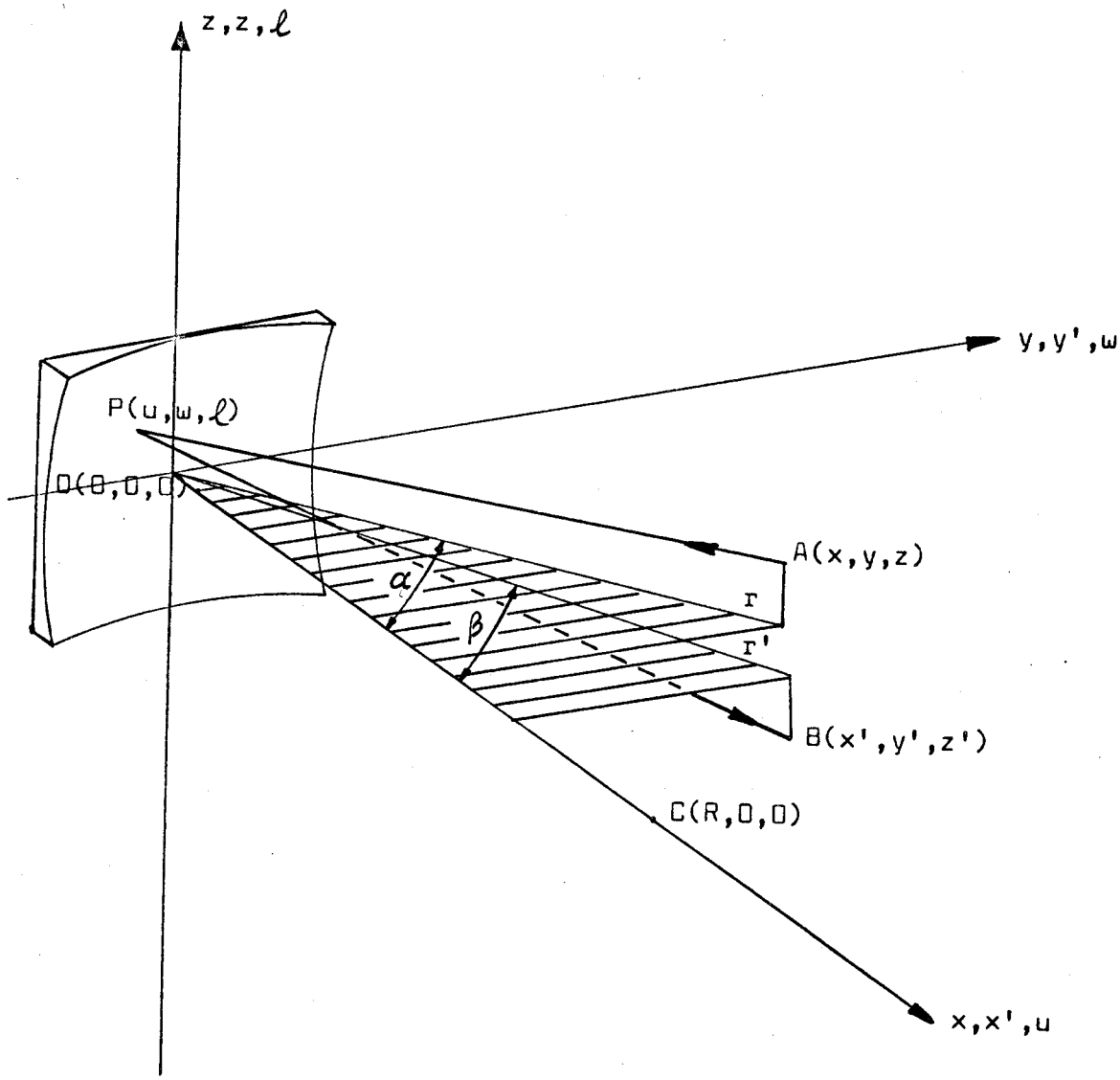

FIGURE 2.1

SCHEMATIC OPTICAL DIAGRAM OF A CONCAVE DIFFRACTION GRATING SPECTROGRAPH

coordinates and expanding in a power series, it is possible to obtain a rather complex equation for F in terms of the parameters r, z, r', z', α, β, w, ℓ, m, R, λ, and d, which is convenient for investigating the optical properties of the concave diffraction grating. This equation for F is Equation A.1.1. of Appendix I.

Fermat's principle[16] states that for point A to be brought to a focus at point B, the light path function F must be equal to within $\pm \lambda/4$ for all points P on the surface of the grating. Thus for all points in the width of the grating to be in focus

$$\frac{\partial F}{\partial w} = 0 \tag{2.2}$$

and for all points along the length of the rulings to be in focus

$$\frac{\partial F}{\partial \ell} = 0 \tag{2.3}$$

Equations A.1.2 and A.1.3 of Appendix I give the full expressions for Equations 2.2 and 2.3, respectively.

For the central ray AOB, since $w = \ell = 0$, Equations 2.2 and 2.3 respectively yield

$$\frac{m\lambda}{d} - \left(1 + \frac{z^2}{r^2}\right)^{-1/2} \sin\alpha - \left(1 + \frac{z_o'^2}{r_o'^2}\right)^{-1/2} \sin\beta_o = 0 \tag{2.4}$$

and

$$\frac{z}{r}\left(1 + \frac{z^2}{r^2}\right)^{-1/2} + \frac{z_o'}{r_o'}\left(1 + \frac{z_o'^2}{r_o'^2}\right)^{-1/2} = 0 \tag{2.5}$$

where the subscript 'o' indicates that the central ray is being considered. Equation 2.5 has the solution

$$\frac{z}{r} = -\frac{z_o'}{r_o'} \tag{2.6}$$

which gives the magnification ratio of the grating. Substitution of this result in Equation 2.4 gives

$$\frac{m\lambda}{d} = \left(1 + \frac{z^2}{r^2}\right)^{-\frac{1}{2}} (\sin\alpha + \sin\beta_0) \qquad (2.7)$$

which is a generalized form of the grating equation for the central ray.

Expansion of the two most important terms of Equation 2.2 about the point (r'_0, β_0, z'_0), together with the use of Equations 2.6 and 2.7, leads to the equation

$$-(\cos\beta_0)\Delta\beta + \tfrac{1}{2}\sum_{n=0}^{\infty} (n+2)\, w^{n+1} \left[\left(\frac{\sin\alpha}{r}\right)^n \left\{\frac{\cos^2\alpha}{r} - \frac{\cos\alpha}{R}\right\} + \left(\frac{\sin\beta}{r}\right)^n \left\{\frac{\cos^2\beta}{r'} - \frac{\cos\beta}{R}\right\}\right] + O\left(\frac{w^2}{R^2}\right) = 0 \qquad (2.8)$$

in which $\Delta\beta$ $(= \beta - \beta_0)$ is related to the spectral line width, and $O\left(\frac{w^2}{R^2}\right)$ indicates small terms of the order of $\frac{w^2}{R^2}$. A similar expansion of Equation 2.3 leads to

$$-\Delta\left(\frac{z'}{r'}\right) + l\left\{\frac{1}{r} - \frac{\cos\alpha}{R} + \frac{1}{r'} - \frac{\cos\beta}{R}\right\} + O\left(\frac{w^2}{R^2}\right) = 0 \qquad (2.9)$$

in which $\Delta(z'/r')$ is related to the astigmatism.

Examination of Equations 2.8 and 2.9 shows that it is not possible to make $\Delta\beta$ and $\Delta(z'/r')$ negligibly small simultaneously. Since in a high resolution spectrograph it is necessary to have the line width a minimum, $\Delta\beta$ in Equation 2.8 must be made as small as possible. To do this, the largest term in the summation (for n = 0) is set equal to zero, i.e.

$$\frac{\cos^2\alpha}{r} - \frac{\cos\alpha}{R} + \frac{\cos^2\beta}{r'} - \frac{\cos\beta}{R} = 0 \qquad (2.10)$$

There are several possible solutions for this equation, but the one of interest here is

$$r = R\cos\alpha \qquad r' = R\cos\beta \tag{2.11}$$

The relations in Equation 2.11 represent a cylindrical surface of diameter R with its axis parallel to the z axis of the Cartesian coordinate system and passing through the point (R/2,0,0). This cylinder is called the Rowland cylinder, since its intersection with the xy plane is the more familiar Rowland circle. Consideration will now be restricted to Rowland cylinder mountings since these are the most important for use in high resolution spectroscopy.

If the slit makes an angle φ with a plane parallel to the z axis passing through the middle point of the slit, then by further consideration of Equation 2.2 (after substitution of Equation 2.11) it can be shown that the value of the angle φ which minimizes the line broadening is given by

$$\varphi = \frac{z_0}{R} \tan\alpha_0 \sec\alpha_0 \tag{2.12}$$

From Equation 2.9 it can be seen that with the line broadening minimized as described above, the point A on the slit will be drawn out into a line when focussed at B. Consideration of Equations 2.3 and 2.9 shows that if the length of slit illuminated is $2a_0$ and the length of the grating rulings is L, then the length of the image is

$$2a_0\left(\frac{\cos\beta_0}{\cos\alpha_0}\right) + L\left[\frac{\sin^2\alpha_0\cos\beta_0}{\cos\alpha_0} + \sin^2\beta_0\right] \tag{2.13}$$

The first term gives the image size caused by the magnification factor of the grating, and the second term gives the lengthening of the image

due to the astigmatism, i.e. it gives the length of the image that would be formed from a point source.

The above treatment covers the more important features of the concave diffraction grating. However, many points have not been considered. For example, coma causes curvature in the spectral images and so limits the permissable length of the slit and grating rulings, while spherical aberration causes the spectral lines to be broadened and thus limits the usable aperture of the grating. Also, in the above, the grating rulings have been treated as lines of zero width having no shape, whereas in actual fact it is usual to shape the grooves (blaze the grating) so that light is reflected preferentially into certain orders of the grating.

2.3 The Off-Plane Eagle Mounting

The Eagle mounting has often been used in the design of large vacuum spectrographs since it is a compact mounting which has low astigmatism and large wavelength coverage. This mounting is used in two modifications. The in-plane Eagle mounting uses a Rowland circle of radius R/2, the slit and plate being placed on the circle and the grating centre being tangent to the circle. The angle of incidence is either smaller or larger than the angle of diffraction, the choice depending on the specific purpose of the spectrograph.

The off-plane Eagle mounting, which is the one of interest here, employs a Rowland cylinder of radius R/2. The grating centre is tangent to the cylinder, with the normal to the centre of the grating defining the plane of the Rowland circle. The slit and

photographic plate are mounted on the Rowland cylinder, displaced equal but opposite amounts from the Rowland circle. It is necessary to bend the photographic plate to a radius of curvature R/2 so that the whole length of the plate is on the Rowland cylinder. Since the slit and the middle of the photographic plate are side by side, the angle of incidence α_o is equal to the angle of diffraction β_o, so that the form of the grating equation that applies is

$$m\lambda_o = \left(1 + \frac{z_o^2}{R^2\cos^2\alpha_o}\right)^{-\frac{1}{2}} 2d\sin\alpha_o \qquad (2.14)$$

The off-plane Eagle mounting is normally used as shown in Figure 2.2, in which the axis system has been rotated relative to that in Figure 2.1 so that the z axis is horizontal and the xy plane (i.e. the plane of the Rowland circle) is vertical. The length of the grating rulings is horizontal, and so the light is dispersed vertically.

From the grating Equation 2.14, it is easily seen that to change the wavelength λ_o reaching the middle of the plate, it is necessary to change the angle α_o. Since the positions of the slit and the middle of the plate are fixed usually, it is necessary to rotate the grating about the z axis (the direction of the length of the grating rulings) by the angle α_o. When this is done, the Rowland cylinder is also rotated and so the slit and the middle of the plate are no longer on the cylinder (see Figure 2.2.b). Thus it is necessary to move the grating towards or away from the plane of the slit and middle of the plate until they are again on the Rowland cylinder. Now the middle of the plate is on the Rowland cylinder, but the whole

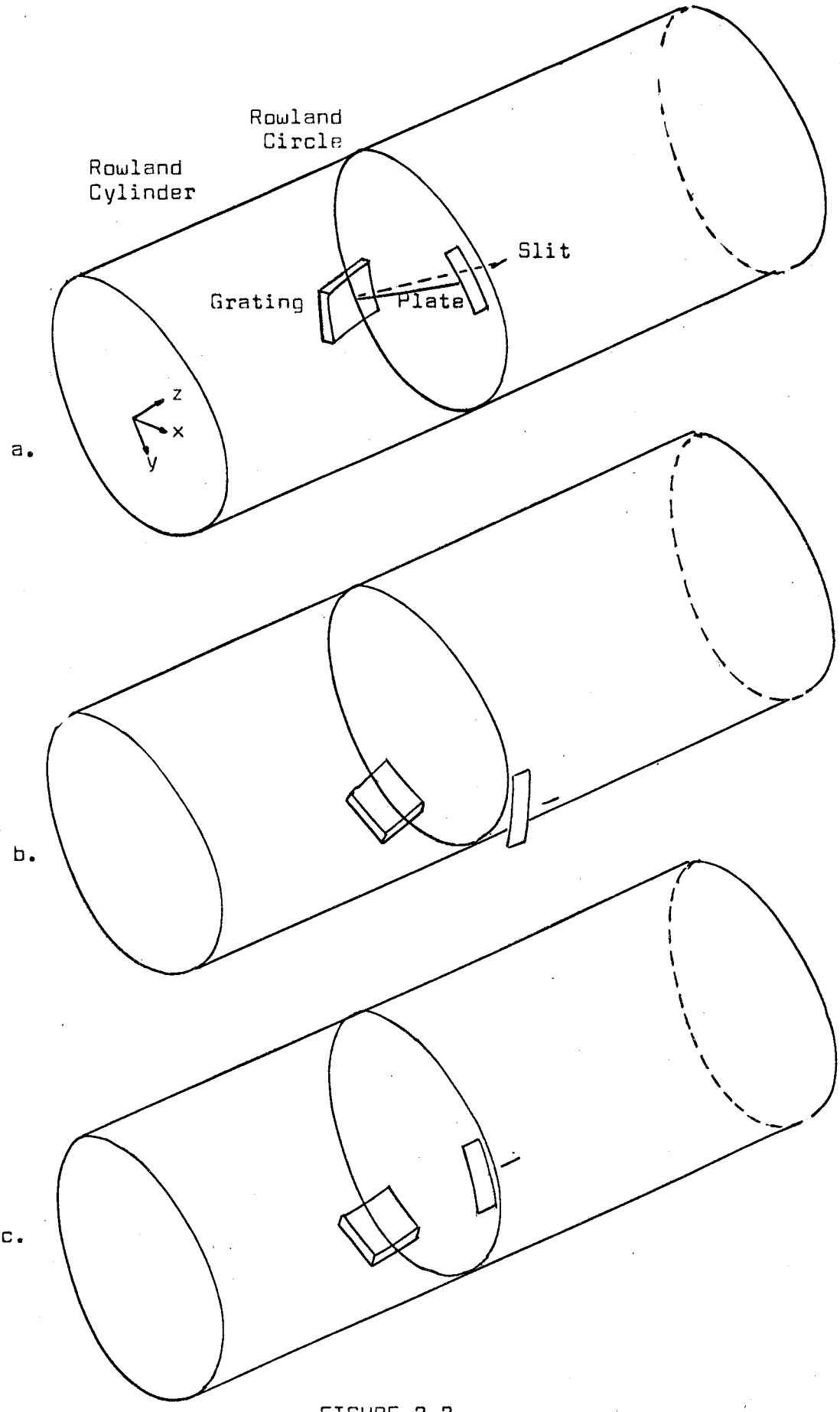

FIGURE 2.2

THE ROWLAND CYLINDER MOUNTING USED IN THE

OFF-PLANE EAGLE VACUUM SPECTROGRAPH

length of the plate is not, so it is necessary to rotate the plate about its mid-point by the angle α_0 so that the whole plate is again on the Rowland cylinder.

Since $z_0 \neq 0$ in the off-plane Eagle mounting, it is clear from Equation 2.12 that as the angle α_0 is changed the angle φ must also be changed. That is, it is necessary to be able to rotate the slit about an axis defined by the direction of the light beam. In practice it is found that for reasonable values of z_0 and R, the angle φ is a slowly changing function of the angle α_0, and so, once the slit angle is set, it is not necessary to adjust it except when the highest resolution is required.

From the preceding discussion, the basic adjustments required for an off-plane Eagle mounting are rotation of the grating about an axis parallel to the grating rulings, translation of the grating in the direction of the slit and plate, rotation of the photographic plate about its mid-point, and rotation of the slit about an axis defined by a line joining the centre of the grating to the middle of the slit.

For initially setting up the spectrograph, certain other adjustments are essential. One of these is rotation of the grating about an axis perpendicular to the direction of the grating rulings (the y axis) in order to ensure that light from the slit is diffracted from the grating to the photographic plate. A second adjustment is an accurate rotation of the grating about the normal to its centre (the x axis) in order first to check that the blazed side of the grating is being used and second to make the grating rulings exactly horizontal.

Using an off-plane Eagle mounting as described above, it is possible to assemble a spectrograph having a concave grating of six metre focal length in a space of about seven metres by one-half metre, which is a considerably smaller volume than that required by any other mounting to give comparable performance. This small volume is important for a vacuum spectrograph since it allows smaller pumps to be used, this not only reducing the cost, but also minimizing the problems with vibration which can cause line broadening. There is also the advantage mentioned before that only one reflection is required.

CHAPTER 3

DESIGN OF THE SPECTROGRAPH

The spectrograph is a twenty-one foot off-plane Eagle mounting designed for use primarily in high orders in the region from about 1200 Å to 2000 Å. The design of the spectrograph follows that described by P. G. Wilkinson[7], who has shown that this mounting is capable of very high resolution in the vacuum ultraviolet.

3.1 General Description

A schematic diagram of the spectrograph is given in Figure 3.1. The main vessel is a three hundred pound test steam pipe, twelve inches in internal diameter and about twenty-two feet long. This vessel is covered in a two inch layer of fibreglass insulation and is mounted on two concrete pillars constructed so as to minimize the effects of building vibrations on the spectrograph. One end of the pipe is closed by a heavy cover plate, and the other end has attached a compartment housing the plate chamber, and allowing connection of the slit assembly. A large flange is attached to the middle of the pipe to allow mounting of the pumping system.

3.2 The Vacuum System

The backing pump is an Edwards Speedivac rotary pump, model 1SC4508, having a pumping speed of 450 litres/min. The diffusion pump is an Edwards type 603 6 in., three stage oil diffusion pump, fitted

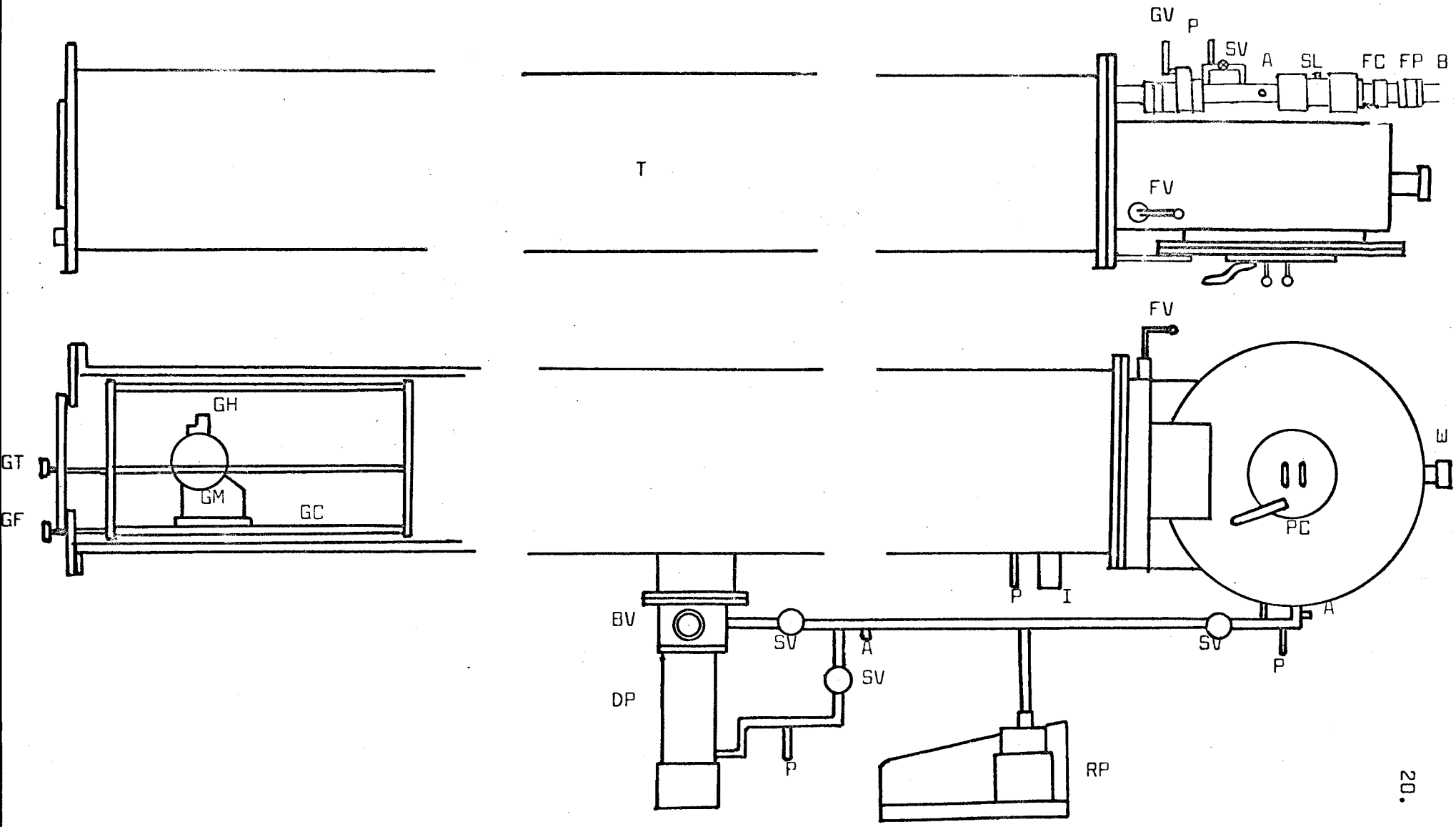

FIGURE 3.1: SCHEMATIC DIAGRAM OF THE VACUUM SPECTROGRAPH

LEGEND FOR FIGURE 3.1.

BV	baffle valve
DP	diffusion pump
RP	rotary pump
SV	speedivalve
P	Piriani gauge head
I	Philips ionization gauge head
A	air admittance valve
FV	flap valve control
PC	plate controls
W	alignment window
GH	grating holder
GM	grating mount
GC	grating carriage
SL	slit
FC	fore-prism focus control
FP	fore-prism holder
B	bellows
GF	grating focus control
GT	grating tilt control
GV	gate valve
T	main vacuum tube

with a type 9LP6 baffle valve, which has a baffled speed of about 350 litres/sec. The diffusion pump is water cooled and has several protective devices. An Asco solenoid valve is fitted to the water line and is connected so that power cannot be supplied to the diffusion pump heaters unless the cooling water is turned on. An Edwards type FSM-1 Flowtrol flowmeter is connected in the water line so that power to the heaters is cut off if the water flow rate falls below a certain required minimum. Finally, a thermostat control in series with the power lines is mounted on the side of the pump and cuts off the power if the pump starts to heat up.

As seen from Figure 3.1, the diffusion pump is connected directly to the main vacuum vessel. Connections from the diffusion pump to the rotary pump, and from the rotary pump to the main chamber and the plate chamber, are standard 1 in. copper pipe, and the connection to the slit chamber is ½ in. copper pipe. The valves used for isolation are the appropriate size Saunders Edwards Speedivalves. Edwards air admittance valves are used for letting air into the various sections of the spectrograph. The locations of these are indicated in the figure.

Pressures in the range from roughly 50 mm down to about 5×10^{-3} mm are measured by an LKB Autovac Piriani type vacuum gauge. This unit has connections for four gauge heads, and these are mounted one each in the main vacuum chamber, the plate chamber, the slit chamber, and the backing line, as indicated in Figure 3.1. For high vacuum measurement, an Edwards Philips type cold cathode ionization gauge, model 3,

covering the range from 5×10^{-3} mm to 1×10^{-5} mm, is used. This is mounted on the main vacuum chamber.

3.3 The Slit

The slit is a Hilger F1386 slit with a smallest division of 1 micron, which has been mounted so that it is possible to adjust the slit width and shutter controls, and to rotate the whole slit about an axis defined by the direction of the light beam, without breaking vacuum. Provision has been made for recording comparison spectra without disturbing the absorption cell and Lyman source. A small mirror may be rotated into the absorption spectrum light path under vacuum so that light passing through the side window of the mirror chamber is reflected onto the slit and so to the grating. Details of this are given in Figure 3.2. The whole slit chamber may be isolated from the rest of the spectrograph by a 1 in. gate valve (Vacuum Research Co., VG-101T).

3.4 The Grating

The grating is a Bausch and Lomb replica mounted on a fused quartz blank 152 mm in diameter and has a radius of curvature of 6.65 m. There are 1200 grooves/mm over a width of 132 mm, each groove being 60 mm long. The grating has a blaze angle of 19° 16', which corresponds to 5500 Å in the first order, and the grating surface has been over-coated with magnesium fluoride to increase the reflectivity in the vacuum ultraviolet. The resolving power of the grating is stated to be in excess of 80% of theoretical, which is 158,400 in the first order.

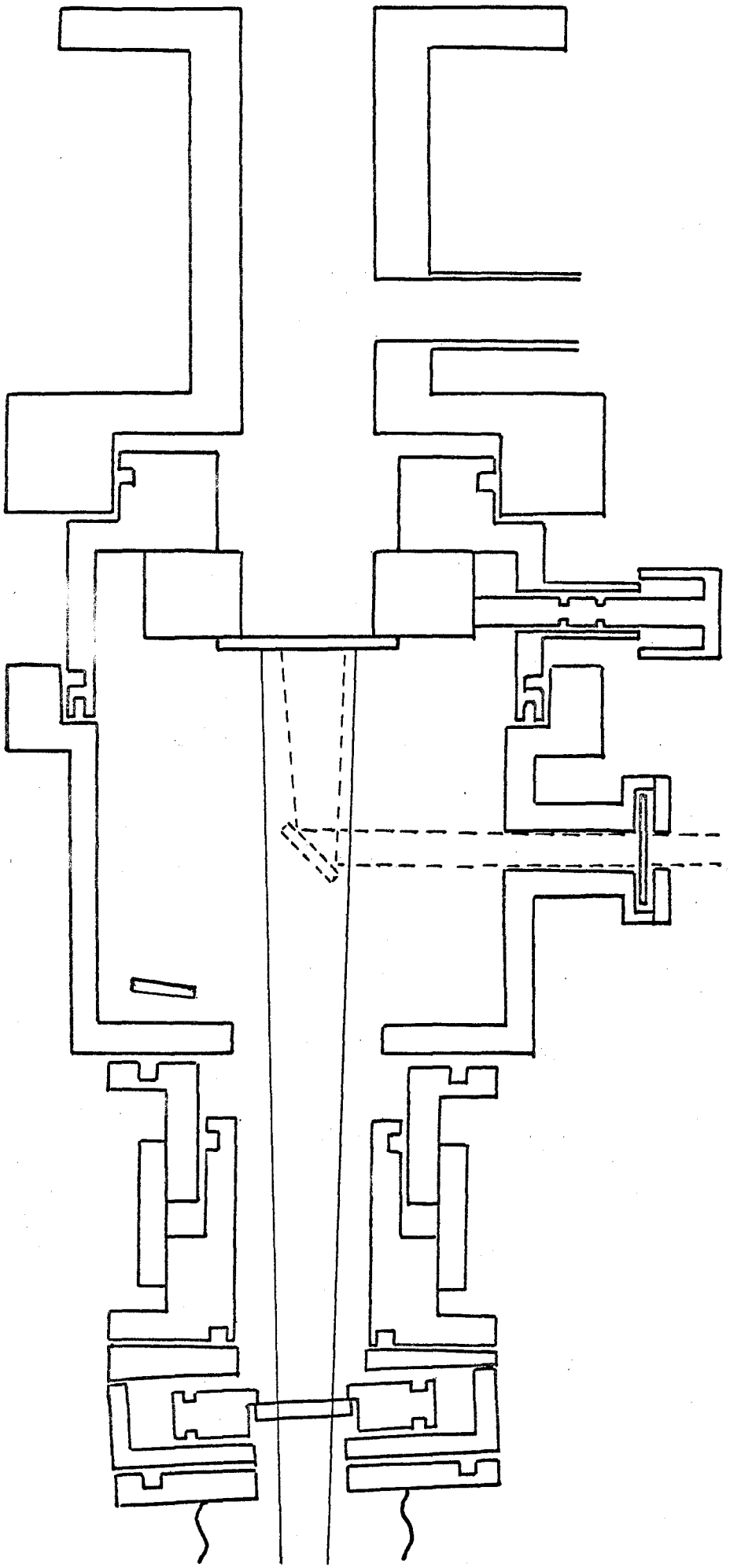

FIGURE 3.2: HORIZONTAL SECTION OF SLIT AND PREDISPERSION UNITS

3.5 The Grating Mount

The grating is mounted in a holder which allows rotation both by small amounts and by 180° about the normal to the centre of the grating (the x axis of Figures 2.1 and 2.2). This holder is mounted on a horizontal axis supported by a carriage which allows several more adjustments of the grating. The grating carriage may be rotated about a vertical axis (the y axis) to bring the image of the slit to the plate. The grating may also be rotated about the horizontal axis (the z axis) to change the wavelength of the light diffracted to the plate. The carriage rides on two machined rods and is driven by a long drive screw so that the grating may be moved towards or away from the slit and plate so as to bring these components onto the Rowland cylinder. An overall motion of the grating of 18 in. is allowed by the length of these rods.

The controls for rotation of the grating about the horizontal axis (grating tilt) and translation of the grating carriage (grating focus) may be adjusted without breaking the vacuum. The other controls have not been brought outside the spectrograph since once set, they need not be changed unless the grating mount is disturbed.

3.6 The Plate Chamber

The plate holder, which takes 2 in. x 10 in. photographic plates, and can be adapted to take 35 mm film, has been accurately machined to a 10.5 ft. radius of curvature so that the whole length of the photographic plate will be on the Rowland cylinder. External controls have been provided for rotation of the plate about its mid-point, for moving the plate so that up to 8 exposures may

be taken on a 2 in. x 10 in. plate, and for taking comparison spectra without moving the plate.

The plate chamber can be isolated from the rest of the spectrograph by a flap valve,[17] thus making changing plates quite simple and fast, the whole process taking only about 15 minutes. The plate chamber is provided with a window so that either the spectrum can be viewed, or an alignment lamp can be shone on the grating to facilitate adjustment of the cell and light sources.

CHAPTER 4

THE LYMAN SOURCE AND PREDISPERSION UNIT

4.1 Survey of Other Sources

There are not many continuous sources known for the vacuum ultraviolet. One that has been used for some time is the hydrogen continuum which extends from about 3500 Å to 1600 Å. The continuum may be produced by a high current discharge,[18] or by microwave excitation,[19] in the gas. Recombination of hydrogen atoms results in the production of hydrogen molecules in the stable excited state $^3\Sigma_g^+$, which then fall to the dissociative lower state $^3\Sigma_u^+$ and so emit continuous radiation.[20]

A newer development in absorption sources for the vacuum ultraviolet are the continua excited in the rare gases. These may be produced by a repetitive condensed discharge in He, Ne, Ar, Kr, and Xe, or by microwave excitation at 2450 Mc/sec in Ar, Kr, and Xe. The wavelength range in which each is useful is summarized in Table 4.1. For high resolution studies, the continua excited by microwave radiation are more useful since they give out less light at longer wavelengths and so minimize the problems of order separation. The mechanism by which the continua are produced is similar to that in the case of the hydrogen continuum, i.e. by collision of atoms, rare gas diatomic molecules are produced in stable excited states (most important are $^{1,3}\Sigma_u^+$, $^{1,3}\Pi_u$) which then undergo a transition to the dissociative ground state $^1\Sigma_g^+$, which results in the production of

TABLE 4.1

WAVELENGTH RANGE OF THE RARE GAS CONTINUA

Rare Gas	Wavelength Range (Å)	
	Condensed Discharge	Microwave Excitation
He	600 - 1100	------
Ne	744 - 1000	------
Ar	1070 - 1650	1060 - 1500
Kr	1250 - 1850	1260 - 1700
Xe	1470 - 2250	1500 - 2000

a continuum. The construction, operation, and theory of these sources have been extensively described.[8,21,22]

4.2 The Lyman Source

A Lyman source was chosen for use here since it has high intensity throughout the wavelength range of interest, i.e. approximately 1200 Å to 2000 Å. There are certain disadvantages to the Lyman source, the most important of which are that it is a spectroscopically dirty source, the capillary lifetime is short, there are emission and absorption lines in the continuum, and there is a problem with overlapping orders when working in high orders of the grating. In the source as described below, an attempt has been made to minimize these disadvantages.

The principle of operation of the Lyman source is the rapid passage of a large amount of energy through a restricted path. Commonly, a few microfarads of capacity are charged to between 10 and 20 kilovolts, and then short-circuited through a capillary containing a gas at a fairly low pressure. The exact mechanism by which the light is emitted is not understood, although it has been suggested that particles eroded from the capillary by the discharge are heated to a high temperature and emit continuous radiation.[23] It is known that in order to get a continuum with a minimum of overlying emission lines, it is necessary to have a current density of about 30,000 amp/cm^2 passing through the capillary. To accomplish this, the inductance of the discharge circuit must be minimized so that the discharge will be as fast as possible.

Various designs for Lyman sources have been given in the literature.[23,24] The Lyman source described here differs considerably from these.

The light source is shown schematically in Figure 4.1. The base is a sheet of Macarta, 20 in. x 4 in. x ¼ in. The electrodes are machined from aluminum and are bored out in order to provide a light path. Each electrode is fitted with a side arm to allow connection to the vacuum and argon flow system.

The rear electrode, which is connected to the high voltage side of the capacitors through the interrupted spark gap, is supported by a holder made from Glassite which may be clamped tightly to hold the rear electrode in position, or loosened to permit replacement of capillaries. The Glassite holder, together with the Macarta base, provides the necessary insulation for the high voltages used. The rear electrode has a window at the back end which is used to view along the axis of the electrodes in order to ensure that the source lies on the optic axis of the spectrograph.

The front electrode is made very long as shown in the diagram in order to minimize the amount of material eroded from the capillary reaching the rear window of the absorption cell, since this reduces the transmission of the window, and tends to ruin its optical finish. The front electrode is connected to ground, and so is supported by two holders of the same design as the rear electrode holder, but made from aluminum. A circular disc with a rectangular slot is press-fitted at the front of this electrode to act as an aperture stop. Also, the front electrode has a flange with an O-ring groove to make a vacuum

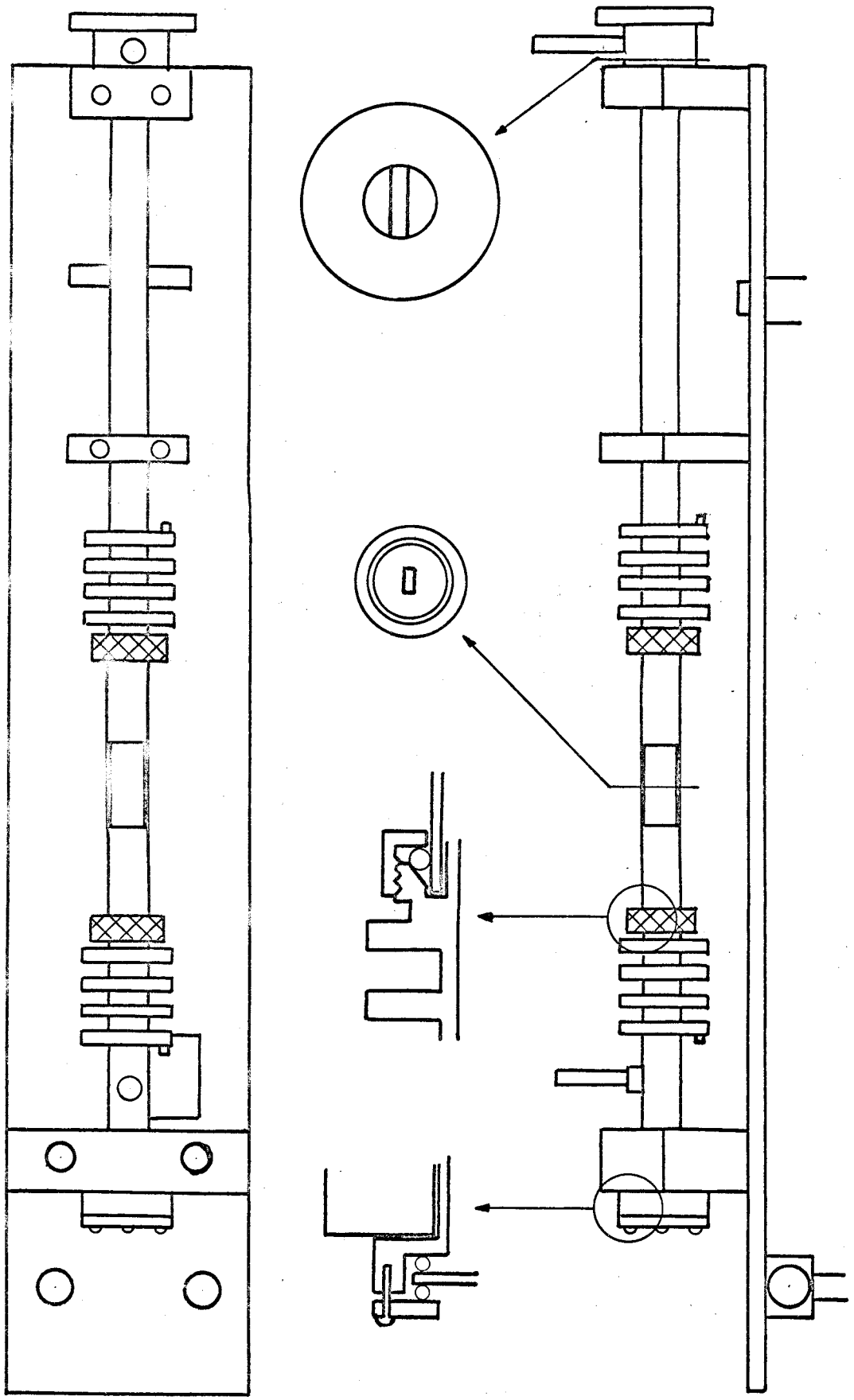

FIGURE 4.1: LYMAN FLASH SOURCE (SCALE: 1 cm≃1 inch)

connection to the rear of the absorption cell.

The capillaries, which are made from zircon, are cylinders 15 mm in diameter and 35 mm long, and have a rectangular slot 1 mm by 3.5 mm along the cylinder axis. These are cemented into 18 mm Pyrex glass tubing with Sauereisen Insa-lute cement. Vacuum connection of the discharge tubes to the two electrodes is made by means of O-rings and threaded collars as shown in the figure.

The source is mounted on Zeiss-type optical stands, which are supported by a 1.5 m optical bench. With these optical stands, it is possible to move the source horizontally and vertically to align it exactly on the optic axis of the spectrograph.

4.3 The Lyman Source Power Supply

A schematic diagram of the circuit is given in Figure 4.2. It is a simple half-wave rectification unit, the high voltage transformer giving an output of 21 kilovolts at 100 milliamperes with a 220 volt input. The primary supply is controlled by a Variac thus allowing the output voltage to be controlled. Rectification is achieved by means of a high vacuum diode (JAN-218) which has its own filament transformer. The output current is limited by a series resistance of 200,000 ohms. The direct current output is used to charge two capacitors, each rated at 1 microfarad, 25 kilovolts, which are connected through a series spark gap to the high voltage electrode of the source.

When the switch for the primary of the high voltage transformer is turned on, a lamp on top of the power supply is lighted to serve as a warning signal. Also, a solenoid-activated shorting switch across the high and low voltage terminals of the capacitors is raised, thus

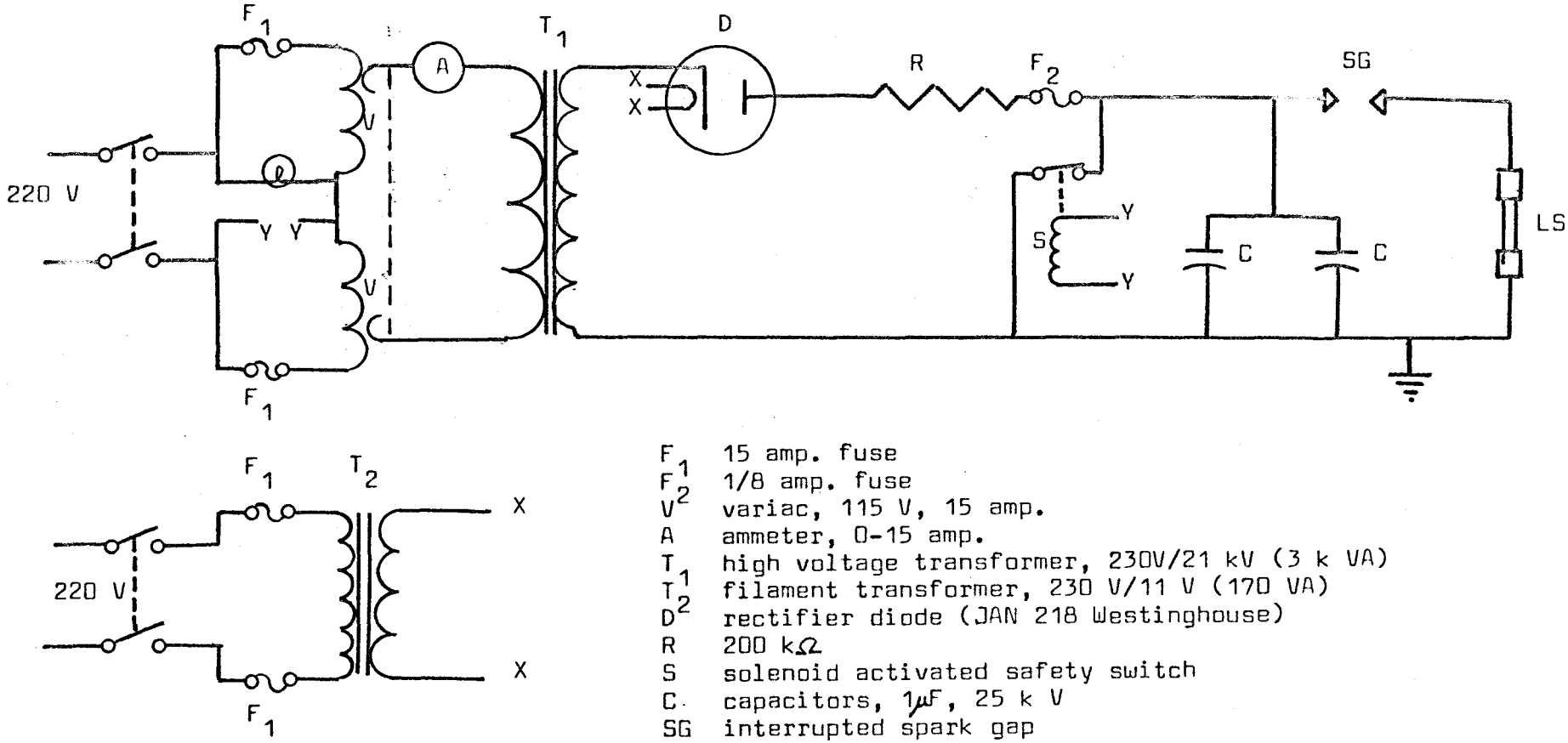

F_1	15 amp. fuse
F_2	1/8 amp. fuse
V	variac, 115 V, 15 amp.
A	ammeter, 0-15 amp.
T_1	high voltage transformer, 230V/21 kV (3 k VA)
T_2	filament transformer, 230 V/11 V (170 VA)
D	rectifier diode (JAN 218 Westinghouse)
R	200 kΩ
S	solenoid activated safety switch
C	capacitors, 1μF, 25 k V
SG	interrupted spark gap
LS	Lyman source

FIGURE 4.2: Lyman Source Power Supply

allowing them to charge. When the primary supply is turned off, the lamp goes out and the shorting switch falls, thus automatically discharging the capacitors.

The interrupted spark gap is shown in Figure 4.3. The lead from the high voltage terminal of the capacitors is connected to one electrode and the lead from the other electrode is connected to the rear electrode of the Lyman source. The electrodes are ¼ in. diameter stainless steel rods, and are supported by posts made from Perspex. The spark gap is interrupted by two small stainless steel rods supported in a large Perspex wheel, the centre of which is connected to the shaft of a motor which has a speed of 20 rev/min. The gap between the stationary and rotating electrodes is made very small (less than 1 mm) so that low voltages as well as high voltages may be used. The actual voltage used is controlled by the Variac in the primary of the high voltage transformer supply, since the time between discharges of the capacitors is constant at about 1.5 seconds.

The whole spark gap assembly is enclosed in a large glass container to reduce the noise in the laboratory. Also, the assembly is kept in an atmosphere of argon to eliminate the corrosion resulting from the formation of ozone when the spark gap is interrupted in air.

4.4 Operation of the Lyman Source

As shown in Figure 4.4, the Lyman source is connected to a vacuum and flow system by means of side arms on the electrodes. When it is to be used, the Lyman source is first evacuated to a pressure less than 1 mm by a rotary pump. Then, tank argon is flowed through the source at a pressure of about 30 mm. Argon is used since it is

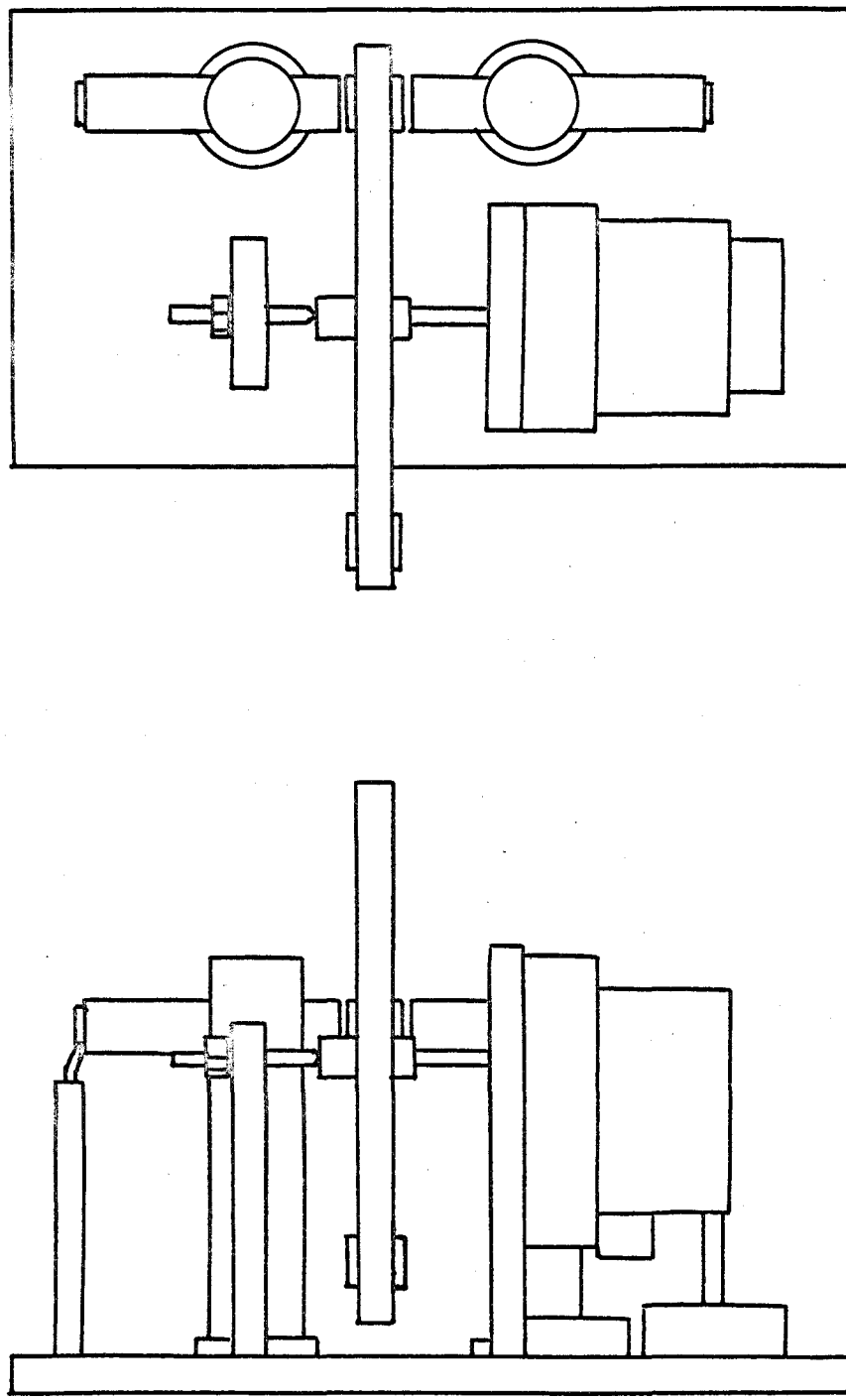

FIGURE 4.3.

SPARK GAP (SCALE: 1 CM = 1 IN.)

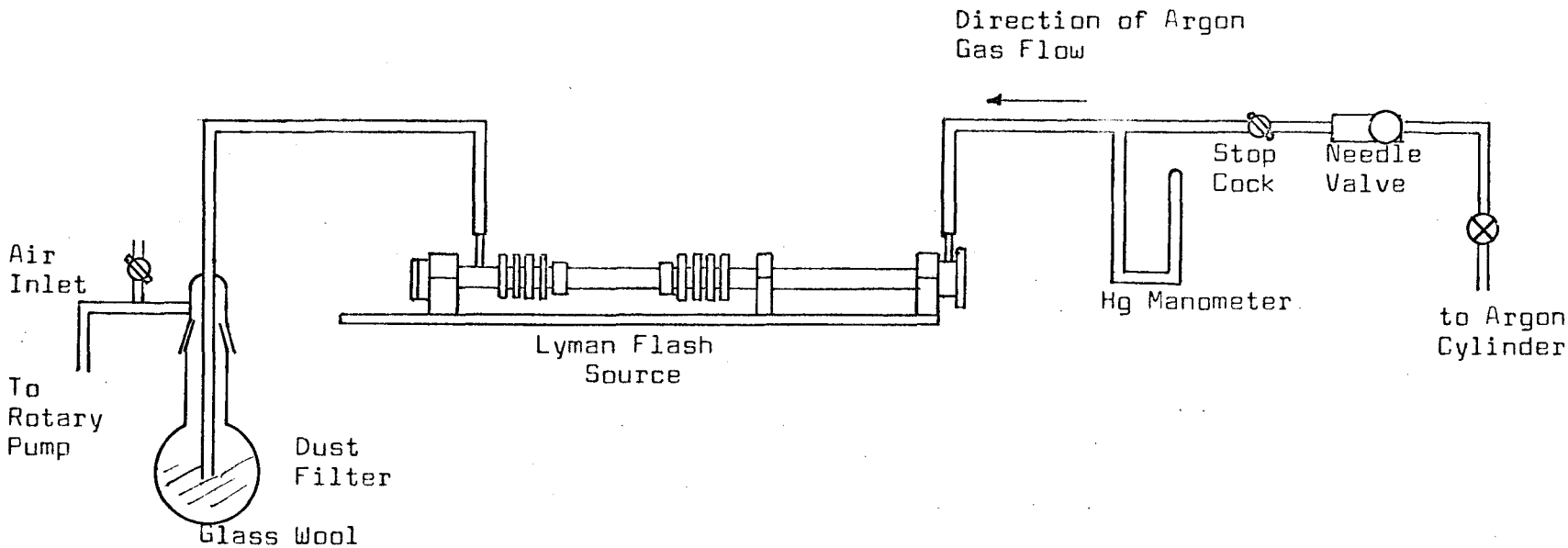

FIGURE 4.4: LYMAN SOURCE VACUUM AND FLOW SYSTEM

a readily available gas which is transparent throughout the region of interest. The argon not only serves to conduct the discharge, but also helps prevent material eroded from the capillary from being deposited on the rear window of the absorption cell since it is flowed through the lamp from front to rear.

It has been found that the pressure of argon, although not critical, must be controlled within a certain range. At low pressures, it is found that there is not enough gas to prevent material from the capillary from reaching the window of the cell, whereas at high pressures, quite often the glass tube holding the capillary will be violently shattered when the discharge occurs. A dust trap, which is just a small amount of glass wool placed in a standard vacuum trap, is positioned between the source and the rotary pump to prevent dust from the capillary from reaching the rotary pump and damaging it.

When a new capillary is being used, it is necessary to use fairly low voltage discharges for a short time until the capillary is conditioned. Immediate use of a high voltage usually results in the cracking of the glass tube holding the capillary.

4.5 The Absorption Cell System

The absorption cell is a 75 cm length of 28 mm Pyrex glass tubing and has standard Edwards 1 in. brass flanges, with O-ring grooves, attached to either end with Picein wax. Depending upon the region being investigated, the windows are either special purity fused silica or Harshaw polished calcium fluoride. These are 1 in. in diameter and 2 mm thick, and are held in brass holders with O-rings and a collar, as shown in Figure 4.5. These holders make the windows easily accessible and so make it easier to clean them.

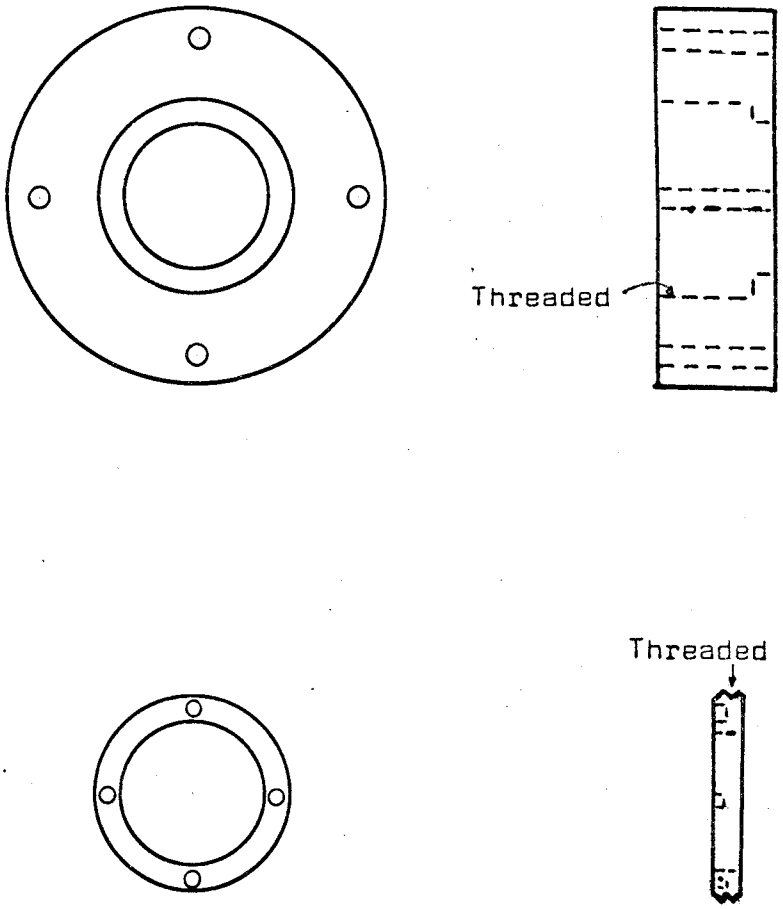

FIGURE 4.5

WINDOW HOLDER (FULL SIZE)

In this work, it was found necessary to flow the compound through the cell, since when static samples were used the polymer formed by photolysis tended to cause excessive coating of the windows, and some of the photolysis products have strong absorption spectra. To minimize the amount of contamination of the windows, only 15 cm of the total 75 cm cell length are used as an absorption path, the inlet and outlet for the compound each being about 30 cm from the nearest window. The flow system is shown in Figure 4.6.

After evacuation with the sample frozen out, the sample container is placed in a dewar held at a temperature giving a reasonable pressure (1 to 20 mm) in the 500 ml reservoir bulb. The vapour is then passed through a needle valve which controls the pressure in the absorption cell, and after flowing through the cell, the compound and any decomposition products are frozen out in a trap held at liquid air temperature. This system was found to give good control over the pressure in the absorption cell, to minimize the amount of polymer deposited on the cell windows, and to eliminate any problems due to absorption by photolysis products.

4.6 The Predispersion Unit

There are various ways of dealing with the problem of overlapping orders when using high orders of a grating spectrograph in the vacuum ultraviolet. The simplest way is to use the microwave excited rare gas continua[8] which have little emission at long wavelengths. A second method is the use of a concave foregrating at grazing incidence,[25] the first order of the wavelength desired being focussed by it on the slit of the spectrograph. This also has the

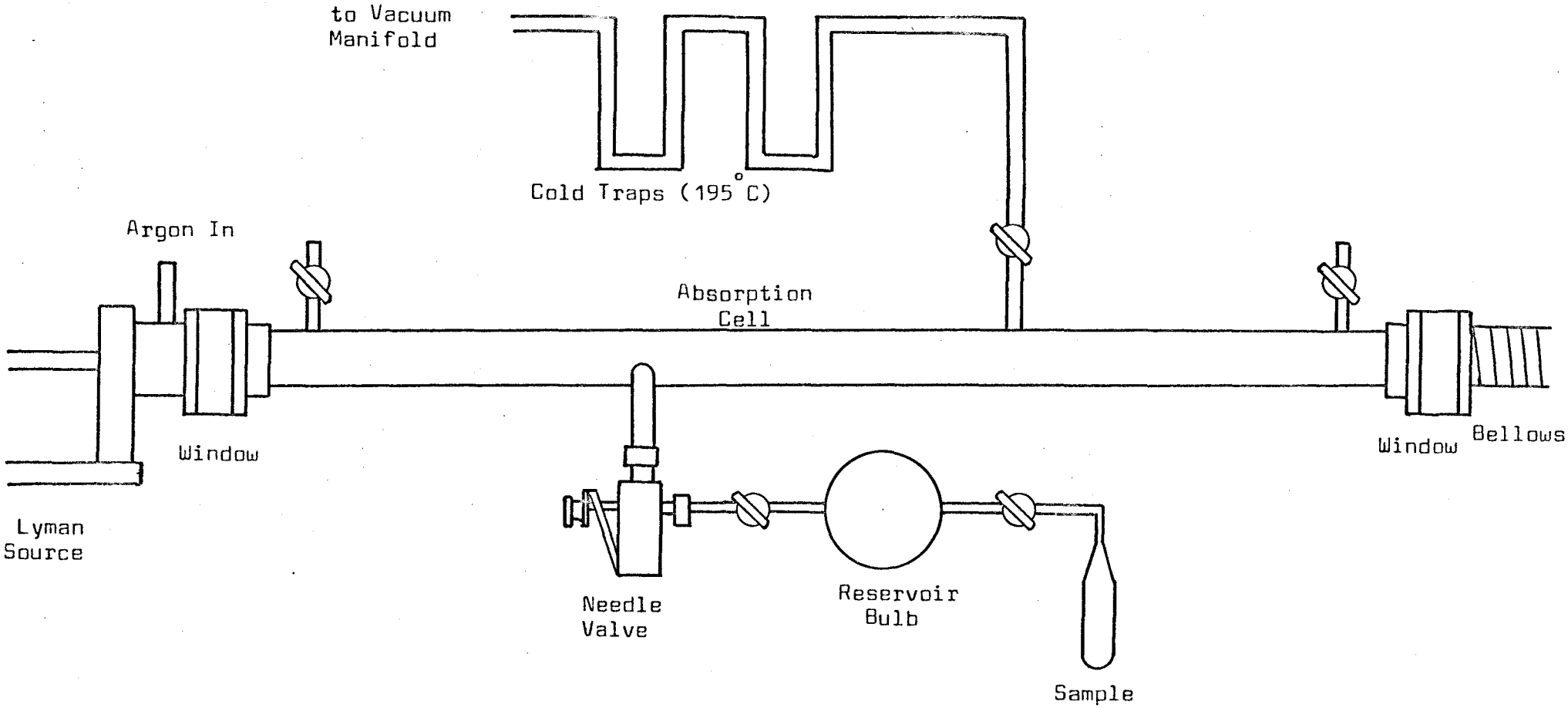

FIGURE 4.6: ABSORPTION CELL AND FLOW SYSTEM

advantage that the natural astigmatism of the spectrograph can be compensated for if the foregrating is placed at the vertical focus of the spectrograph. However, it is found that the order separation is not complete, the grating is damaged by "dirty" sources, and the reflectivity of the grating is not as high as is desirable.

The method chosen here for order separation is the use of a foreprism.[26] The foreprism used here is one-half of a lithium fluoride plano-convex cylindrical lens of radius of curvature 6.9 cm. As a lens, this allows the desired wavelength to be focussed on the slit of the spectrograph. The lens acts as a thin prism with an effective angle δ, and deviates a given wavelength through an angle which depends upon the wavelength and the value of δ.

The foreprism is mounted in a special holder shown in cross-section in Figure 3.2. This holder allows the foreprism to be moved in a direction that varies the effective prism angle without breaking the vacuum. This is a useful adjustment since it allows control over the amount of dispersion by the foreprism, which is necessary because the optimum value for δ is different for different orders. It is necessary to disperse the light sufficiently so that different orders do not overlap, but not so much that a full photographic plate is not covered by the wavelength range of light entering the spectrograph slit.

To allow focussing of the desired wavelength on the slit, a double screw assembly, which is also shown in Figure 3.2, is used. One end of this attaches to the slit chamber and the other end to the foreprism holder. Since this unit has a left hand thread on one piece and a right hand thread on the other, simply turning the central collar

allows the foreprism-to-slit distance to be varied. Again, this unit has O-ring seals so that this adjustment can be made without letting air into the slit chamber.

4.7 Mounting of the Absorption Cell and Lyman Source

The absorption cell is supported by standard optical fittings, and vacuum connections to the slit assembly and the Lyman source are made at each end by O-rings. The Lyman source is supported by optical stands which allow it to be moved both vertically and horizontally. These optical stands are mounted on a 1.5 m optical bench which is screwed to a length of channel iron. The front end of the channel iron is supported by a yoke pivoted about the position of the foreprism. The rear end is guided by two machined upright pieces of steel and is supported by a bearing on the end of a coarse screw. This coarse screw has a handle attached to the lower end and allows the end of the channel iron to be raised or lowered. These details are shown in Figure 4.7.

Since the front end of the optical bench supporting the absorption cell and Lyman source is pivoted about the foreprism position, lowering or raising the rear end of the bench varies the angle at which the incident light falls on the foreprism and, as a result of the dispersion of the prism, changes the wavelength of the light falling on the slit.

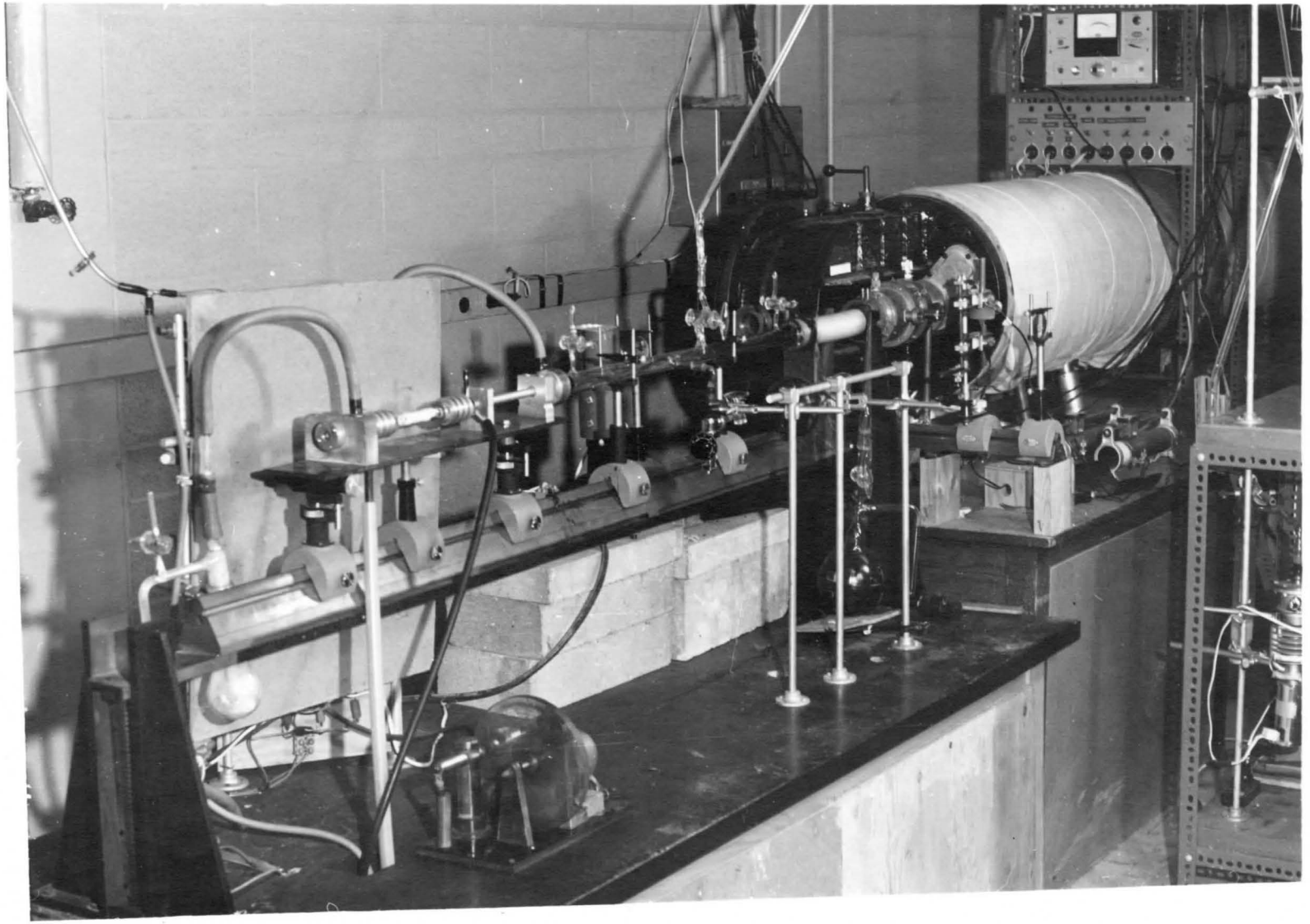

FIGURE 4.7

OVERALL VIEW OF VACUUM SPECTROGRAPH AND ASSOCIATED APPARATUS

CHAPTER 5

CALIBRATION OF APPARATUS

5.1 Calibration of Plate Tilt

As shown in Section 2.3, the grating equation for an off-plane Eagle mounting is

$$m\lambda_o = \left(1 + \frac{z_o^2}{R^2\cos^2\alpha_o}\right)^{-\frac{1}{2}} 2d \sin\alpha_o \qquad (2.14)$$

For this instrument, the constants are z_o = 7.5 cm, R = 665 cm, and d = 1/12000 cm = 8.33×10^{-5} cm, and so the equation is

$$m\lambda_o = \frac{(1.67 \times 10^4) \sin\alpha_o}{\left(1 + \frac{1.27 \times 10^{-4}}{\cos^2\alpha_o}\right)^{\frac{1}{2}}} \qquad (5.1)$$

for λ_o expressed in Å. To obtain α_o, this equation should be solved for the desired values of m and λ_o. However, the term $(1.27 \times 10^{-4})/\cos^2\alpha_o$ is very small, and so for the calculations here the simple grating equation

$$m\lambda_o = 2d \sin\alpha_o = (1.67 \times 10^4) \sin\alpha_o \qquad (5.2)$$

has been used. The difference between the values calculated from the two equations is less than 0.1%, and is negligible. Figure 5.1 shows a plot of α_o against $m\lambda_o$.

For measurement of α_o, a large protractor was attached to the plate rotation mechanism and adjusted to zero with the plate in a vertical position. During use of the spectrograph, it has been

found that setting the plate tilt angle to somewhat better than 1° has been sufficient to obtain good spectra.

5.2 Calibration of Grating Tilt

The grating tilt (rotation about the z axis of Figures 2.1 and 2.2) is controlled by rotation of a shaft from outside the vacuum chamber. The drive shaft is connected by a gear system to a Veeder counter which is used for calibration.

For the preliminary adjustments of the grating, a small tungsten lamp was placed before the slit, all but the middle portion of the slit being masked off. The grating tilt was adjusted so that the zeroth order (direct image) was reflected into the plate chamber. Then, the grating mount was rotated about a vertical axis (the y axis) until the image passed through the diaphragm placed before the plate. (This diaphragm is necessary since the spectrograph is astigmatic.) The grating tilt was changed until green light (about 5500 $\mathring{A}$) was visible at the plateholder. The grating was then "rolled" 180° about the normal to its centre (the x axis), and the image intensity compared with that before rolling. It was found that the intensity in one position was more than twice that in the other position, and so this position, i.e. the blaze side of the grating, was used thereafter.

The grating tilt was varied to pass the visible spectrum across the plate position. The grating was then rotated by small amounts about the normal to its centre until the whole visible spectrum passed through the same position on the plate when the grating was tilted to either side of the normal. This procedure ensures that the image for any intermediate setting of the grating tilt also passes through this

position.

For calibration of the grating tilt, the grating was illuminated by light from a mercury lamp, and the spectrum observed visually through the window on the plate chamber. The Veeder counter was set to 500 for the zeroth order. Then, the grating tilt was varied until one of the visible mercury lines was brought to the middle of the plateholder. The grating focus was next adjusted until the line was in focus at the plateholder as determined by use of the Foucault knife edge test,[30] and then a more accurate setting of the grating tilt that brought the line to the middle of the plateholder was recorded. Using this visual setting as a guide, a number of photographs of the line were taken for various settings of the grating focus and tilt controls until the best settings were obtained. For the photographs, the mercury lamp was excited by a microwave generator (2450 Mc/sec) run at low power to make the natural line width of the mercury lines a minimum. This procedure was repeated for a number of visible mercury lines.

Using the data obtained above, graphs of grating focus and tilt setting versus wavelength were plotted, and extrapolated to the ultraviolet. Using values obtained from these graphs as preliminary settings, the best values of the grating focus and tilt for various ultraviolet mercury lines were obtained photographically. At a later date, grating tilt settings for the first order below 2000 Å were obtained from the positions of known atomic absorption and emission lines. The calibration curve for the grating tilt counter is given in Figure 5.2.

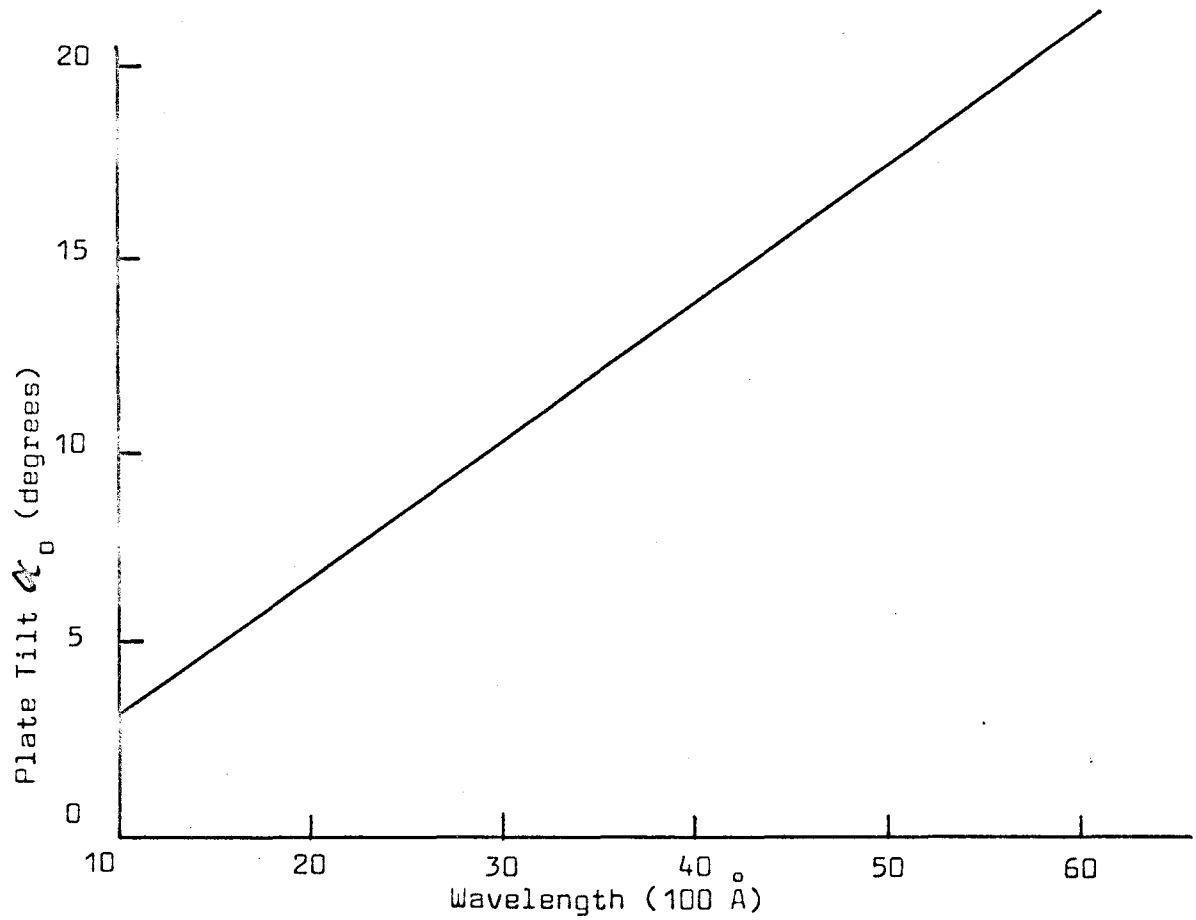

FIGURE 5.1: Plate Tilt Calibration Curve

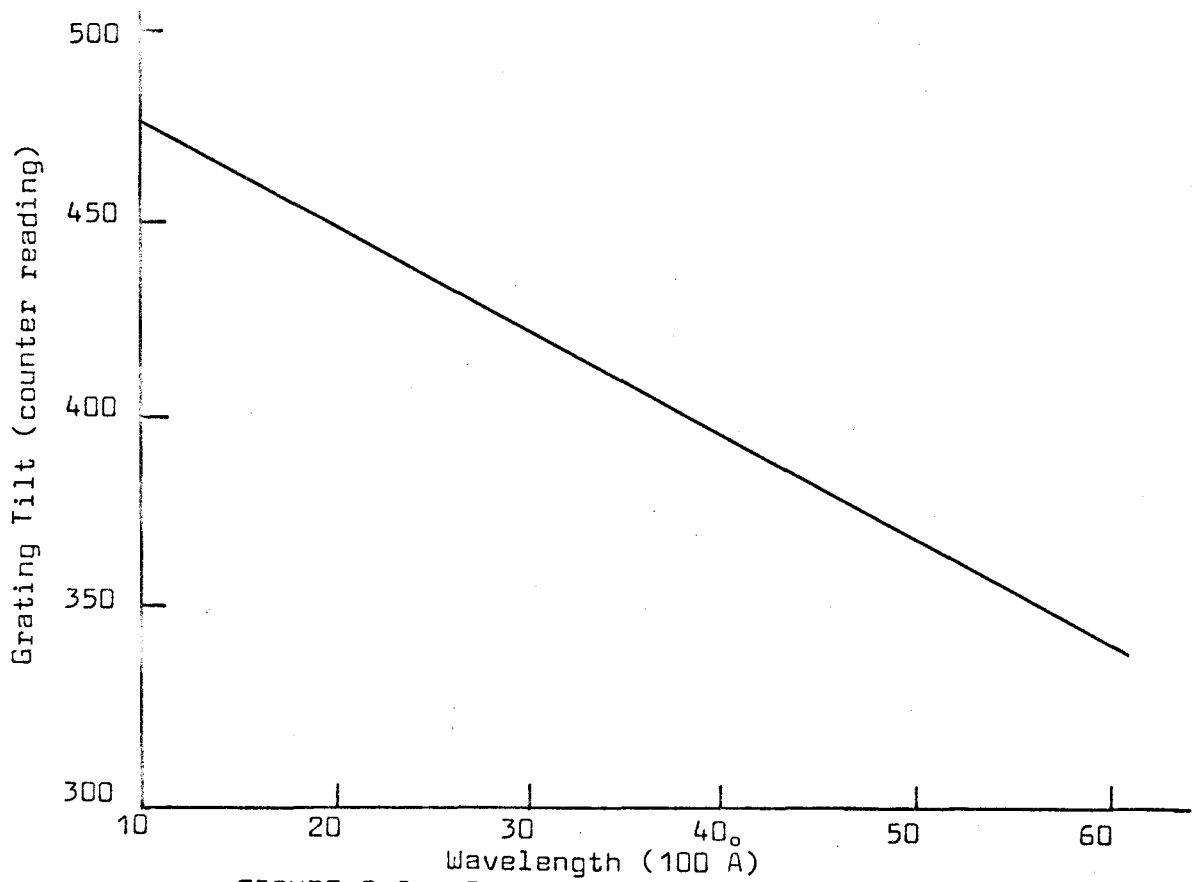

FIGURE 5.2: Grating Tilt Calibration Curve

5.3 Calibration of Grating Focus

In the off-plane Eagle mounting, the angle of incidence α_o is equal to the angle of diffraction β_o, so that it is clear from Equation 2.11 that the distance r from the slit to the grating is equal to the distance r' from the grating to the plate. A view of the grating mounting in which the slit and plate have been projected onto the Rowland circle is given in Figure 5.3. From this it is easily seen that the distance r" from the grating to the plane of the slit and plate is given by

$$r'' = R\cos\alpha_o \tag{5.3}$$

Using the simple grating Equation 5.1.2 and the constants for this spectrograph, r" in cm is given by

$$r'' = 399.0\ (2.778 - m^2\lambda_o^2 \times 10^{-8})^{1/2} \tag{5.4}$$

for λ_o expressed in Å.

Since the length of the rods on which the grating carriage rides restricts the focussing movement of the grating to 45.5 cm, it is not possible to cover all wavelengths in all orders for a particular setting of the grating mount. As a compromise, it was decided that the lowest first order wavelength that could be reached in focus would be 1200 Å. From Equation 5.4, it is seen that the maximum distance from the grating to the plane of the slit and plate should then be r"(1200) = 66.5 cm. Since it is not convenient to measure this distance, the following procedure was used to position the grating mount correctly. The grating was adjusted so that the Hg 5460.7 Å line was in focus at the middle of the plate. From equation 5.4, it is found that r"(5460.7) = 628.5 cm. Thus, the distance from the back of the grating mount to

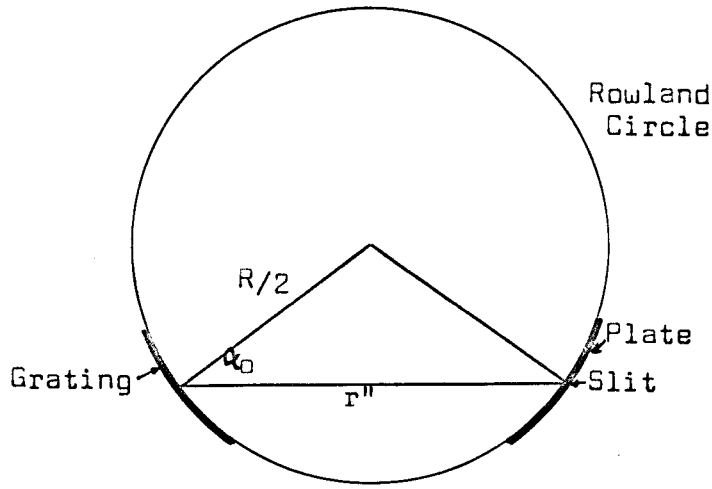

FIGURE 5.3

ROWLAND CIRCLE PROJECTION OF THE OFF-PLANE EAGLE VACUUM SPECTROGRAPH

TABLE 5.1

WAVELENGTH RANGE OF THE VACUUM SPECTROGRAPH IN VARIOUS ORDERS

m	λ_o(min), Å	λ_o(max), Å
1	1400	6200
2	700	3100
3	470	2100
4	350	1550

the grating holder should be 663.5 - 628.5 = 35.0 cm. After the relative positions of the grating carriage and mount were changed to satisfy the above conditions approximately, it was found by refocussing the Hg 5460.7 Å line that r"(max) = 662.6 cm and r"(min) = 617.1 cm. Under these conditions, the wavelength ranges in the various orders are as shown in Table 5.1.

When the grating carriage was positioned, an attempt was made to adjust the two rods on which the grating mount rides so that the grating mount was level from side to side and from front to back over the whole motion of the grating mount. But, it was not possible to do this with any accuracy. Thus, there is some motion of the image as the grating focus is changed. However, this should not cause any trouble since the calibration and alignment procedures will take this into account.

The grating focus control has been brought outside the vacuum vessel and connected to a Veeder counter in the same way as described for the grating tilt control. The Veeder counter was set to zero for the grating as far from the slit and plate as possible. The grating focus settings for the various mercury lines were actually determined at the same time as the grating tilt controls, as described in the previous section. The Veeder counter readings were plotted against $m\lambda_0$ to give a calibration curve.

For use in the first order, it was necessary to extrapolate the grating focus calibration curve beyond the calibrated region. Since the graph is curved, the following procedure was used for the extrapolation. The distance r" from the grating to the plane of the

slit and plate was calculated from Equation 5.4 for each mercury line used in the calibration. Then, the observed Veeder counter reading C was plotted against r". As expected, this plot was linear, and so it was assumed that the two variables are related by an equation of the form

$$C = k_1 r'' + k_2 \qquad (5.5)$$

and the constants k_1 and k_2 were determined from the plot. After substitution of Equation 5.4 for r", the following equation was obtained.

$$C = 31{,}162\ (2.778 - m^2 \lambda_o^2 \times 10^{-8})^{\frac{1}{2}} + 51{,}709 \qquad (5.6)$$

This was used to obtain the calibration curve shown in Figure 5.4.

5.4 Calculation of the Slit Width

The criterion for this calculation was that the optimum slit width should be equal to the smallest wavelength difference that can be resolved. Using the grating Equation 5.2, together with the equation

$$R = \frac{\lambda}{d\lambda} = \frac{mW}{d} \qquad (5.7)$$

which gives the resolving power of a grating as a function of the order m, the grating width W, and the grating spacing d, it can be shown that the slit width $d\ell$ is given by

$$d\ell = \frac{2dR}{mW} \tan \alpha_o = 84\ \frac{\tan \alpha_o}{m} \text{ microns} \qquad (5.8)$$

For the wavelength regions in the vacuum ultraviolet accessible in the various orders, this equation gives slit widths between 5 and 10 microns. However, slit widths as small as this are not practical in the vacuum

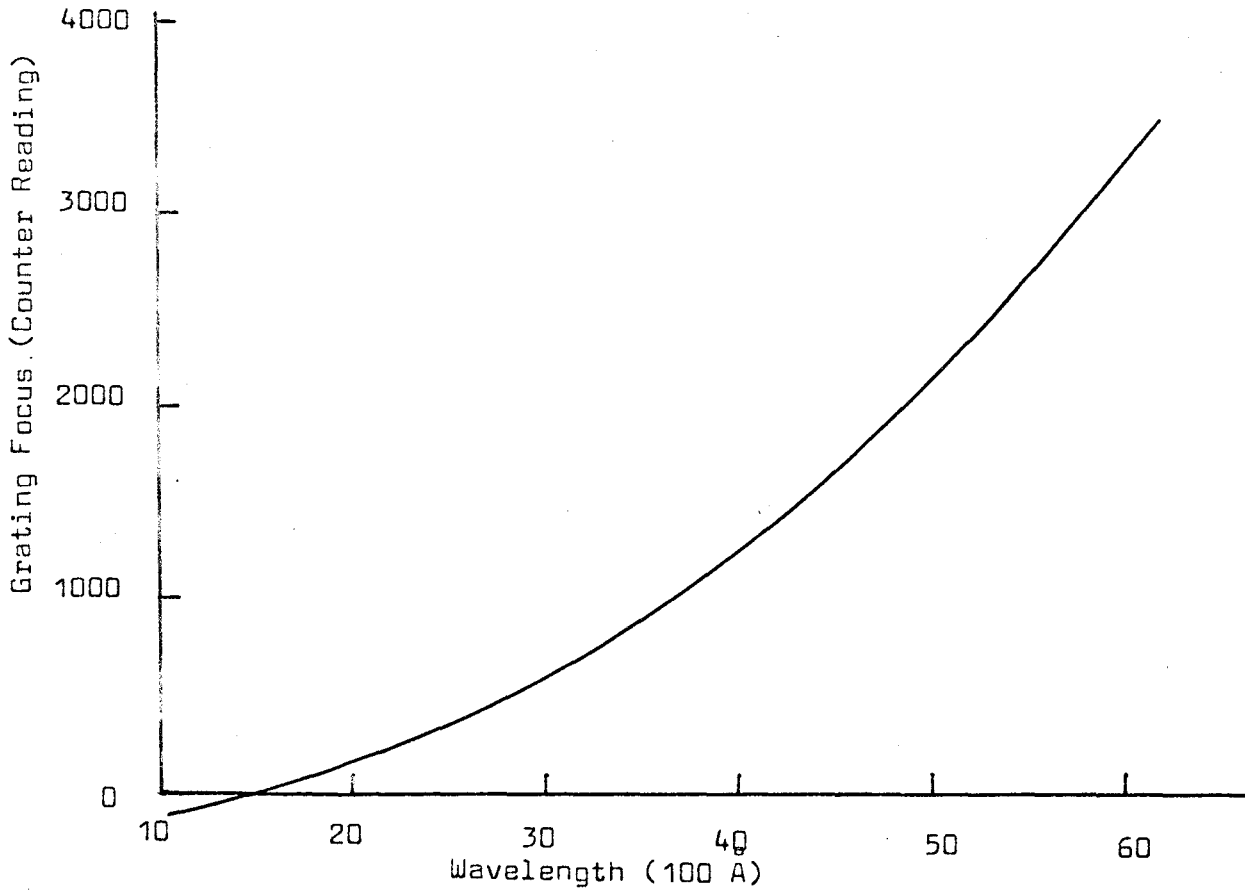

Figure 5.4: Grating Focus Calibration Curve

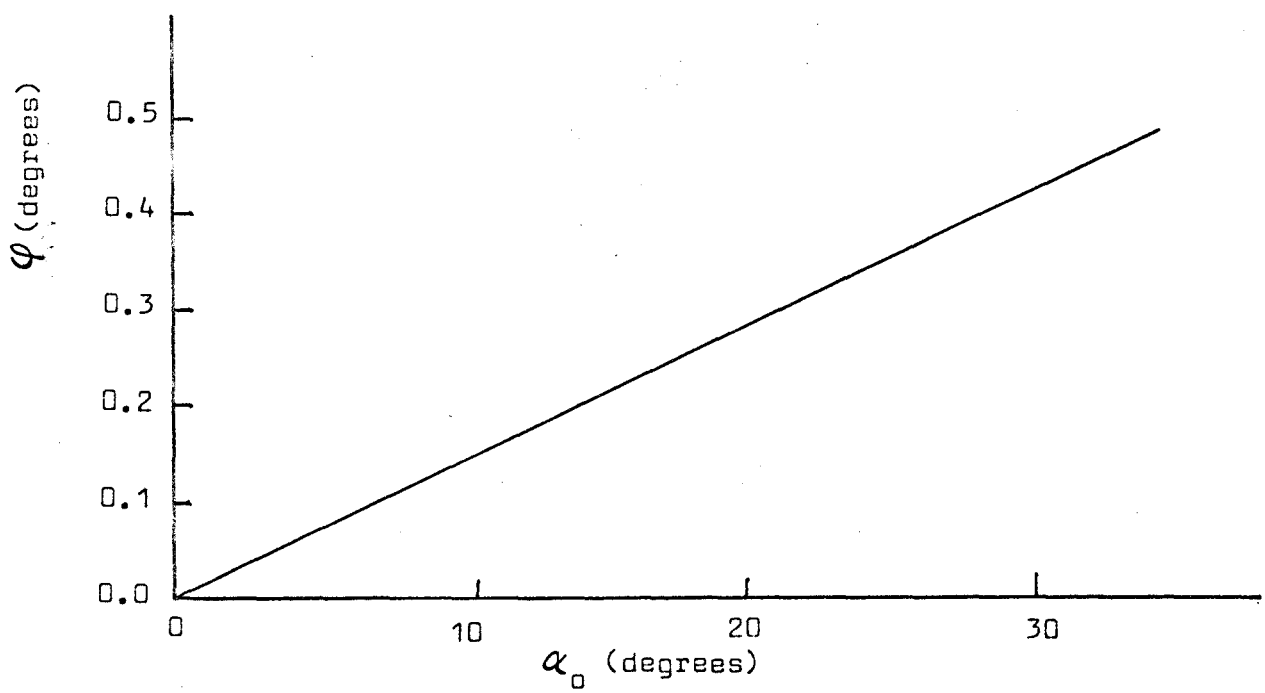

Figure 5.5: Slit Rotation Angle φ Versus Angle of Incidence α_0

ultraviolet for two main reasons. First, the grain size of the photographic plates used is larger than this (about 14 microns), and second, the intensity of most light sources is too low to use such a small slit. The slit widths used were set empirically, being quite large for low resolution pictures, and as small as convenient for higher resolution pictures.

5.5 Adjustment of the Slit Rotation

For a given angle of incidence, the angle between the direction of the grating rulings and the length of the slit is given by Equation 2.12. Since this angle cannot be measured directly, the following procedure was used in setting it. The grating was illuminated by light from a mercury lamp excited by a microwave generator run at a low power level in order to keep the natural line width as small as possible. The controls for the grating focus, grating tilt, plate tilt, and slit width were set to the correct values for the Hg 4358.4 Å line. Then, a series of exposures were taken as the slit was rotated by small amounts about the optic axis. The angle of rotation was finally set to that which gave the best resolution of the hyperfine structure of the Hg 4358.4 Å line. A photograph of this line is shown in Chapter 6.

Substituting the constants for this spectrograph (z_o = 7.5 cm, R = 665 cm) in Equation 2.12 gives Equation 5.9, which is plotted in Figure 5.5.

$$\varphi = 0.0113 \tan\alpha_o \sec\alpha_o \qquad (5.9)$$

As can be seen, the angle of slit rotation φ is a slowly varying

function of the angle of incidence α_o. Over the range of angles of incidence likely to be used for high resolution studies (roughly 12° to 22°), φ varies only from 0.14° to 0.28°, and so it is not necessary to change φ unless the highest resolution is required.

5.6 Calibration of the Predispersion Unit as a Lens

As mentioned before, the predisperser is simply half of a plano-convex cylindrical lens of radius of curvature 6.9 cm made from lithium fluoride. As a lens, it can be used to focus the light from the Lyman source on the slit of the spectrograph. Because it is a cylindrical lens, it will image a point as a line, but since the spectrograph is astigmatic this is useful, as it is necessary to illuminate a certain length of slit to get a uniform intensity over the required image size on the plate.

The focal length f of a plano-convex lens at any wavelength λ, where the refractive index of lithium fluoride is n, is given by [28]

$$f = \frac{r}{n - 1} = \frac{6.9}{n - 1} \text{ cm} \qquad (5.10)$$

The image distance p for any object distance q may be calculated simply from the thin lens equation[29]

$$\frac{1}{f} = \frac{1}{p} + \frac{1}{q} \qquad (5.11)$$

For this apparatus, the distance q from the source to the lens is not constant, since as the lens is moved to bring the desired wavelength into focus at the slit (p varied), q also varies because the position of the Lyman source is fixed. However, the value of q is quite large (about 136 cm) and variation is only about ± 3 cm at most. Using the

constant value of 136 cm for q, values of p for various wavelengths were calculated. On the basis of the variation of the values calculated for p, a refined source-to-lens distance q' was calculated for each wavelength as given by

$$q' = q + (p_{av} - p) \tag{5.12}$$

where p_{av} is the average value of p over the range. Using this value q', a new lens-to-image distance p' was calculated for each wavelength using Equation 5.11. It was found that the values for p and p' at each wavelength agreed to within 0.05 cm, and so this was not considered further. The variation of the lens-to-image distance with wavelength is shown in Figure 5.6.

The lens-to-slit distance is varied by the double-screw mechanism described previously. As can be seen from Figure 3.2, the length of this is just part of the total lens-to-slit distance. The length of the other parts was measured to be 11.0 cm, and so the actual setting P of the focal adjuster is

$$P = p' - 11.0 \text{ cm} \tag{5.13}$$

5.7 Calibration of the Predispersion Unit as a Prism

Since the predisperser is half a cylindrical lens, it acts as a prism as well as a lens. The lens has an effective prism angle δ depending upon the section of the lens that is used. As described previously, provision has been made for varying δ. Since the prism is thin, the thin prism equation[27]

$$\theta = (n - 1)\delta \tag{5.14}$$

may be used to calculate the angle θ through which the prism deviates light of wavelength λ at which the refractive index of lithium fluoride is n.

Calibration of the prism is quite simple. By measuring the amount of deviation d of light of wavelength λ at a distance ℓ from the prism, it is possible to calculate θ as

$$\theta = \frac{\ell}{d} \tag{5.15}$$

and thus

$$\delta = \frac{\theta}{n - 1} = \frac{\ell}{d(n - 1)} \tag{5.16}$$

Using this value for δ, it is possible to calculate the angle and amount of deviation for any other wavelength.

5.8 General Alignment Procedure

The grating focus control is set depending upon the wavelength and order that is to be used, and the lens-to-slit distance is set according to the wavelength. The grating tilt is usually set for the green (counter setting about 360) since the eye is most sensitive to it. Then, with the plateholder removed, but the plate diaphragm in position, light from a 12 volt bulb, permanently positioned for alignment purposes, is shone through the alignment window and the plate diaphragm to the grating and is reflected back through the slit and predispersion unit. The angle of the prism is set to give roughly the amount of dispersion required, and then with the cell removed, the predispersion unit is rotated about the light beam until a sharp image is formed. The angle of the optical bench supporting the cell and

source is then adjusted by means of the screw mechanism so that the light beam passes through the front centre of the Lyman source, which is placed in the position that it will occupy after the cell is in place. With the capillary out, the source is then adjusted so that the light beam passes along the axis of the electrodes.

Next, the cell and windows are put in position and the alignment checked. The capillary is then inserted, and the source adjusted slightly so that the maximum intensity passes through the capillary opening.

As described in Section 5.7, it is now possible to calculate δ, and so the value of θ and d for the wavelength desired. Because the setting calculated this way is usually not the optimum one, it is necessary to take a few trial exposures on one plate at various values of d, to find the best setting. Once this has been done, the d for any other wavelength can be easily calculated.

As mentioned before, it is possible to change δ depending upon the amount of dispersion required. For each value of δ, it is necessary to recalibrate the foreprism. Also, it is necessary to realign the optics after a new capillary is inserted, to get the maximum intensity.

CHAPTER 6

TESTS OF THE APPARATUS

6.1 The Vacuum System

The pumps employed will evacuate the 520 litre volume of the spectrograph from atmospheric pressure to less than 10^{-3} mm in about 1 hour. Pumping overnight outgasses the system and gives an ultimate vacuum of approximately 2×10^{-5} mm.

The majority of the spectrograph is quite leak free, the only significant leaks being in the plate chamber. Figure 6.1 shows the pressure versus time for the isolated system. As the graph is close to a straight line, the pressure rise is chiefly due to leakage, the leak rate being about 0.28 microns/min. This leakage is slightly inconvenient since it makes it impossible to shut off the pumps for long exposures. With the pumps running, there is a slight broadening of the spectral lines due to the vibrations of the pumps, although it has been attempted to minimize this by mounting the rotary pump on shock absorbers and having bellows in the connections between the rotary pump and the spectrograph.

6.2 The Lyman Source

A Lyman source emits radiation from roughly 500 to 7000 Å. The intensity of the radiation decreases with decreasing wavelength, thus making order separation very important when using high orders of the grating.

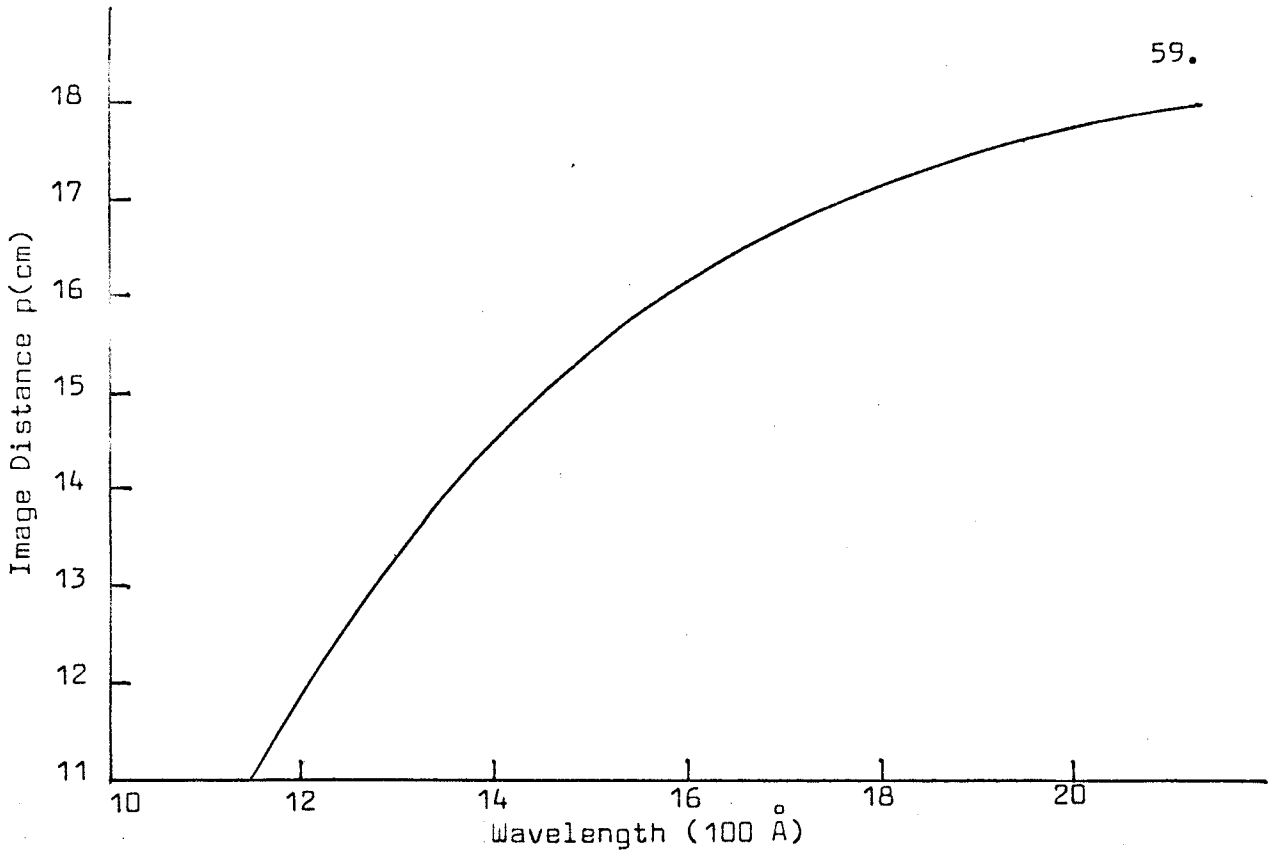

Figure 5.6: Image Distance p versus Wavelength for Lithium Fluoride Fore-prism

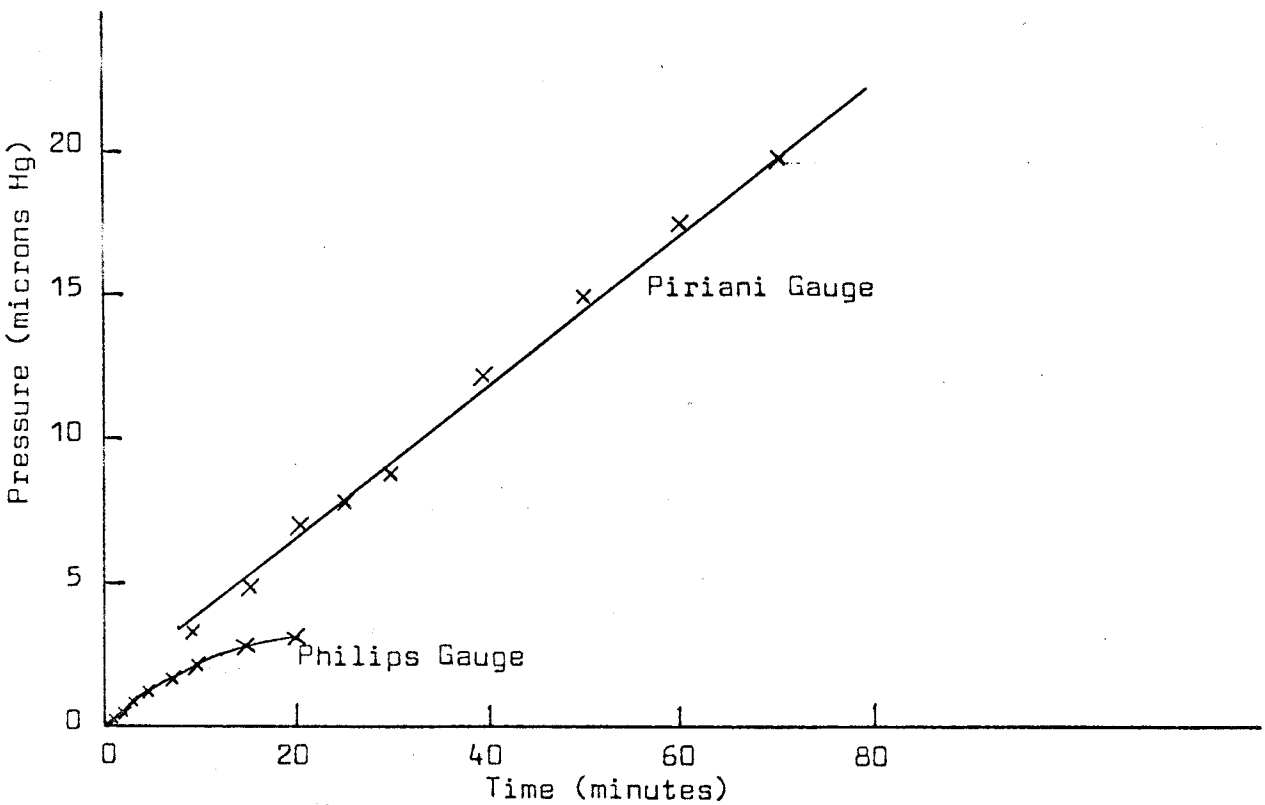

Figure 6.1: Leak Rate of Vacuum Spectrograph

The discharge profile for the Lyman source has been observed using a voltage divider and oscilloscope, as shown in Figure 6.2.a. The profile, which is given in Figure 6.2.b, shows that the discharge takes somewhat more than 100 μsec, which is rather long. If this were shortened, the performance of the Lyman source would be improved considerably. However, to do this, it is necessary to reduce the inductance of the discharge circuit, and since most of the inductance is in the capacitors, this is not possible unless special low inductance capacitors are used. The discharge profile also allows an estimate of 17 kV to be made for the peak voltage of the discharge.

6.3 Resolution Tests

No attempt has been made to measure the resolution since this is a difficult and controversial task. However, spectra of some atomic lines and molecular bands have been taken to compare with those in the literature.

Figure 6.3 shows a first order photograph of the Hg 4358.4 Å line, taken as described in Section 5.5, in which partial resolution of the hyperfine structure has been attained. From this picture, it can be estimated that the resolving power in the first order is at least 100,000 (theoretical resolving power in first order is 158,400).

Figure 6.3 shows a photograph of some of the oxygen Schumann-Runge bands taken in the third order of the spectrograph. This photograph seems to be of the same quality as those in the recent literature.[3,8]

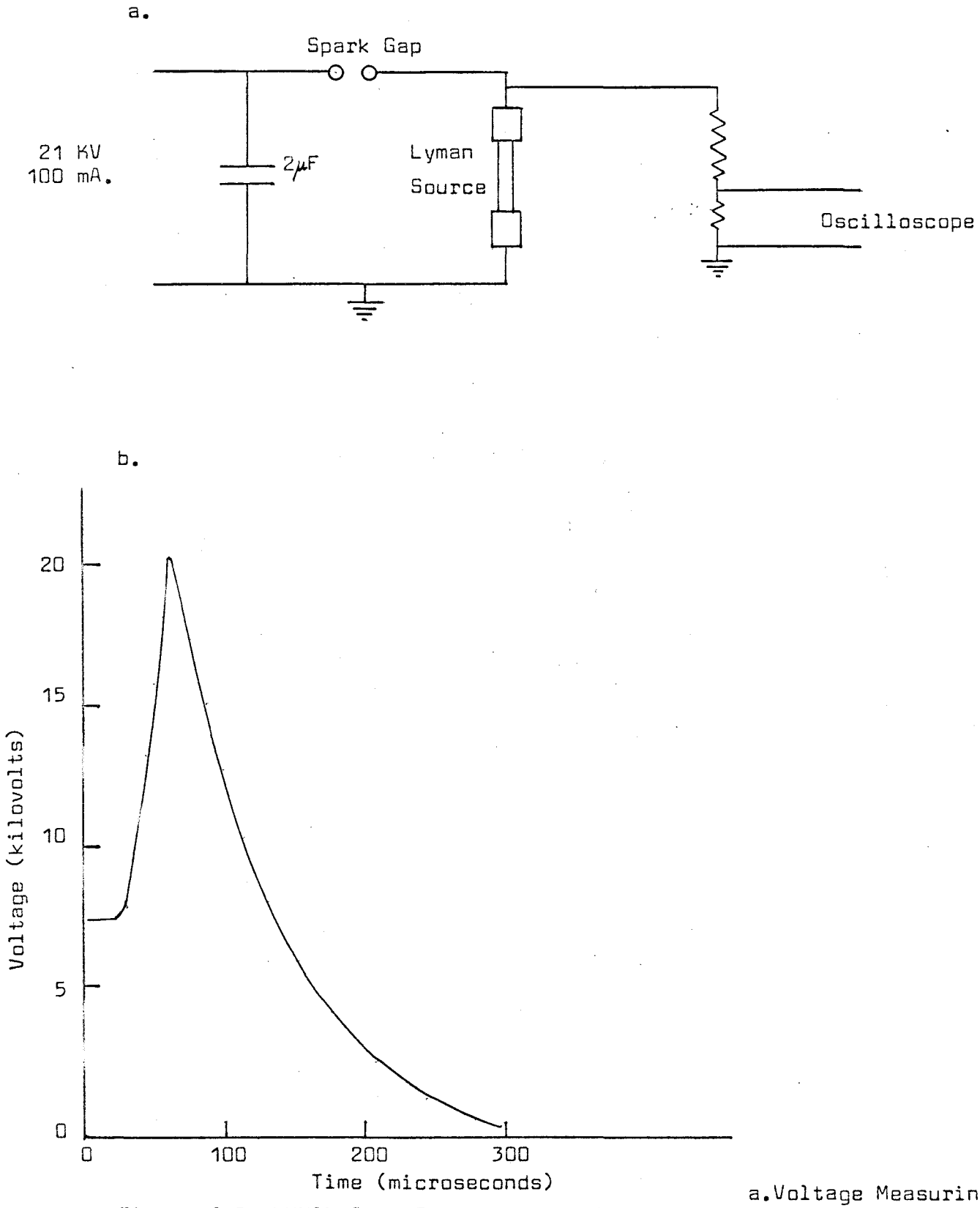

Figure 6.2: LYMAN SOURCE CIRCUIT CHARACTERISTICS

a. Voltage Measuring Circuit
b. Voltage versus time

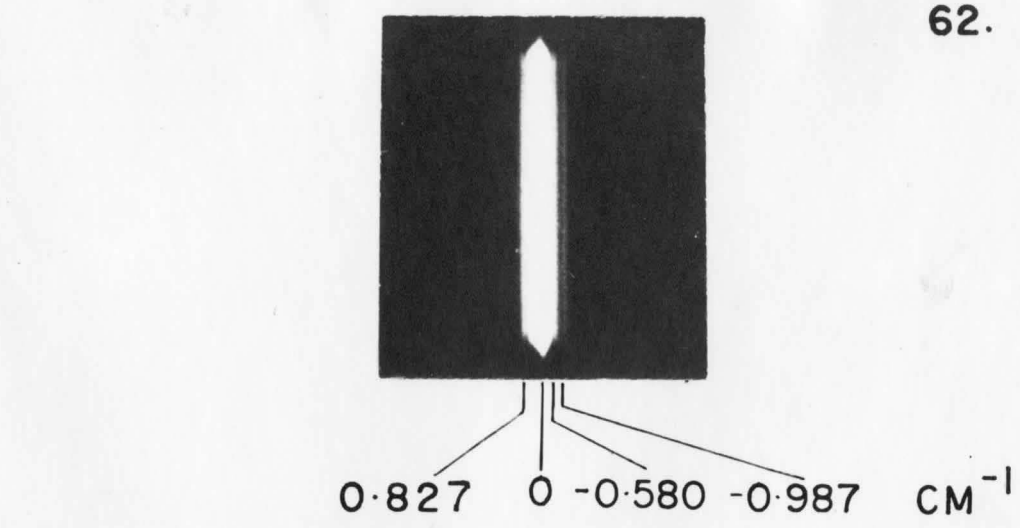

Hg 4358 Å

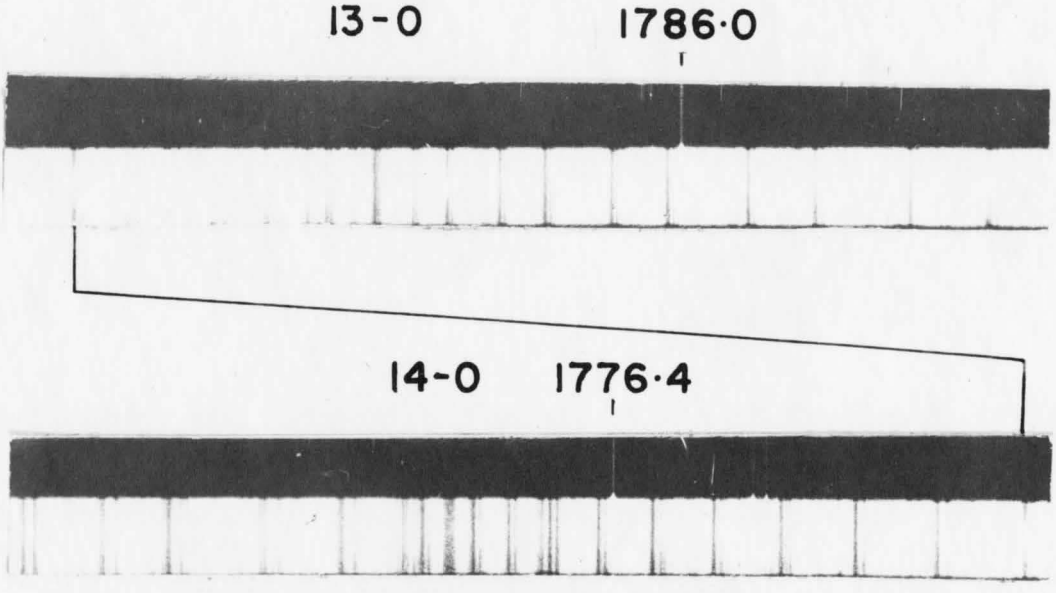

O_2 SCHUMANN-RUNGE

FIGURE 6·3

PART II

THE ELECTRONIC SPECTRA OF THE CYANOGEN HALIDES

Scope of Part II

The off-plane Eagle vacuum spectrograph and associated apparatus which are described in Part I of this thesis have been used to observe the electronic spectra in the vacuum ultraviolet of cyanogen iodide, cyanogen bromide, and cyanogen chloride. Cyanogen fluoride was not studied because its preparation and purification are very difficult and attempts to obtain samples, both privately and commercially, were unsuccessful.

After a short review of previous work on the cyanogen halides, the methods used to observe the electronic spectra of the cyanogen halides are described. The theory necessary to interpret the spectra is presented and then the spectra are described, analyzed, and assigned to specific electronic transitions. For the two electronic spectra of each molecule which show extended vibrational structure, vibrational analyses are given and the molecular structure in each of the excited states is determined by use of the Franck-Condon principle in a quantitative form. The shorter wavelength absorption observed for cyanogen iodide and cyanogen bromide is assigned to Rydberg transitions and estimates of the two lowest ionization potentials are made. The coupling of angular momenta in the Rydberg states is discussed and estimates of the spin-orbit coupling constants for the monopositive molecular ions are given.

CHAPTER 7

INTRODUCTION TO THE SPECTROSCOPIC PROBLEM

7.1 Separation of the Wave Equation

In general, the forces acting between molecules in the vapour phase are negligible, and so each molecule may be treated as an isolated entity. Thus, if translation of the molecule and electron and nuclear spin are neglected, the quantum mechanical Hamiltonian operator $\mathcal{H}$ for the molecule may be expressed as the sum of the kinetic energy operators for the electrons and nuclei plus the potential energy of the electrostatic interactions between all pairs of particles in the molecule. If the mass and coordinates of the electrons are given subscripts i, j, ... and those of the nuclei are given subscripts α, β, ..., the Hamiltonian may be written

$$\mathcal{H} = -\sum_i \frac{\hbar^2}{2m_i}\nabla_i^2 - \sum_\alpha \frac{\hbar^2}{2M_\alpha}\nabla_\alpha^2 - \sum_{\alpha,i} \frac{Z_\alpha e^2}{r_{\alpha i}} + \sum_{i>j} \frac{e^2}{r_{ij}} + \sum_{\alpha>\beta} \frac{Z_\alpha Z_\beta e^2}{r_{\alpha\beta}} \qquad (7.1)$$

In this equation $\hbar$ is Planck's constant h divided by 2π, m_i and M_α are the masses of electron i and nucleus α, respectively, ∇^2 is the Laplacian operator, Z_α is the atomic number of nucleus α, e is the absolute value of the electronic charge, and r_{pq} is the distance between particles p and q.

The Hamiltonian operator $\mathcal{H}$ has eigenfunctions $\Psi_T(r,R)$ and eigenvalues E_T, where r and R represent collectively the coordinates

of all electrons and nuclei, respectively. The eigenfunctions $\Psi_T(r,R)$ are solutions of the wave equation

$$\mathcal{H}\,\Psi_T(r,R) = E_T\,\Psi_T(r,R) \tag{7.2}$$

and describe stationary states of the molecule.

In order to simplify the treatment of molecular systems, it is usual to separate the wave equation into an electronic part and a nuclear part in the manner first given by Born and Oppenheimer.[31] Classically, the separability assumption is justified by the fact that the electrons, because of their much smaller mass, move very much faster than the nuclei and so adapt almost instantaneously to the nuclear configuration. Therefore, the electronic part of the problem can be solved independently for each nuclear configuration. Quantum mechanically, the Born-Oppenheimer approximation states that the wave function $\Psi_T(r,R)$ may be expressed as the product

$$\Psi_T(r,R) = \psi_E(r,R)\,\psi_N(R) \tag{7.3}$$

where $\psi_N(R)$ is a function of the nuclear coordinates alone and $\psi_E(r,R)$ is a function of the coordinates of both the electrons and the nuclei. For fixed nuclei, the electronic Hamiltonian $\mathcal{H}_E$ is

$$\mathcal{H}_E = -\sum_i \frac{\hbar^2}{2m_i}\nabla_i^2 - \sum_{\alpha,i}\frac{Z_\alpha e^2}{r_{\alpha i}} + \sum_{i>j}\frac{e^2}{r_{ij}} \tag{7.4}$$

The functions $\psi_E(r,R)$ are defined to be eigenfunctions of $\mathcal{H}_E$, that is,

$$\mathcal{H}_E\,\psi_E(r,R) = E_E\,\psi_E(r,R) \tag{7.5}$$

Substitution of Equation 7.3 into Equation 7.2 leads to an equation

with terms coupling $\psi_E(r,R)$ and $\psi_N(R)$. It can be shown that in general these cross-terms are very small (in the order of m_i/M_α). If these cross-terms are neglected and use is made of Equation 7.5, the following wave equation can be derived.[32]

$$(\mathcal{H}_N + E_E)\,\psi_N(R) = E_T\,\psi_N(R) \tag{7.6}$$

$\mathcal{H}_N$ is the nuclear Hamiltonian and is defined by the equation

$$\mathcal{H}_N = -\sum_\alpha \frac{\hbar^2}{2M_\alpha}\nabla_\alpha^2 + \sum_{\alpha>\beta} \frac{Z_\alpha Z_\beta e^2}{r_{\alpha\beta}} \tag{7.7}$$

The wave equation has now been separated into an electronic part containing the nuclear coordinates R as parameters, and a nuclear part containing the electronic energy E_E as part of its potential field.

For each electronic state, the electronic energy E_E has a minimum value, usually denoted E_e, when the nuclei are in their equilibrium positions for that electronic state. The nuclear energy E_N for each electronic state is usually expressed relative to E_e, so that the total energy E_T is

$$E_T = E_e + E_N \tag{7.8}$$

The nuclear wave function $\psi_N(R)$ describes both the vibrational and rotational motions of a molecule in a given electronic state. Since the vibration and rotation of a molecule are independent to a first (rigid rotor) approximation,[33] it is possible to express $\psi_N(R)$ as the product

$$\psi_N(R) = \psi_V(Q)\,\psi_R(\theta,\phi,\chi) \tag{7.9}$$

where $\psi_V(Q)$ is the vibrational wave function which depends upon all the normal coordinates Q of a molecule except those for translation, which we can ignore here, and $\psi_R(\theta,\phi,\chi)$ is the rotational wave function which depends upon the Eulerian angles θ, ϕ, χ. If the vibrational energy is written E_V and the rotational energy is written E_R, then the nuclear energy E_N is the sum

$$E_N = E_V + E_R \tag{7.10}$$

Use of the Born-Oppenheimer and rigid rotor approximations makes it possible to express the total wave function as the product, and the total energy as the sum, of components due to electronic, vibrational, and rotational motion.

$$\Psi_T(r,R) = \psi_e(r,R)\,\psi_V(Q)\,\psi_R(\theta,\phi,\chi) \tag{7.11}$$

$$E_T = E_e + E_V + E_R \tag{7.12}$$

If small interactions occur among these three components, it is possible to treat them by perturbation theory. However, if the interactions are large, as in the Renner and Jahn-Teller effects, the above approximations are no longer valid.

7.2 Spectroscopic Transitions

By the use of time dependent perturbation theory,[34] it can be shown that the probability of an electric dipole transition between an upper state having total wave function Ψ_T' and a lower state having total wave function Ψ_T'' is proportional to the square of the transition

moment $\vec{R}$, defined by the equation

$$\vec{R} = \int \Psi_T'^{*} \vec{\mu} \Psi_T'' \, d\tau \qquad (7.13)$$

where $d\tau$ indicates an element of coordinate space, and $\vec{\mu}$ is the electric dipole moment operator given by

$$\vec{\mu} = \vec{i}\,\mu_x + \vec{j}\,\mu_y + \vec{k}\,\mu_z \qquad (7.14)$$

In this equation, $\vec{i}$, $\vec{j}$, and $\vec{k}$ are the unit vectors along the x, y, and z Cartesian axes and μ_x, μ_y, and μ_z are defined in terms of the charge q_i at the point (x_i, y_i, z_i) by the equations

$$\mu_x = \sum_i q_i x_i, \qquad \mu_y = \sum_i q_i y_i, \qquad \mu_z = \sum_i q_i z_i \qquad (7.15)$$

Only electric dipole transitions will be considered here since magnetic dipole and electric quadrupole transitions are usually weaker by factors of approximately 10^{-5} and 10^{-7}, respectively, and are not encountered in this work.

The application of group theory to the transition moment $\vec{R}$ to derive symmetry selection rules, and the intensity distribution in progressions of vibrational bands of an electronic transition will be considered in more detail in later chapters.

The unit of energy used in most spectroscopic work is the wavenumber (cm^{-1}), given here the symbol σ. For a transition between an upper state and a lower state having total energy eigenvalues E_T' and E_T'', respectively, the wavenumber of the absorbed or emitted quantum of electromagnetic radiation is given by

$$\sigma = \frac{E_T' - E_T''}{hc} \qquad (7.16)$$

where h is Planck's constant and c is the velocity of light.

Molecular spectra are normally divided into three quite different classes. Pure rotation spectra result from transitions between rotational levels associated with one vibrational level (usually the vibrationless level or a low-lying vibrational level of the ground electronic state) and are observed in the microwave region (0.1-10 cm^{-1}). Since microwave spectroscopy is not only very accurate but also feasible at low molecular concentrations, measurements can easily be made for several isotopes of a molecule and very accurate structural data for vapour phase molecules may be obtained.

Transitions between different vibrational levels of the ground electronic state are observed in the region 50-4000 cm^{-1} by infrared and Raman spectroscopy. Changes in rotational energy occur in each vibrational transition and give rise to rotational fine structure accompanying each band. Infrared and Raman investigations give the fundamental vibrational frequencies for the molecule in the ground state and can give the molecular structure for various vibrational levels if the rotational fine structure is resolved.

Electronic excitation causes spectra which normally fall in the visible and ultraviolet regions (10,000-100,000 cm^{-1}). In each electronic transition there may be accompanying changes in vibrational energy which result in vibrational bands, each of which is composed of rotational fine structure. It will be shown in Chapter 9 that analysis of the vibrational band structure of an electronic spectrum can lead to qualitative or quantitative information about the molecular structure in the electronically excited state. If analysis of the rotational

fine structure is possible, very accurate molecular dimensions in the electronically excited state can be determined.

7.3 Previous Structural Studies of the Cyanogen Halides

In this thesis, an investigation of the electronic spectra of cyanogen iodide, cyanogen bromide and cyanogen chloride is described. Consequently, this literature survey will be restricted to these three compounds, although the preparation[35] of cyanogen fluoride has been reported, and its microwave[36] and infrared[37,38] spectra have been studied.

In agreement with the predictions of simple molecular orbital theory,[39] all the structural studies of the cyanogen halides have shown that they are linear molecules belonging to the $C_{\infty v}$ point group in the ground electronic state.

7.3.1 Microwave Studies

The microwave spectra of the cyanogen halides have been investigated many times;[36,40-44] several isotopes have been studied for each molecule and very accurate values for the molecular constants in the ground state have been determined. The quantities of primary interest here are the internuclear distances. However, there are several expressions for the internuclear distances that are commonly used in the literature and it is necessary to distinguish between these.

Internuclear distances are most commonly calculated from the moments of inertia for the molecule in the vibrationless level and these are denoted r_0. Because of anharmonicity in the potential function, the r_0 values differ from the internuclear distances r_e for

the hypothetical case when the molecule is at the minimum of the potential surface. The r_e values are the most useful since they are independent of the isotopic composition of the molecule.[106] But, they can be calculated by extrapolation only for the few cases where the variation of the moments of inertia when the different vibrations are excited has been determined. In order to obtain internuclear distances which are less dependent on the isotopes of the atoms in the molecule than r_o values, the two following types of internuclear distances are sometimes used. Substitution internuclear distances r_s can be calculated if a number of the nuclei in the molecule have more than one isotope for which the moments of inertia of the molecule can be determined.[107] Average internuclear distances $\langle r \rangle$ can be calculated by applying a correction for the harmonic part of the vibrational motion to the moments of inertia for the vibrationless level.[108] There will be differences between these various expressions for the internuclear distances, but in general, the differences will be less than ± 0.01 Å.

The two most recent microwave studies of the cyanogen halides are by Lafferty, Lide and Toth[44] for cyanogen chloride and by Tyler and Sheridan[36] for cyanogen chloride, cyanogen bromide and cyanogen iodide. The former authors give r_o, r_e and $\langle r \rangle$ values for the two bonds in cyanogen chloride and the latter authors r_s values for the bond lengths of all three molecules. Comparison of the values of r_o, r_e, r_s and $\langle r \rangle$ for cyanogen chloride shows that all four of these quantities for each bond agree to within ± 0.005 Å. Tyler and Sheridan give values for all three molecules, and their values are used here. These are listed in Table 7.1, together with the dipole moments

TABLE 7.1

INTERNUCLEAR DISTANCES AND DIPOLE MOMENTS FOR THE CYANOGEN HALIDES (FROM REFERENCE 36)

Compound	r_s(XC), Å	r_s(CN), Å	μ, Debyes ($\overset{+}{\text{X}}\text{-C}\equiv\overset{-}{\text{N}}$)
ClCN	1.631	1.159	2.80
BrCN	1.789	1.158	2.94
ICN	1.994	1.159	3.71

TABLE 7.2

FUNDAMENTAL VIBRATIONAL FREQUENCIES (cm^{-1}) FOR THE CYANOGEN HALIDES (FROM REFERENCE 50)

Compound	Vapour			Solid (-180°C)		
	ν_1	ν_2	ν_3	ν_1	ν_2	ν_3
ClCN	714	380	2219	734?	398	2212
BrCN	575	342.5	2200	572.5	363.5	2194
ICN	---	---	---	451.5	328.5	2176

which have also been determined by these authors from the microwave spectrum.

7.3.2 Infrared and Raman Studies

The infrared spectra of the three cyanogen halides have been investigated several times.[44,47-52] Freitag and Nixon[50] observed the spectra of all three cyanogen halides under low resolution. They recorded the spectra of cyanogen chloride and cyanogen bromide in the vapour phase and those of cyanogen chloride, cyanogen bromide, and cyanogen iodide as polycrystalline solids at -180°C. The fundamental vibrational frequencies which they obtained are given in Table 7.2.

Lafferty, Lide and Toth[44] observed the infrared spectrum of cyanogen chloride vapour and Maki and Gott[51,52] obtained that of cyanogen bromide vapour under high resolution. These studies yielded improved vibrational frequencies which are given in Table 7.3, plus internuclear distances and rotational constants for vibrationally excited levels of the ground electronic state.

It is found quite commonly in linear triatomic molecules that a perturbation caused by anharmonic terms in the molecular potential function occurs between pairs of vibrational levels described by the sets of quantum numbers* (v_1, v_2^0, v_3) and $(v_1-1, (v_2+2)^0, v_3)$ since

---

*Linear triatomic molecules have three normal vibrations. Two of these, labelled ν_1 and ν_3, are non-degenerate stretching vibrations and the third, labelled ν_2, is a doubly-degenerate bending vibration. The vibrational levels of a given electronic state of a linear triatomic molecule are described by the set of quantum numbers $(v_1, v_2^{\ell_2}, v_3)$, where v_1, v_2, and v_3 are vibrational quantum numbers for the three normal vibrations and the superscript ℓ_2 on the vibrational quantum number v_2 is a quantum number which measures the vibrational angular momentum about the internuclear axis and can take the values v_2, v_2-2, v_2-4, ..., 1 or 0. The vibrational levels have symmetry $\Sigma^+, \Pi^2, \Delta^2, \ldots$ for $\ell_2 = 0, 1, 2, \ldots$

they are of the same symmetry and often lie close in energy in zeroth order approximation. These perturbations are called Fermi resonances[110] and cause the vibrational levels to be shifted from their zeroth order values by an amount that is larger the closer the zeroth order levels lie. Such Fermi resonances have been observed in the ground electronic state for cyanogen chloride and cyanogen bromide and are discussed in references 44, 50, and 51. The calculated zeroth order vibrational frequencies, that is, the vibrational frequencies which would be observed in the absence of Fermi resonance, are listed in Table 7.3.

The Raman spectra of all three cyanogen halides have been observed,[45,46] cyanogen chloride and cyanogen bromide as the pure liquids and cyanogen iodide in solution. All three fundamental vibrational frequencies have been assigned for all three molecules, and these agree well with the infrared values when shifts in frequency between the gas and liquid phase values are taken into consideration.

7.3.3 Ultraviolet Studies

There have been several investigations of the spectra of the three cyanogen halides in the visible and near ultraviolet, both in the vapour phase[53,54] and in solution.[55] In all cases, at least one region of continuous absorption has been found below 3000 Å, there being no absorption to longer wavelengths. The wavelengths at which the absorption starts has been reported several times for the various molecules, and the wavelength of the absorption maximum has also been reported for cyanogen iodide. These data are summarized in Table 7.4. It is reported that the wavelength of the absorption maximum for cyanogen chloride is below 1840 Å, the shortest wavelength accessible to the

TABLE 7.3

FUNDAMENTAL VIBRATIONAL FREQUENCIES (cm^{-1}) OF THE CYANOGEN HALIDES FROM HIGH RESOLUTION INFRARED MEASUREMENTS (UNCERTAINTY LESS THAN $\pm 0.5\ cm^{-1}$)

Compound	ν_1	ν_2	ν_3	Reference
$^{35}ClCN$	714.0 (744.2)*	378.4	2215.6	44
$^{37}ClCN$	710 (736.0)*	378.0	2215.3	44
$^{79}BrCN$	--- (584.9)*	341.7	2198.3	51,52
$^{81}BrCN$	--- (583.1)*	341.6	2198.3	51,52

* zeroth order values

TABLE 7.4

ABSORPTION BY THE CYANOGEN HALIDE VAPOURS IN THE NEAR ULTRAVIOLET (WAVELENGTHS IN Å)

Compound	Reference 53	Reference 54	
	λ onset	λ onset	λ max
ClCN	>2270	2240	<1840
BrCN	>2450	2540	----
ICN(first)	>2900	3100	~2500
ICN(second)	>2100	2150	----

investigators. For cyanogen iodide, all reports state that there is a second absorption system which is slightly more intense than the first and has its onset in the region 2200-2100 Å.

In the vacuum ultraviolet, there have been only two reports of spectroscopic investigations of the cyanogen halides. Price and Walsh[56] have mentioned observing the absorption spectra for the three cyanogen halides. However, they give no details about the spectra aside from estimates of 10.6 and 11.2 eV for the first two ionization potentials of cyanogen iodide. Yakovleva[57] has examined the spectrum of cyanogen iodide down to about 1550 Å on a small fluorite spectrograph and has given wavelengths and oscillator strengths for the various regions of absorption which are summarized in Table 7.5.

7.3.4 Other Structural Studies

An electron diffraction study[58] of cyanogen chloride and cyanogen bromide indicates that the molecules are linear, but the internuclear distances which were obtained are not very accurate.

X-ray studies[59,60,61] of all three cyanogen halides in the solid state have been carried out, but accurate internuclear distances were obtained only for cyanogen chloride. Two interesting features were found in this work. First is the fact that cyanogen chloride and cyanogen bromide are iso-structural but different from cyanogen iodide. The essential difference between the two structures is that although both are linear chains packed in an approximation to the closest packing of cylinders, adjacent chains are antiparallel for cyanogen chloride and cyanogen bromide, whereas all chains are parallel for cyanogen iodide. The second feature is that there appears to be a sizeable

TABLE 7.5

ABSORPTION BY CYANOGEN IODIDE IN THE VACUUM ULTRAVIOLET

(FROM REFERENCE 57)

λ_{max}, Å	f	log ϵ	Designation	
			Ref. 57	This Work
2500	2.8×10^{-3}	---	A	A
1890	2.9×10^{-3}	---	B_1	α
1860	2.5×10^{-6}	---	B_2	
1739	---	---	B_3	
1710	---	3.00	B_4'	
1700	---	3.36	B_4	
1697	---	---		B
1681	---	3.09	B_5	
1573	---	3.64	C_1	C
1560	---	3.13	C_1'	

contraction of the molecules in the solid.

An electron impact study[62] of the three cyanogen halides has been made. From this, it has been found that the most abundant species produced by electron impact is the monopositive molecular ion. The appearance potentials for these ions have been measured and are listed in Table 7.6.

Flash photolysis experiments[63] have been made with cyanogen bromide and cyanogen iodide, and these show that the cyanogen halides dissociate into a halogen atom and a CN radical on absorption of ultraviolet radiation. The CN radical is thought to be produced in either the X $^2\Sigma^+$ state or the A $^2\Pi$ state, but it has not been possible to decide between these two possibilities.

TABLE 7.6

APPEARANCE POTENTIALS FOR THE CYANOGEN HALIDE MONOPOSITIVE MOLECULAR IONS (FROM REFERENCE 62)

Compound	Appearance Potential (eV)
ClCN	12.49 ± 0.04
BrCN	11.95 ± 0.08
ICN	10.98 ± 0.05

CHAPTER 8

EXPERIMENTAL

8.1 Preparation of the Compounds

8.1.1 Cyanogen Iodide

The preparation followed that reported by Ketelaar and Kruyer.[64] Twenty-one grams of iodine and 33 ml of water were placed in a 500 ml round bottom flask and stirred magnetically. A solution of 12 g of potassium cyanide in 167 ml of water was added to this from a dropping funnel. After half of the potassium cyanide solution was added, chlorine gas was bubbled through the reaction mixture. The chlorine flow was regulated to maintain excess iodine in the flask while the rest of the potassium cyanide solution was added. The cyanogen iodide was extracted in ether which was then dried over anhydrous calcium sulphate. After filtration, the ether was allowed to evaporate at room temperature in a fume hood. The crude cyanogen iodide was purified by sublimation and then stored in a closed container at $-78^{o}C$ to prevent decomposition.

In order to check the purity of the sample, the infrared spectrum of cyanogen iodide in a potassium bromide disc was taken. The only peaks observed agreed with those reported for cyanogen iodide.[50]

8.1.2 Cyanogen Bromide

The sample was purchased from the Eastman Kodak Company and was used without purification, except for pumping on the sample held at about $-30^{o}C$ to remove volatile impurities. The infrared spectrum of the vapour showed that no detectable impurities were present.

8.1.3 Cyanogen Chloride

The sample of cyanogen chloride was provided by Drs. J. L. Hencher and S. H. Bauer of Cornell University, Ithaca, New York. The infrared spectrum of the vapour showed the presence of carbon dioxide (bands at 2340 and 667 cm^{-1}), plus a small amount of water (weak absorption at 3710 and 3605 cm^{-1}). To remove the carbon dioxide, the sample was held at -78°C and pumped on until the bands of carbon dioxide were no longer observable in the infrared spectrum. No attempt was made to remove the water since it was not troublesome.

8.2 Ultraviolet Spectra

8.2.1 Visible and Near Ultraviolet

The spectra of each of the three cyanogen halides were recorded in the region 7000 Å to 1840 Å on a Cary Model 14 spectrophotometer. The Cary spectrophotometer accomodates cells of 10 cm maximum length.

Since the vapour pressure of cyanogen iodide is quite low at room temperature (less than 1 mm), it was necessary to measure its spectrum in this region in solution. Matched sets of 1.0 and 2.0 cm fused silica liquid cells were used to record the spectra of various concentrations of cyanogen iodide in n-heptane (Fisher Spectroanalyzed) and distilled water.

The vapour pressure of cyanogen bromide at room temperature is about 100 mm and so it was possible to record the spectrum both in solution and in the vapour on the Cary spectrophotometer. The spectra in n-heptane and aqueous solutions were recorded in the same way as for cyanogen iodide. The vapour spectra were measured using a cell approximately 10 cm in length fitted with fused silica windows. A 10 cm fused

silica cell filled with dry nitrogen was used as a reference cell.

The spectrum of cyanogen chloride was recorded only for the vapour since it is a gas at room temperature. This was done in the same way as for cyanogen bromide vapour.

The near ultraviolet spectra of all three compounds were also examined under higher resolution. The spectrum of cyanogen iodide vapour at about 1 mm pressure in a 50 cm fused silica absorption cell was observed using a deuterium lamp and a Hilger medium quartz spectrograph. The spectrum of cyanogen iodide vapour at pressures in the range 0-1 mm were also taken in the first order of the 21 foot off-plane Eagle vacuum spectrograph using a 75 cm cell fitted with calcium fluoride windows. The spectra of cyanogen bromide and cyanogen chloride vapour at pressures of 0-20 mm were also taken in the first order of the Eagle vacuum spectrograph using the 75 cm cell.

All photographs were taken on Ilford Q2 plates which were developed for 4 minutes in Kodak D19 developer at 20^{o}C, fixed for about 5 minutes and then washed thoroughly and allowed to dry in a dust-free place.

8.2.2 Vacuum Ultraviolet

The spectra in the vacuum ultraviolet of all three cyanogen halides were taken in the first order of the 21 foot Eagle vacuum spectrograph using slit widths of 25 to 100 microns. Selected portions of the spectra of the compounds were also observed in higher orders of the grating of this spectrograph using slit widths of 25 and 50 microns.

In the vacuum region it was necessary to flow the compound through the absorption cell using the system described in Section 4.5.

The pressure of the sample vapour in the reservoir bulb was maintained at a constant value in the range 1-20 mm by keeping the vessel containing the sample at a suitable temperature in a Dewar flask. The sample was kept at room temperature (about 23°C) for cyanogen iodide, at 0°C for cyanogen bromide and at about -65°C for cyanogen chloride. Some experiments were also done using a one litre bulb filled to about 20 mm pressure of cyanogen chloride in place of the cooled sample.

In the vacuum region the spectra were usually recorded on Ilford Q2 plates although some of the spectra in the higher orders were taken on Kodak SWR plates. These plates were developed as described previously.

8.3 Wavelength Measurements

8.3.1 Near Ultraviolet

Wavelengths were read from the recorder scale for all spectra taken on the Cary spectrophotometer. The error in this is less than ± 5 Å, which is quite adequate for the spectra observed. No wavelength measurements were taken from the spectra observed at high resolution since their only purpose was to check whether the absorption spectra observed for the cyanogen halides in the near ultraviolet were continuous as they appeared under low resolution.

8.3.2 Vacuum Ultraviolet

The travelling microscope was not used in the wavelength measurements because all the bands observed in the vacuum ultraviolet were not sharp even under high resolution. Instead, the wavelengths of the bands were determined in the following way. Microdensitometer traces of the plates were taken on a Leeds and Northrup travelling microdensitometer.

The Lyman source has certain characteristic emission and absorption lines, the wavelengths of which have been accurately measured,[65,66,67] and these were used as internal standards on the microdensitometer traces. The bands were measured at the point of maximum absorption and the wavelengths were calculated by interpolation between the standards. The wavelengths reported are the averages of measurements from microdensitometer traces of at least five different plates.

8.4 Intensity Measurements

8.4.1 Near Ultraviolet

The Beer-Lambert law may be written in the form

$$\frac{I}{I_0} = 10^{-\epsilon c \ell} \qquad (8.1)$$

where I_0 is the intensity of the radiation incident on the sample, I is the intensity of the radiation transmitted by the sample, ϵ is the extinction coefficient, c is the sample concentration and ℓ is the path length of the cell. The absorbance A is defined by the equation

$$A = \log_{10} \frac{I_0}{I} = \epsilon c \ell \qquad (8.2)$$

The absorbance readings for the spectra recorded on the Cary spectrophotometer were taken from the scale on the chart. The extinction coefficients were then calculated since the concentrations and cell path lengths were known. It should be noted that extinction coefficients calculated in this way are meaningful only if the Beer-Lambert law is obeyed. Plots of absorbance against concentration for all three cyanogen halides were found to be linear within the accuracy of the experimental measurements, thus showing that the Beer-Lambert

law is obeyed.

In order to obtain a measure of the total intensity of the spectra, oscillator strengths were calculated in the following way. The oscillator strength f can be calculated from the equation[68]

$$f = 4.317 \times 10^{-9} K \int \epsilon_\sigma d\sigma \qquad (8.3)$$

where ϵ_σ is the extinction coefficient in litre mole^{-1} cm^{-1} at wavenumber σ and the integration is over the whole absorption band. K is a factor depending upon the refractive index of the solvent.[69] For spectra in n-heptane K has the value 0.810, whereas for spectra in the vapour phase it is unity.

The integral in Equation 8.3 is simply the area under the curve resulting from a plot of extinction coefficient versus wavenumber, and can be approximated quite well for symmetric bands[68] by

$$\int \epsilon_\sigma d\sigma = \rho \epsilon_{max} \Delta\sigma_{1/2} \qquad (8.4)$$

where ϵ_{max} is the extinction coefficient at the absorption maximum and $\Delta\sigma_{1/2}$ is the width in cm^{-1} of the absorption band at half-height. ρ is a parameter depending upon the shape assumed for the absorption band; here the value 1.00 was used since the band shape was taken to be triangular.

The oscillator strength reported for each of the cyanogen halides is the average of at least three values measured at different concentrations. The precision in the measurements is in the order of 15%, but the accuracy is probably not this good.

8.4.2 Vacuum Ultraviolet

It was shown in the previous section that the intensity of a

spectral band is measured by the oscillator strength and that the oscillator strength can be expressed in the form

$$f = 4.317 \times 10^{-9} \rho \epsilon_{max} \Delta\sigma_{\frac{1}{2}} \qquad (8.5)$$

The absorbance A_{max} at the wavelength of maximum absorption of a spectral band is defined by the equation

$$A_{max} = \log_{10} \frac{I_0}{I_{max}} = \epsilon_{max} c \ell \qquad (8.6)$$

where I_0 is the intensity of the radiation incident on the sample and I_{max} is the intensity of the radiation transmitted by the sample at the wavelength of maximum absorption. The oscillator strength can now be expressed in terms of the absorbance by the following equation.

$$f = \frac{4.317 \times 10^{-9} \rho A_{max} \Delta\sigma_{\frac{1}{2}}}{c \ell} \qquad (8.7)$$

In the vacuum region, it was necessary to make intensity measurements from photographic plates. Great care must be taken in making such measurements because the response of a photographic emulsion depends upon the seven factors listed below.[70]

(i) intensity of the incident radiation

(ii) wavelength of the incident radiation

(iii) time of exposure to the radiation

(iv) nature of the photographic emulsion

(v) time of development

(vi) type of development

(vii) temperature of development

In the investigation described here, relative intensity measurements were made only for bands observed on the same exposed strip of a given

photographic plate. Therefore, any variations in the response of the emulsion were due only to the effects of the intensity and the wavelength of the radiation incident on the emulsion.

For the radiation used in molecular electronic spectroscopy (approximately 2-10 eV), the density D of blackening of a photographic emulsion is related to the exposure E by the equation

$$D = \gamma \log_{10} E \tag{8.8}$$

over the central range of blackening.[109] γ is a constant which depends upon the seven factors listed above. The exposure E is related to the intensity I of the radiation and the time t of the exposure by the reciprocity law[109] which can be written in the form

$$E = It^{p} \tag{8.9}$$

where p is a constant.

If, at the wavelength of maximum absorption for a given spectral band, the intensity of the radiation incident on the sample is I_0 and the intensity of the radiation transmitted by the sample is I_{max}, then the densities D_0 and D_{max} of blackening of the photographic emulsion that would be caused by I_0 and I_{max}, respectively, are

$$D_0 = \gamma \log I_0 t^{p} \tag{8.10}$$

$$D_{max} = \gamma \log I_{max} t^{p} \tag{8.11}$$

Since the time of exposure is the same for the two cases, the differences in densities are related to the absorbance by the following equation.

$$D_0 - D_{max} = \gamma \log \frac{I_0}{I_{max}} = \gamma A_{max} \tag{8.12}$$

Therefore, the oscillator strength can be expressed in terms of the densities of darkening on the plate as

$$f = \frac{4.317 \times 10^{-9} \rho (D_0 - D_{max}) \Delta\sigma_{1/2}}{\gamma c \ell} \qquad (8.13)$$

In this investigation, absolute oscillator strengths could not be calculated from Equation 8.13 because a number of the constants could not be measured. It was not possible to calibrate the emulsion for variation of response with the wavelength of the radiation. Therefore, it was necessary to assume that response was independent of wavelength over the region of interest, that is, that γ is a constant. This is a good assumption here since the wavelength range on a single exposure was always considerably less than 100 Å. Another problem was that the concentration of the sample and the cell path length could not be measured since fresh sample was flowed continuously through the absorption cell. However, since only bands recorded on the same exposure were compared, the sample concentration and cell length were the same for all bands. Therefore, the relative intensities of two bands j and k can be related by the equation

$$\frac{f^j}{f^k} = \frac{\rho^j (D_0^j - D_{max}^j) \Delta\sigma_{1/2}^j}{\rho^k (D_0^k - D_{max}^k) \Delta\sigma_{1/2}^k} \qquad (8.14)$$

The band shape and band width at half-height were all very similar for the bands being compared. So, ρ and $\Delta\sigma_{1/2}$ could be assumed to be constant for all the bands. This allowed the relative intensities to be expressed in the simplified form

$$\frac{f^j}{f^k} = \frac{D_0^j - D_{max}^j}{D_0^k - D_{max}^k} \qquad (8.15)$$

This equation allowed the relative intensities of two bands to be calculated from the plate densities.

In this investigation, plate densities were measured on a Leeds and Northrup travelling microdensitometer, which has a logarithmic intensity scale from which plate densities can be read directly. The accuracy of the plate densities obtained with this instrument was checked in the following way. A rotating sector was used to vary the intensity of the radiation from a deuterium lamp entering a Hilger medium quartz spectrograph so that exposures with intensity ratios of 1:3/4:1/2:1/4:1/8:1/16 could be taken. The exposures were taken on Ilford Q2 plates which are the same as were used in the vacuum ultraviolet. All exposures were for equal times so that problems with reciprocity law failure were eliminated; and the rotating sector was operated at a speed in the order of several thousand revolutions per minute so that intermittency effects introduced no error. The plates obtained in this manner were developed and fixed in the same way as described previously.

By use of Equations 8.8 and 8.9, it can be shown that the intensity I_M and density D_M for the most intense exposure and the intensity I_F and density D_F for any other exposure should be related by the equation

$$D_M - D_F = \gamma \log \frac{I_M}{I_F} = \gamma A_{MF} \qquad (8.16)$$

For several different plates the densities of each of the six standard exposures were measured at four different wavelengths (3000, 2600, 2300, and 2100 Å) with the Leeds and Northrup microdensitometer. The

differences in density $D_M - D_F$ were plotted against the appropriate absorbance values calculated from the known relative intensities. These plots yielded straight lines for plates which were neither over-exposed nor under-exposed. There was a small scatter of the points about the straight line, but this could easily be accounted for by fluctuations of the lamp intensity over the time necessary to take the exposures.

Microdensitometer traces of the cyanogen halide spectra for which intensity measurements were desired were made with the Leeds and Northrup microdensitometer. The density D_{max} at the wavelength of maximum absorption for each vibronic band was measured directly from the chart. In order to obtain a value for the density D_0 which the radiation incident on the sample would have produced if it had fallen on the emulsion, a smooth curve was drawn joining the continuum on either side of each vibronic band. The value of D_0 was then measured at the appropriate wavelength. This procedure assumes that the intensity of the Lyman source varies smoothly with wavelength; plates taken without any sample have shown that this is true.

The results reported are the averages of values measured from at least five different plates. The precision of the measurements will be given when the results are discussed. The uncertainty of the results is probably in the order of 10-20% in general.

CHAPTER 9

THEORY OF ELECTRONIC SPECTRA

9.1 Classification of Electronic States

Triatomic molecules such as the cyanogen halides XCN (X=Cl, Br, or I) can have either a linear or non-linear equilibrium nuclear configuration in a given electronic state. In the former case the molecule is classified under the $C_{\infty v}$ point group given in Table 9.1, whereas in the latter case the molecule is classified under the C_s point group given in Table 9.2. The electronic wave functions form bases for irreducible representations of the molecular point groups and these are used in classifying the electronic states.

Only that component of the electronic wave function that is a function of space coordinates is considered here. Spin-orbit interactions are assumed to be negligibly small so that spin angular momentum is separately conserved. Later in this thesis, it will be shown that spin-orbit coupling must be considered when describing the Rydberg states of the cyanogen halides; modifications to the theory will be made at that time.

9.2 Molecular Orbital Considerations

9.2.1 Molecular Orbitals

Approximate semi-localized molecular orbitals have been constructed for the cyanogen halides both for 180° and 90° valence angles and are used here to give a qualitative interpretation of some of the observed electronic spectra. The methods of construction of the

TABLE 9.1

THE IRREDUCIBLE REPRESENTATIONS OF THE $C_{\infty v}$ POINT GROUP

$C_{\infty v}$	E	$2C_{\phi}$	$\infty\sigma_v$		
Σ^+	1	1	1	T_z	
Σ^-	1	1	-1		R_z
Π	2	$2\cos\phi$	0	T_x, T_y	R_x, R_y
Δ	2	$2\cos 2\phi$	0		
Φ	2	$2\cos 3\phi$	0		
.	.	.	.		
.	.	.	.		
.	.	.	.		

TABLE 9.2

THE IRREDUCIBLE REPRESENTATIONS OF THE C_s POINT GROUP

C_s	E	$\sigma_h(yz)$		
A'	1	1	T_y, T_z	R_x
A"	1	-1	T_x	R_y, R_z

molecular orbitals and the relative energies of the electrons in them are given in Appendix II.

In Figure 9.1 the molecular orbitals of the linear and non-linear (valence angle 90°) cyanogen halides are shown schematically on the right and left hand sides, respectively. The approximate localization of the pi-type molecular orbitals, implied by large relative values of the coefficients of the component atomic orbitals, is indicated by cross-hatching in these diagrams.

9.2.2 Correlation of Molecular Orbitals

The principles for determining which molecular orbitals of the linear and bent cyanogen halides correlate with each other and how the binding energy of a molecular orbital varies as the bond angle changes were first given by Mulliken[112] and later extended by Walsh.[72]

For a valence angle of 90° it is assumed that the s atomic orbital on the carbon atom does not hybridize with the p atomic orbitals, but that as the angle increases the amount of hybridization increases until there is sp hybridization for a 180° angle. The variation of the binding energy of the electrons in a molecular orbital as the valence angle changes is primarily dependent upon the change of hybridization at the carbon atom. The electrons in a molecular orbital have greater binding energy, that is, they become more tightly bound, as the amount of s character at the carbon atom increases. For a molecular orbital in which the hybridization at the central atom does not change as the bond angle changes, a second principle applies; the binding energy increases as the angle decreases if the orbital is bonding between the halogen and nitrogen atoms, but decreases as the angle decreases if the orbital is anti-bonding between the halogen and

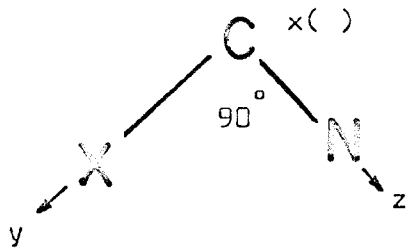

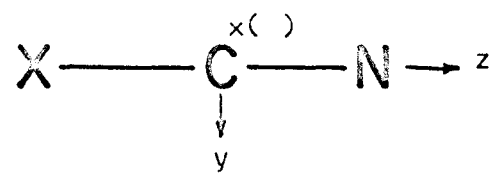

1a'

1σ

2a'

2σ

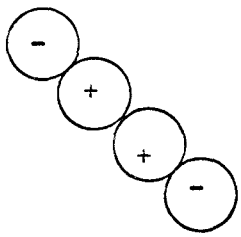

3a'

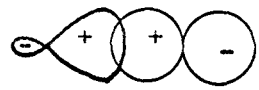

3σ

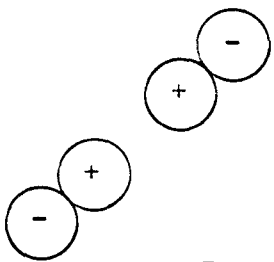

4a'

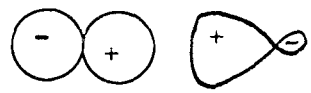

4σ

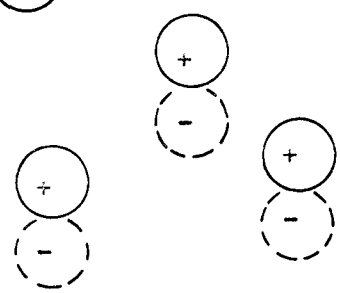

1a"

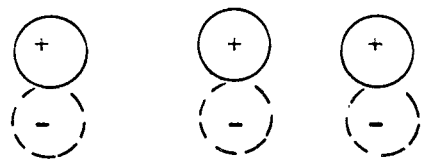

$1\pi_x$

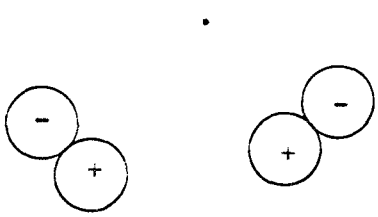

5a'

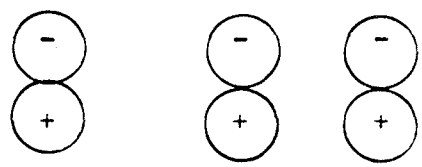

$1\pi_y$

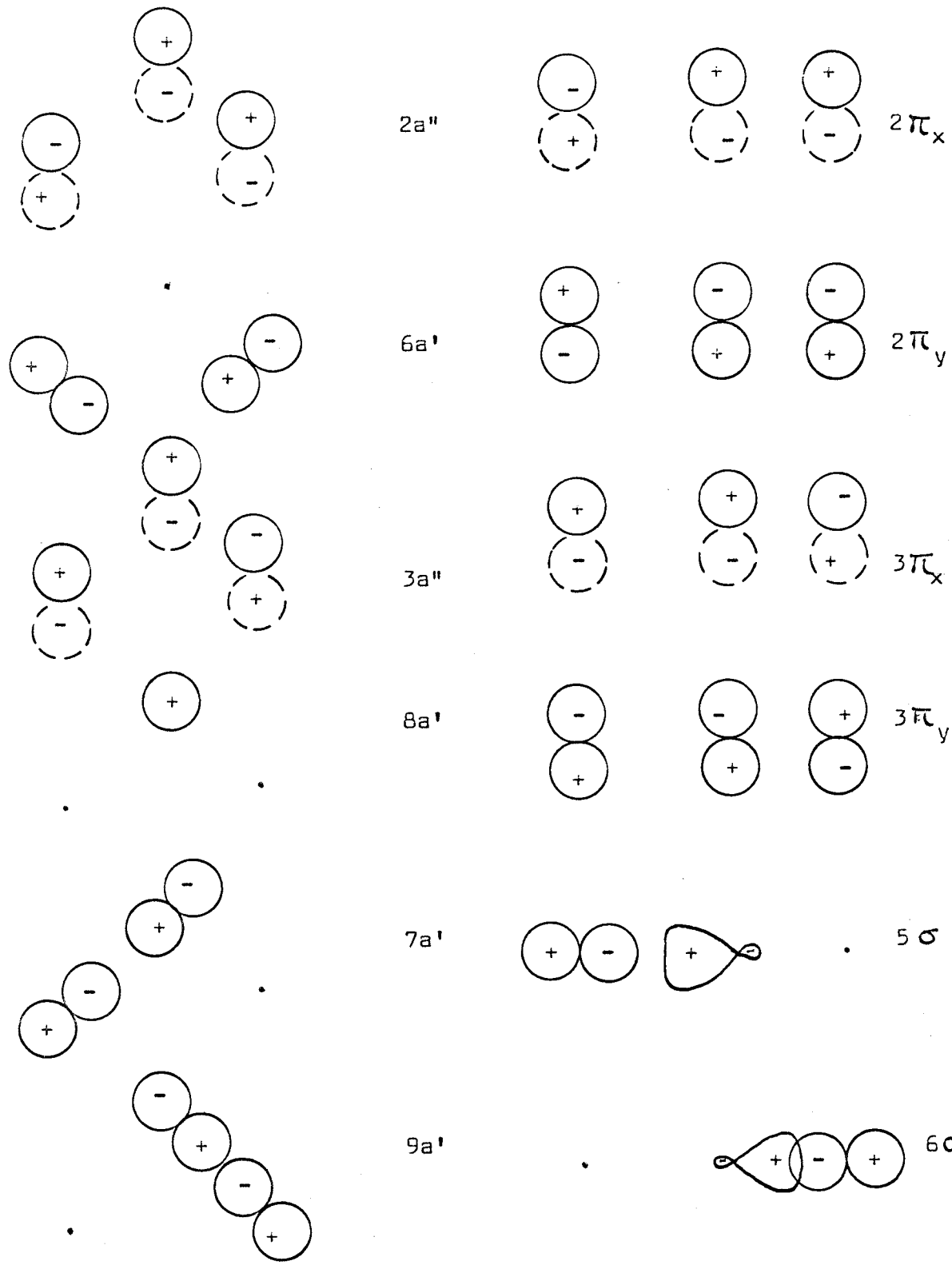

FIGURE 9.1.

MOLECULAR ORBITALS FOR THE LINEAR AND NON-LINEAR CYANOGEN HALIDES

(SCHEMATIC)

nitrogen atoms.

In correlating the molecular orbitals for the 90° and 180° bond angles, it is necessary to follow the non-crossing rule.[117] This correlation is accomplished quite simply in most cases by examination of the mathematical and pictorial representations of the molecular orbitals. Only in the case of the π molecular orbitals of the linear molecule is there some difficulty. But by following Walsh's examples,[72] the correlations can be made without trouble. The molecular orbitals which correlate with each other are listed side by side in Figure 9.1.

Figure 9.2 gives the molecular orbital correlation diagram for the cyanogen halides. In this diagram the binding energy of the electrons decreases from bottom to top along the ordinate and the cyanogen halide bond angle increases from 90° to 180° from left to right along the abscissa. The relative energies of electrons in the molecular orbitals of the linear molecule, which are discussed in Appendix II, are plotted on the right hand side of Figure 9.2, and the molecular orbitals of the linear and bent molecules which correlate with one another are joined by solid lines. The binding energy scale in Figure 9.2 is only qualitative. The relative energy separation of the molecular orbitals for the linear molecule and the slope of a line joining molecular orbitals which correlate with one another probably vary considerably between the cyanogen halides.

9.2.3 Molecular Orbital Predictions

Molecular orbital correlation diagrams such as Figure 9.2 are extremely useful since they allow predictions about the molecular geometry and the symmetry of the electronic wave function in various

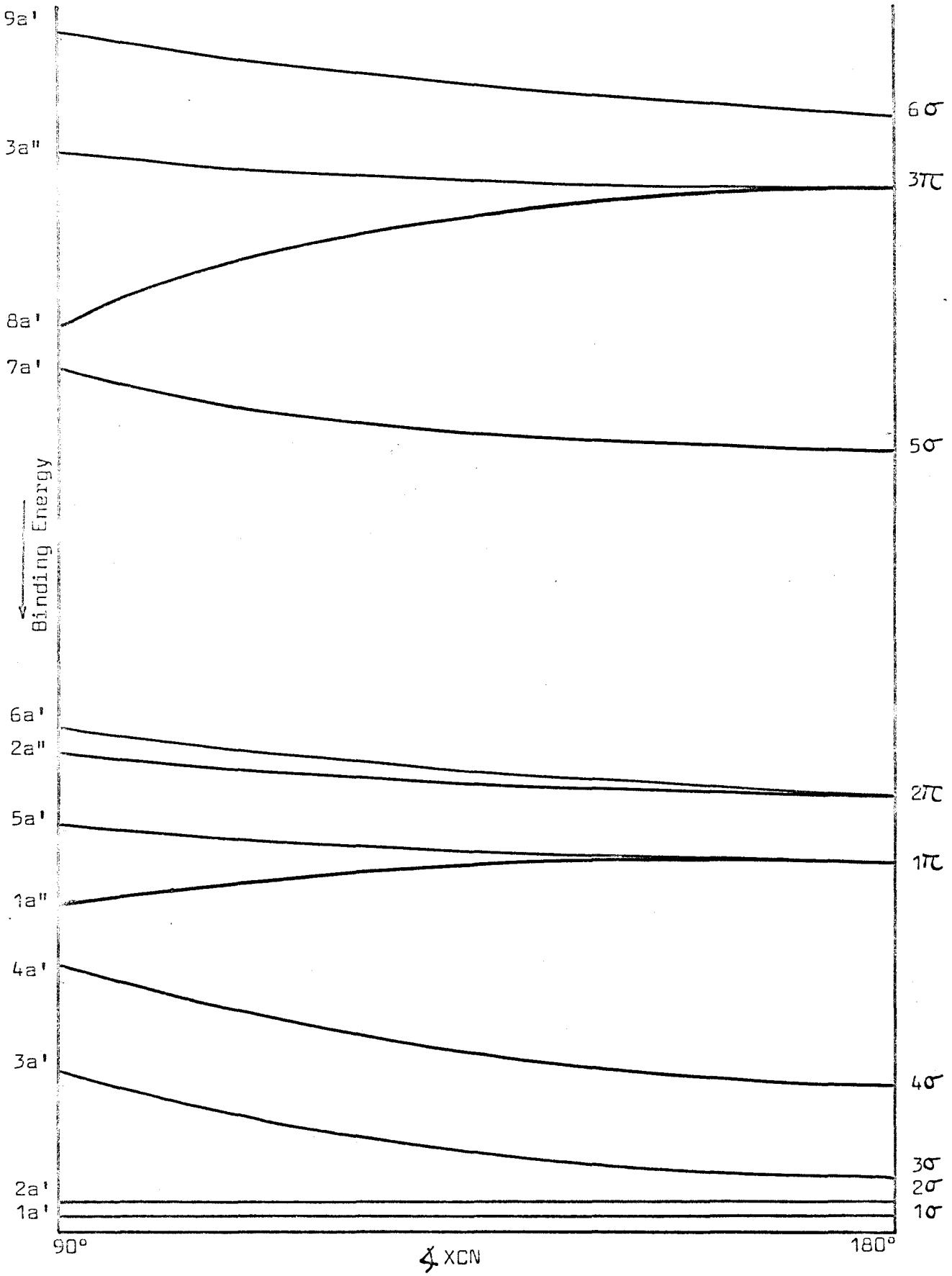

FIGURE 9.2

MOLECULAR ORBITAL CORRELATION DIAGRAM FOR THE CYANOGEN HALIDES

electronic states to be made according to the number of valence electrons that are present. The cyanogen halides have sixteen valence electrons and these fully occupy the molecular orbitals 1σ to 2π for the linear molecule or the molecular orbitals 1a' to 6a' for the 90° bent molecule. Figure 9.2 shows that the total electronic energy is less in the linear configuration so that in the ground electronic state the cyanogen halides are predicted to be linear with the following electron configuration and electronic wave function symmetry.

$$(1\sigma)^2(2\sigma)^2(3\sigma)^2(4\sigma)^2(1\pi)^4(2\pi)^4 \qquad X\,{}^1\Sigma^+ \qquad (9.1)$$

This agrees with the results found from the microwave spectra.

Figure 9.2 shows that the lowest energy electronic spectrum of the cyanogen halides should result from promotion of an electron from the 2π to the 5σ molecular orbital. Since the 5σ molecular orbital is also more binding for a linear molecule, the cyanogen halides should be linear in this excited state and have the following electron configuration and state symmetry.

$$(1\sigma)^2(2\sigma)^2(3\sigma)^2(4\sigma)^2(1\pi)^4(2\pi)^3(5\sigma)^1 \qquad {}^{1,3}\Pi \qquad (9.2)$$

Another low-lying electronic spectrum of the cyanogen halides should result from promotion of an electron from the 1π to the 5σ molecular orbital. The binding energy is again greater for the linear molecule so that the excited state electron configuration and state symmetry should be

$$(1\sigma)^2(2\sigma)^2(3\sigma)^2(4\sigma)^2(1\pi)^3(2\pi)^4(5\sigma)^1 \qquad {}^{1,3}\Pi \qquad (9.3)$$

Another relatively low-lying electronic spectrum might be expected to result from promotion of an electron from the 2π to the

3π molecular orbital. If the molecule stays linear, the electron configuration and state symmetries are

$$(1\sigma)^2(2\sigma)^2(3\sigma)^2(4\sigma)^2(1\pi)^4(2\pi)^3(3\pi)^1 \qquad {}^{1,3}\Sigma^+, \; {}^{1,3}\Sigma^-, \; {}^{1,3}\Delta \tag{9.4}$$

whereas if the molecule bends, the electron configurations and state symmetries that are possible are

$$(1a')^2(2a')^2(3a')^2(4a')^2(1a'')^2(5a')^2(2a'')^2(6a')^1(3a'')^1 \quad {}^{1,3}A'' \tag{9.5.a}$$

$$(2a'')^1(6a')^2(3a'')^1 \quad {}^{1,3}A' \tag{9.5.b}$$

$$(2a'')^2(6a')^1(8a')^1 \quad {}^{1,3}A' \tag{9.5.c}$$

$$(2a'')^1(6a')^2(8a')^1 \quad {}^{1,3}A'' \tag{9.5.d}$$

The 3π molecular orbital of the linear molecule correlates with the 3a" and 8a' molecular orbitals of the non-linear molecule and is more binding than the former but less binding than the latter. Therefore, it is predicted that the states of (9.5.a) and (9.5.b) are linear and that those of (9.5.c) and(9.5.d) are non-linear.

9.3 The Energy of Spectral Transitions

In molecular spectroscopy, energy is usually measured in terms of wavenumbers (cm^{-1}) and the zero of energy is usually taken at the minimum of the potential energy surface of the ground electronic state. Relative to this, the energy of any vibrational level of any electronic state may be written as

$$T = T_e + G(v_1, v_2 \ldots) \tag{9.6}$$

where T is the term value of the vibrational level, T_e is the energy of the minimum of the potential surface of the electronic state, and $G(v_1, v_2,..)$ is the energy of the vibrational level relative to T_e.

In the limit that the vibrational motions of the atoms in a molecule are infinitely small, the vibrations of a molecule may be analyzed in terms of normal vibrations which total 3N-6 for non-linear molecules and 3N-5 for linear molecules, where N is the number of atoms in the molecule. In this approximation, the vibrational energy $G(v_1, v_2, \ldots)$ is

$$G(v_1, v_2, \ldots) = \sum_i \omega_i (v_i + \frac{d_i}{2}) \qquad (9.7)$$

where ω_i is the frequency (in cm^{-1}) for infinitely small classical vibrations, v_i is the vibrational quantum number, and d_i is the degeneracy of the i^{th} normal vibration. However, the amplitudes of molecular vibrations are not infinitely small so that the concept of normal vibrations is not strictly valid. To take this into account, the vibrational energy of an actual molecule is empirically expressed in the form

$$G(v_1, v_2, \ldots) = \sum_i \omega_i (v_i + \frac{d_i}{2}) + \sum_i \sum_{k \geq i} x_{ik} (v_i + \frac{d_i}{2})(v_k + \frac{d_k}{2}) + \ldots \qquad (9.8)$$

where the x_{ik} are constants (expressed in cm^{-1}) which arise from anharmonicity of the molecular vibrations.

The wavenumber σ of a vibronic band resulting from a transition between two vibrational levels of an upper and lower electronic state, denoted by single and double primes, respectively, is given by

$$\sigma = \sigma_e + G'(v_1', v_2', \ldots) - G''(v_1'', v_2'', \ldots) \qquad (9.9)$$

where

$$\sigma_e = T'_e - T''_e \tag{9.10}$$

If the anharmonicity constants x_{ik} are neglected, the wavenumber σ is given by

$$\sigma = \sigma_e + \sum_i \omega'_i(v'_i + \frac{d'_i}{2}) - \sum_i \omega''_i(v''_i + \frac{d''_i}{2}) \tag{9.11}$$

The wavenumbers of vibronic bands observed in an electronic transition can usually be expressed quite well in terms of this equation except when long progressions are observed since then the quadratic terms of Equation 9.8 may become quite large.

9.4 Intensity Considerations

9.4.1 Selection Rules

It was shown in Section 7.2 that the intensity of an electronic transition is proportional to the square of the transition moment $\vec{R}$ which is given by

$$\vec{R} = \int \Psi'^{*}_T \vec{\mu} \Psi''_T d\tau \tag{9.12}$$

for an electric dipole transition between two states with wave functions Ψ'_T and Ψ''_T. For the transition to be allowed, that is, to have non-zero intensity, $\vec{R}$ must not be zero for symmetry reasons. Since the value of $\vec{R}$ cannot be changed by the exchange of identical particles, the integrand of Equation 9.12 must be invariant to all the symmetry operations of the point group to which the molecule belongs. This means that the direct product of the irreducible representations to which the components of the integrand belong must contain the totally symmetric representation. The Wigner-Eckart theorem expresses this requirement in the form

$$\Gamma\Psi_T'^{*} \otimes \Gamma\Psi_T'' = \Gamma\vec{\mu} \qquad (9.13)$$

where the symbol Γ stands for an irreducible representation of the molecular point group.

In general, it is a good approximation to express the total wave function as the product of electronic, vibrational, and rotational wave functions (see Section 7.1). The rotational wave function may be neglected in the following discussion since it does not affect the results to be derived. Thus, the total wave function Ψ_T can be expressed as the product of an electronic and a vibrational wave function.

$$\Psi_T = \psi_e(r,Q)\,\psi_V(Q) \qquad (9.14)$$

In this equation, r represents the coordinates of the electrons and Q represents the normal coordinates of the nuclei. By substitution of Equation 9.14 in Equation 9.12, the transition moment can be expressed in the form

$$\vec{R} = \int \psi_V'^{*}(Q)\,\psi_V''(Q)\,\vec{R}_e(Q)\,dQ \qquad (9.15)$$

where $\vec{R}_e(Q)$ is the electronic transition moment defined by

$$\vec{R}_e(Q) = \int \psi_e'^{*}(r,Q)\,\vec{\mu}(r)\,\psi_e''(r,Q)\,dr \qquad (9.16)$$

In many cases it is a good approximation to assume that the electronic wave function $\psi_e(r,Q)$ is independent of the nuclear coordinates. This means that $\vec{R}_e(Q)$ is a constant independent of the nuclear motion and can be set equal to $\vec{R}_e(0)$, the value when all the

nuclei are in their equilibrium positions.* The transition moment $\vec{R}$ can thus be written

$$\vec{R} = \vec{R}_e(0) \int \psi_v'^{*}(Q)\, \psi_v''(Q)\, dQ \qquad (9.17)$$

which can be used to obtain selection rules for transitions between vibrational levels in the combining electronic states.

For the integrand in Equation 9.16 to be non-zero, the direct product of the irreducible representations of the components of the integrand must have a component which transforms like the totally symmetric irreducible representation. Therefore, the combining electronic states must obey the selection rule

$$\Gamma_{\psi_e'^{*}} \otimes \Gamma_{\psi_e''} = \Gamma_{\vec{\mu}} \qquad (9.18)$$

The electric dipole moment operator $\vec{\mu}$ is a vector whose Cartesian components transform like translations along these three space directions. In Tables 9.1 and 9.2, the irreducible representations for which any vector forms a basis are indicated by the symbols T_x, T_y, and T_z, where these symbols represent the Cartesian components of the vector.

For electronically allowed transitions, a selection rule on the vibrational levels that can combine is derived from Equation 9.17. For the integral over the normal coordinates to be non-zero, it is necessary

---

*The treatment given by Robinson[78] is followed here. $\vec{R}_e(Q)$ is expanded in a Taylor series in the normal coordinates Q_i about the equilibrium nuclear configuration (Q=0)

$$\vec{R}_e(Q) = \vec{R}_e(0) + \sum_i \left(\frac{\partial R_e}{\partial Q_i}\right)_0 Q_i + \cdots$$

and only the first term of the expansion is retained. This differs from the procedure in diatomic molecules[116] where $\vec{R}_e$ is given the value $\vec{R}_e$ for a mean internuclear distance $\bar{r}$, called the r-centroid.

that

$$\Gamma_{\psi_V'^*} \otimes \Gamma_{\psi_V''} = \Gamma_1 \qquad (9.19)$$

where Γ_1 is the totally symmetric representation ($\sum^+$ for $C_{\infty v}$ and A' for C_s). For a transition between two vibrational levels to be possible, the vibrational wave functions in both electronic states must have the same symmetry. Because of this, progressions* are observed only for totally symmetric normal vibrations. Transitions involving non-totally symmetric normal vibrations can occur only if the change in the vibrational quantum number is $0, \pm 2, \pm 4, \ldots$

9.4.2 Vibronic Interactions

In the preceding section, it has been assumed that the electronic transition moment is independent of the nuclear coordinates. In this section, the effects of the dependence of the electronic motion on the nuclear coordinates will be described in the way first given by Herzberg and Teller.[74]

Expression of the total wave function as the product of an electronic and a vibrational wave function as in Equation 9.14 is still valid. However, it is no longer possible to ignore the dependence of the electronic wave functions on the nuclear coordinates. Thus, the transition moment $\vec{R}$ must be considered in the full form given below.

$$\vec{R} = \int\int \psi_e'^*(r,Q)\, \psi_V'^*(Q)\, \vec{\mu}(r)\, \psi_e''(r,Q)\, \psi_V''(Q)\, dr\, dQ \qquad (9.20)$$

*In electronic spectroscopy, a progression refers to a series of vibrational bands in which a given vibrational quantum number changes by unity between bands.

For a transition to be allowed in this approximation, it is necessary that the following condition be satisfied.

$$\Gamma\psi_e'^{*} \otimes \Gamma\psi_v'^{*} \otimes \Gamma\psi_e'' \times \Gamma\psi_v'' = \Gamma\vec{\mu} \qquad (9.21)$$

If the transition is electronically forbidden, that is, if Equation 9.18 is not satisfied, transitions may still be observed if vibrations of the correct symmetry to satisfy Equation 9.21 exist. Transitions to vibrational levels which are forbidden by the selection rule of Equation 9.19 may become vibronically allowed if Equation 9.21 is satisfied. Transitions which are vibronically allowed but electronically forbidden are considerably weaker than electronically allowed transitions.

9.4.3 The Franck-Condon Principle

The intensity distribution within progressions of bands is determined by the Franck-Condon principle. The classical concept of Franck[75] states that the nuclear positions and velocities do not change appreciably during an electronic transition because the nuclear masses are much greater than the electron mass. This means that for any ground state nuclear configuration the electronic transition is to a vibrational level of the excited electronic state in which the nuclear positions and velocities are essentially unchanged.

Condon[76] has shown that Franck's classical concept can be explained more satisfactorily using quantum mechanics. It was shown in the previous section that the intensity of an allowed electronic transition between any pair of vibrational levels of the ground and excited electronic states can be written in the form

$$I \propto \left|\vec{R}_e(0)\right|^2 \left| \int \psi_v'^{*}(Q)\, \psi_v''(Q)\, dQ \right|^2 \qquad (9.22)$$

where $\vec{R}_e(0)$ is the electronic transition moment and is constant for a given electronic transition. Thus, the relative intensities of the transitions are determined by the relative values of the squares of the appropriate vibrational overlap integrals. Since most molecules are in the vibrationless level of the ground electronic state, the most intense transitions arise from that level and their relative intensities depend upon the magnitudes of the vibrational overlap integrals. The vibrational overlap integral is greatest for transitions to the vibrational level whose classical turning point lies "vertically" above the vibrationless level and so this transition is the most intense. For any other excited state vibrational level, the vibrational overlap integral is smaller the farther the level lies from the most probable level, and the intensity is correspondingly reduced.

If there is a change in the geometry (but not the symmetry) of a molecule, then progressions in the totally symmetric normal vibrations corresponding to the normal coordinates which cause this geometry change are excited in the spectrum. The larger the change in the geometry of the molecule, the greater the number of bands observed in a progression and the farther the intensity maximum lies from the origin band of the electronic transition.

9.5 Molecular Structure From the Franck-Condon Principle

It is possible to use a quantitative expression of the Franck-Condon principle to determine the structural changes in molecules upon

electronic excitation. This method does not give as accurate information as the rotational analysis of vibronic bands, but it allows changes in geometry to be determined in cases where rotational analysis is not possible or does not yield sufficient information for a complete structure determination.

The theory will be developed here for the case of an allowed electronic transition between two electronic states for which the symmetry of the molecule is the same.[77] The oscillator strength of a transition from the vibrational level v" of the ground electronic state to the vibrational level v' of an excited electronic state is given by the expression[78]

$$f^{v',v''} = \frac{4\pi mc}{3\hbar e^2} G \sigma^{v',v''} \left| \vec{R}^{v',v''} \right|^2 \qquad (9.23)$$

where c, m, $\hbar$, and e have their usual significance, G is the degeneracy of the excited electronic state, $\sigma^{v',v''}$ is the wave number of the vibronic transition, and $\vec{R}^{v',v''}$ is the transition moment. If Equation 9.17 for the transition moment is used and all the factors which are constant for a given electronic transition are grouped into a constant K, the oscillator strength may then be written

$$f^{v',v''} = K \sigma^{v',v''} \left| \int \psi_v'^{*}(Q') \psi_v''(Q'') \, dQ' \right|^2 \qquad (9.24)$$

where Q' and Q" represent, collectively, the normal coordinates for the excited and ground electronic states, respectively.

The total vibrational wave function $\psi_V(Q)$ is written as the product[79] of a wave function $\phi_i(Q_i)$ for each normal coordinate Q_i.

$$\psi_V(Q) = \prod_{i=1}^{n} \phi_i(Q_i) \tag{9.25}$$

where n is the number of normal coordinates, which is 3N-5 for a linear molecule with N nuclei. The oscillator strength can then be expressed in the following form.

$$f^{v',v''} = K \sigma^{v',v''} \left| \int \left[\prod_j \phi'^{*}_j(Q'_j) \right] \left[\prod_i \phi''_i(Q''_i) \right] dQ'_1 dQ'_2 \ldots dQ'_n \right|^2 \tag{9.26}$$

Duschinsky[80] has shown that the ground and excited state normal coordinates are related by the equation

$$Q''_i = \sum_j a_{ij} Q'_j + d_i \tag{9.27}$$

For transitions in which the symmetry of the molecule does not change, $a_{ij} \neq 0$ only if Q''_i and Q'_j have the same symmetry and $d_i \neq 0$ only for totally symmetric normal coordinates. If only those transitions originating from the zeroth vibrational level (v" = 0) of the ground electronic state are considered, then it is a good approximation to assume that the ground state wave function is spherically symmetric. This means that the ground state normal coordinates can be taken to be parallel to the excited state normal coordinates,[77] thus simplifying Equation 9.27 to the form

$$Q''_i = Q'_i + d_i \tag{9.28}$$

where, as before, $d_i \neq 0$ only for totally symmetric vibrations.

The oscillator strength can now be simplified to the form

$$f^{v',0} = K \sigma^{v',0} \left| \vec{R}^{v',0} \right|^2 \qquad (9.29)$$

where the vibrational transition moment $\vec{R}^{v',0}$ is given by

$$\vec{R}^{v',0} = \prod_{i=1}^{n} R_i(v_i',0) \qquad (9.30)$$

and

$$R_i(v_i',0) = \int \phi_i'^{*}(Q_i') \, \phi_i''(Q_i' + d_i) \, dQ_i' \qquad (9.31)$$

If a progression for only the i^{th} normal vibration in the excited state is considered, then the $R_j(v_j',0)$ for all the other normal vibrations will be constant. Thus, the intensity of a transition between the vibrational levels v_i' and 0 of the excited and ground electronic states, respectively, relative to the intensity of the transition between the vibrationless levels of the two electronic states (0-0 transition) will be given by

$$\frac{f^{v_i',0}}{f^{0,0}} = \frac{\sigma^{v_i',0}}{\sigma^{0,0}} \left| \frac{R_i(v_i',0)}{R_i(0,0)} \right|^2 \qquad (9.32)$$

The $\phi_i(Q_i)$ can be expressed as harmonic oscillator wave functions.[79]

$$\phi_i(Q_i) = N_{vi} H_{vi}(\alpha_i Q_i) \exp\left[-\tfrac{1}{2} \alpha_i^2 Q_i^2\right] \qquad (9.33)$$

α_i is related to the vibrational frequency ν_i (in cm^{-1}) of the i^{th} normal vibration by

$$\alpha_i^2 = \frac{4\pi^2 c}{h} \nu_i \tag{9.34}$$

N_{v_i} is a normalization constant,

$$N_{v_i} = \frac{\alpha_i}{\pi^{1/2} 2^{v_i} v_i!}^{1/2} \tag{9.35}$$

and $H_{v_i}(\alpha_i Q_i)$ is the Hermite polynomial of order v_i.

The values of $R_i(v_i', 0)$ for harmonic oscillator wave functions centred at different points on a given normal coordinate axis have been evaluated in closed form.[77] Some of the values of $R_i(v_i', 0) / R_i(0,0)$ which are most useful are listed below.

$$\frac{R_i(1,0)}{R_i(0,0)} = \frac{\sqrt{2}\,\beta_i^2\,\gamma_i}{(1+\beta_i^2)} \tag{9.36}$$

$$\frac{R_i(2,0)}{R_i(0,0)} = \frac{1}{\sqrt{2}(1+\beta_i^2)} \left[\frac{2\beta_i^4 \gamma_i^2}{(1+\beta_i^2)} + (1-\beta_i^2) \right] \tag{9.37}$$

In these equations, the parameters β_i and γ_i are defined by

$$\beta_i = \frac{\alpha_i''}{\alpha_i'} \tag{9.38}$$

$$\gamma_i = -\alpha_i' d_i \tag{9.39}$$

In Section 8.4.2, it was shown how the relative intensity of any two spectral bands can be determined experimentally. The wavenumbers of the bands and the vibrational intervals can also be obtained by measurement of the spectrum. Therefore, Equations 9.32 - 9.39 can be used to calculate d_i, the change in the i^{th} normal coordinate. This can be repeated for each totally symmetric normal vibration, thus giving the changes in each totally symmetric normal coordinate upon electronic excitation. However, since the squares of the vibrational overlap integrals $R_i(v_i',0)$ are involved in the calculation of d_i, the sign of d_i for each normal coordinate cannot be determined from the above calculation. This means that there will be several possible structural changes consistent with the observed intensity distribution.

The cyanogen halides have only two totally symmetric normal coordinates and the normal vibrations corresponding to these are usually labelled ν_1 and ν_3, the former being essentially the carbon-halogen stretching vibration and the latter the carbon-nitrogen stretching vibration.[81] For progressions in each of these vibrations, the change in each of the normal coordinates can be calculated using the methods described. The problem now is to relate these changes in normal coordinates to changes in bond lengths of the molecule. Changes in bond angle are not considered since these would change the symmetry of the molecule and so invalidate the discussion above.

Equation 9.28 gives the relation between the ground and excited state normal coordinates. This can be re-expressed in matrix form as

$$\begin{bmatrix} Q_1'' \\ Q_3'' \end{bmatrix} = \begin{bmatrix} Q_1' \\ Q_3' \end{bmatrix} + \begin{bmatrix} d_1 \\ d_3 \end{bmatrix} \qquad (9.40)$$

or, more simply,

$$[Q''] = [Q'] + [D] \tag{9.41}$$

From the theory of molecular vibrations, it is known that the normal coordinate matrix $[Q]$ is related to the matrix of the mass-weighted Cartesian displacement coordinates $[\eta]$ by a matrix usually denoted $[L]$

$$\begin{bmatrix} \eta_1 \\ \eta_2 \\ \eta_3 \end{bmatrix} = \begin{bmatrix} \ell_{11} & \ell_{13} \\ \ell_{21} & \ell_{23} \\ \ell_{31} & \ell_{33} \end{bmatrix} \begin{bmatrix} Q_1 \\ Q_3 \end{bmatrix} \tag{9.42}$$

The $[L]$ matrix given here is a modification of the usual $[L]$ matrix, the reason for this being that the normal coordinate for translation has been neglected. The elements of the $[L]$ matrix for the totally symmetric vibrations of the cyanogen halides can be calculated from the theory of molecular vibrations in the way shown in Appendix III.

For the excited state, Equation 9.42 can be written in the following form after substitution of Equation 9.41.

$$[\eta'] = [L'][Q'] = [L']\{[Q''] - [D]\} \tag{9.43}$$

Relative to the equilibrium configuration of the ground electronic state, for which $[Q''] = 0$, this equation becomes

$$[\eta'] = [L'][D] \tag{9.44}$$

The negative sign has been dropped here since, as explained previously, the signs of the $[D]$ matrix elements cannot be determined from this

calculation.

The mass-weighted Cartesian displacement coordinate η_i for atom i is calculated as above, and the corresponding Cartesian displacement coordinate ξ_i is obtained from the relation

$$\xi_i = m_i^{-\frac{1}{2}} \eta_i \qquad (9.45)$$

where m_i is the mass of atom i. ξ_i is the physical displacement of atom i from its equilibrium position in the ground electronic state upon electronic excitation. Therefore, the change Δr_{ij} in the bond length between atoms i and j is simply given by

$$\Delta r_{ij} = \xi_j - \xi_i \qquad (9.46)$$

Δr_{ij} is the change in the equilibrium bond length between atoms i and j upon electronic excitation, and so if the ground state bond lengths are known, the excited state bond lengths are obtained.

The only problem with this method of structure determination is that there are several possible structure changes which can account equally well for the observed intensity distribution since the signs of the d_i are not determined. For the cyanogen halides, the changes in the two totally symmetric normal coordinates can be calculated; but the sign of each change can be either positive or negative. Thus, there are four ($= 2^2$) possible excited state structures which can account for the intensity distribution in the spectrum of each molecule. To distinguish between these, it is necessary to appeal to other evidence. Some possibilities are band contour calculations, simplified Franck-

Condon calculations, and semi-empirical relations of bond lengths and vibrational frequencies. These will be discussed in more detail when the experimental results are examined.

9.6 Rydberg Transitions

Transitions to the lower excited states of molecules are classed as intra-valence shell transitions when the upper molecular orbitals are formed, in LCAO/MO approximation, from valence shell atomic orbitals of the atoms of the molecule. At higher energy, spectra are observed which are due to transitions to excited molecular orbitals in which the principal quantum number of the atomic orbitals is greater than the value in the valence shell; these transitions are extravalence shell transitions. A series of spectra resulting from extravalence shell transitions in which the principal quantum number of one of the atomic orbitals in the upper molecular orbital increases by unity is called a Rydberg series, and the energies of the origin bands of the spectra fit the following equation from atomic spectroscopy.[84]

$$\sigma_n = \sigma_{\infty} - \frac{R}{(n-\delta)^2} = \sigma_{\infty} - T_n \qquad (9.47)$$

Here, σ_n is the wavenumber of the origin band of the spectrum resulting from the transition to the orbital for which the index number is n, n is an integer, σ_{∞} is the series limit which is equal to an ionization potential of the molecule, R is the Rydberg constant for infinite mass (109,737 cm^{-1}), and δ is called the quantum defect. The part of the equation denoted T_n is called the term value and is equal to the energy difference (in cm^{-1}) between the series limit and the origin band of

the spectrum.

The fit of Equation 9.47 to the observed energies of the spectra improves as the index number n increases because the size of the molecular orbital increases and the field which the excited electron experiences becomes closer to a central field; that is, the transitions become more atomic - like and fit the atomic Rydberg equation better. In cases where well-developed Rydberg series are observed, very accurate ionization potentials can be obtained by use of Equation 9.47. Ionization potentials determined spectroscopically are adiabatic values, that is, they are the energies required to produce the molecular ion in the vibrationless level of an electronic state. Ionization potentials determined by other methods are usually vertical ionization potentials; they are the energies required to form the molecular ion in the vibrational level required by the Franck-Condon principle and so are usually greater than spectroscopic values.

In molecules containing non-bonding electrons localized to a large extent on one atom, it is often found that these non-bonding electrons are most readily excited in Rydberg series since they are most loosely bound. As a first approximation, the upper molecular orbitals of the Rydberg transitions may be considered to be atomic orbitals centred on the atom containing the non-bonding electrons. Atomic orbitals that are degenerate in the atom will become split into components of different symmetry under the point group of the molecule. Therefore, Rydberg molecular orbitals are labelled $n\ell\Gamma_i$, where n and ℓ are the principal and orbital angular momentum quantum numbers of the atomic orbital and Γ_i is the irreducible representation under the

molecular symmetry group. Table 9.3 shows the irreducible representations for s, p, and d atomic orbitals under the $C_{\infty v}$ and C_s point groups.

The selection rules for Rydberg transitions are the same as those discussed in Section 9.4. However, since the transitions are atomic-like in nature, the atomic selection rule $\Delta \ell = \pm 1$ is also approximately valid.

More than one Rydberg series leading to the same series limit is often observed in molecules just as in atoms. The reason for this is that different atomic orbitals having the same principal quantum number can be used to form molecular orbitals which differ in energy. Also, because of the lowered symmetry of the molecule, there will be a splitting of the degeneracy of the atomic orbitals as discussed above. The molecular orbitals formed from atomic orbitals of the same principal quantum number differ in energy, but the differences decrease as the principal quantum number increases since the potential field becomes closer to spherically symmetric. Therefore, Rydberg series involving these molecular orbitals have the same series limit. It is also possible to have Rydberg series leading to series limits which are greater than the lowest ionization potential of the molecule. These correspond to formation of the molecular ion in an excited state.

In Rydberg transitions involving non-bonding electrons, it is found empirically that although the series limit σ_∞ is often changed considerably from the atom to the molecule, the term values T_n, and so the quantum defect δ, are usually little changed from the atom to the molecule[85] because of the non-bonding nature of the orbitals involved

TABLE 9.3

THE IRREDUCIBLE REPRESENTATIONS OF SOME ATOMIC ORBITALS UNDER THE C_s AND $C_{\infty v}$ POINT GROUPS

Atomic Orbital	C_s	$C_{\infty v}$
s	a'	σ
p_x	a"	π
p_y	a'	
p_z	a'	σ
d_{z^2}	a'	σ
d_{yz}	a'	π
d_{xz}	a"	
$d_{x^2-y^2}$	a'	δ
d_{xy}	a"	

in the transitions. It has also been found in many cases that there is often little change of the molecular structure upon excitation to Rydberg states, again because of the non-bonding nature of the molecular orbitals involved.

CHAPTER 10

DESCRIPTION AND ANALYSIS OF THE SPECTRA

10.1 Survey of the Spectra

The electronic spectra observed for cyanogen chloride, cyanogen bromide and cyanogen iodide are shown schematically in Figure 10.1, which indicates very approximately the regions of absorption, the relative intensities of the spectra, and whether the absorption is continuous or vibrationally discrete. As can be seen from this figure, the spectra for the three compounds are quite similar in their general appearance, the major difference being that the spectra are shifted to longer wavelengths in the order cyanogen chloride, cyanogen bromide, cyanogen iodide.

For all three cyanogen halides, a region of weak continuous absorption, here labelled A, is observed at longest wavelengths. At somewhat shorter wavelengths, a second absorption system labelled α, which is not well characterized but has about the same intensity as system A, is observed. Two regions of vibrationally discrete intense absorption, labelled B and C, are situated further to shorter wavelengths. Because the short wavelength limit of the spectrograph is in the region 1250-1300 Å, no absorption beyond the B and C systems has been observed for cyanogen chloride. For cyanogen bromide a small amount of absorption and for cyanogen iodide considerably more absorption has been observed to short wavelengths of the B and C systems. This absorption is discrete but rather complex.

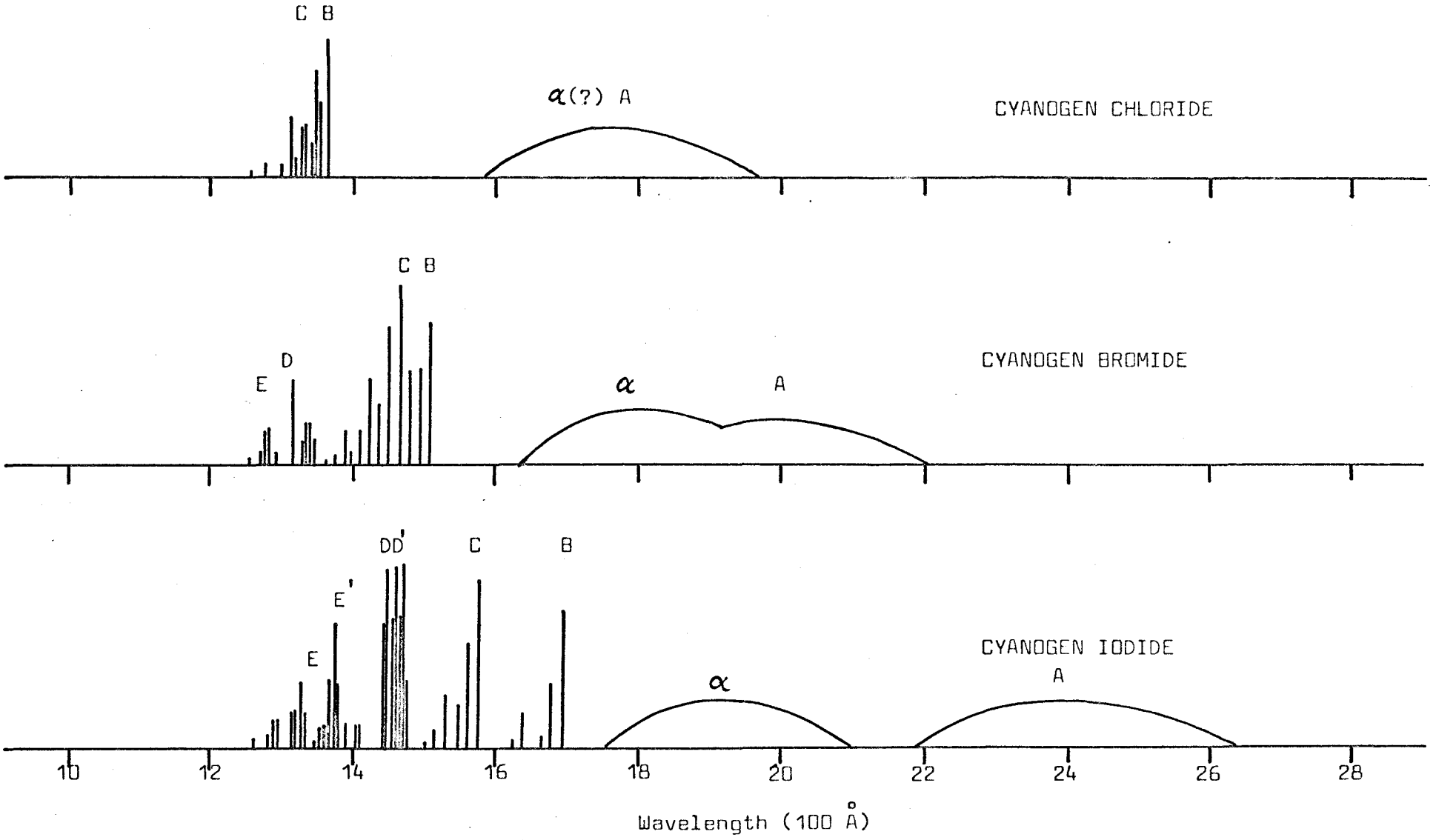

FIGURE 10.1: SCHEMATIC REPRESENTATION OF THE ELECTRONIC ABSORPTION SPECTRA OF THE CYANOGEN HALIDES

The absorption regions which have been given the same labels in the three cyanogen halides are quite similar in their general appearance and their intensities of absorption. Therefore, the regions with the same labels are considered together in the following sections. The spectra which have been observed are described and analyzed, and similarities in the electronic transitions causing the various spectra of the cyanogen halides are discussed.

10.2 Cyanogen Halide A Systems

10.2.1 Experimental Data

The cyanogen halide absorption spectra labelled A were observed for cyanogen iodide in n-heptane and aqueous solutions, for cyanogen bromide in n-heptane and aqueous solutions and in the vapour phase, and for cyanogen chloride in the vapour phase on a Cary Model 14 spectrophotometer. Under these conditions, the A systems for all three molecules appear to be continuous, the band widths at half-height being about 7000 cm^{-1}. Average wavelengths for the regions of maximum absorption for cyanogen iodide and cyanogen bromide as determined from the Cary spectrophotometer are given in Table 10.1; the precision in these values is about ± 5 Å. Average oscillator strengths calculated for the A systems of cyanogen iodide and cyanogen bromide in the way described in Section 8.4.1 are also given in Table 10.1. The precision in the oscillator strengths calculated for different concentrations or different pressures is about $\pm 15\%$.

The wavelength of maximum absorption for the cyanogen chloride A system was found to be about 1775 Å from plates taken on the off-plane Eagle vacuum spectrograph. The whole A system of cyanogen chloride

TABLE 10.1

WAVELENGTHS OF MAXIMUM ABSORPTION (λ_{max}) AND OSCILLATOR STRENGTHS FOR THE CYANOGEN HALIDE A SYSTEMS

Compound	λ_{max}, Å			Oscillator Strength	
	n-heptane	water	vapour	n-heptane	vapour
ICN	2410	2230	----	4.8×10^{-3}	----
BrCN	1990	1915	1990	5.5×10^{-3}	2.5×10^{-3}
ClCN	----	----	~1775	----	~4.8×10^{-3}

TABLE 10.2

LONG WAVELENGTH ABSORPTION FOR SOME ORGANIC HALIDES

Compound	λ_{max}, Å	Oscillator Strength	Reference
CH_3I	2575	8.7×10^{-3}	87
s-C_4H_9I	2606	12.5	87
CH_2=CHI	2500	5-8	89
RC≡CI	2555	8.1	92
CH_3Br	2020	10.6	87
s-C_4H_9Br	2065	8.1	87
RC≡CBr	2195	12.5	92
CH_3Cl	~1740	----	102
RC≡CCl	~1740	----	92

could not be recorded on the Cary spectrophotometer because the short wavelength limit of this instrument is 1840 Å. In order to obtain an estimate of the intensity of the cyanogen chloride A system, the oscillator strength was calculated on the assumption that the absorption was symmetric about 1840 Å, and the value thus obtained was doubled to make allowance for the fact that the absorption maximum is actually at about 1775 Å. This value, which is given in Table 10.1, is not as accurate as those for cyanogen bromide and cyanogen iodide, but should certainly be of the right order of magnitude.

High resolution spectra taken in the vapour phase on the off-plane Eagle vacuum spectrograph show that the A systems for all three cyanogen halides are definitely continuous.

10.2.2 Assignment of the A Systems

The cyanogen halides all have sixteen valence electrons. Therefore, in terms of the simple molecular orbital treatment outlined in Section 9.2 and Appendix II, the ground electronic state should be linear and have the following electron configuration and state symmetry for all three molecules.

$$(1\sigma)^2(2\sigma)^2(3\sigma)^2(4\sigma)^2(1\pi)^4(2\pi)^4 \qquad X\,{}^1\Sigma^+ \qquad (10.1)$$

This has been shown to be the correct symmetry from the microwave spectra.

The A systems of the cyanogen halides are the lowest energy electronic spectra observed for them. The upper electronic state is assigned to the electron configuration resulting from the promotion of an electron from the 2π molecular orbital to the 5σ molecular orbital.

Figure 9.2 shows that the cyanogen halides should be linear in this excited state and have the following electron configuration and state symmetry.

$$(1\sigma)^2(2\sigma)^2(3\sigma)^2(4\sigma)^2(1\pi)^4(2\pi)^3(5\sigma) \qquad A\,^1\Pi \qquad (10.2)$$

Although this electron configuration gives a $^3\Pi$ state also, the upper state of the A systems is probably the singlet one because the intensity of the spectra for the three molecules are all about the same, although there is a slight increase from cyanogen iodide to cyanogen bromide to cyanogen chloride. If the triplet state were the upper state in these spectra, then the changes in intensity would be expected to be more pronounced and in the opposite order to that observed because the spin-orbit coupling is greater for the cyanogen halides containing the heavier halogens.

The 2π molecular orbital is an $np\pi$ orbital, that is, it is essentially a non-bonding p atomic orbital of π symmetry localized on the halogen atom. The 5σ molecular orbital is a σ^* orbital which is anti-bonding between the halogen and carbon atoms; in a first approximation, 5σ can be taken to be $np\sigma$ orbital, that is, a p atomic orbital of σ symmetry localized on the halogen atom. Therefore, the electronic transition causing the A systems of the cyanogen halides is essentially an $np\sigma \leftarrow np\pi$ transition and is denoted Q←N in Mulliken's notation. Transitions of this type are expected to be relatively weak because they are forbidden by the atomic selection rule $\Delta\ell = \pm 1$. This explains the low intensity observed for the cyanogen halide A systems.

There are several reasons for the assignment given above for the cyanogen halide A systems. The first is that a spectrum which is

continuous and has a band half-width in the order of 6000 cm^{-1} is observed at longest wavelengths in many compounds containing a carbon-halogen bond. Table 10.2 lists the wavelengths of maximum absorption and the measured oscillator strengths for a few of these compounds in hydrocarbon solvents. This table shows that the oscillator strengths are about the same as have been observed for the cyanogen halide A systems and that the wavelengths of maximum absorption are mainly dependent on the nature of the halogen atom. These facts support the idea that the electronic transition is localized to a large extent in the region of the carbon-halogen bond. Mulliken[86] first gave an assignment for these absorption systems of the methyl halides analogous to that given here for the cyanogen halide A systems. More recently, Mulliken's assignment has been confirmed for the first absorption systems of various alkyl halides by Kimura and Nagakura[87] and similar assignments have been suggested for the first absorption systems of various halogenated alkynes and vinyl iodide by Moreau and Serre[88] and by Schaufele and Goodman,[89] respectively.

A fact that supports the identification of the 2π molecular orbital as an $np\pi$ orbital as stated above is that upon changing from n-heptane to distilled water as solvent, the A systems of cyanogen bromide and cyanogen iodide are shifted to higher energies. Similar behaviour is observed in the $\pi^* \leftarrow$ n transitions in carbonyl compounds in which an electron is promoted from the n orbital, which is a non-bonding p orbital localized on the oxygen, to the π^* orbital, which is an anti-bonding π orbital localized on the carbonyl group, and is attributed to formation of a hydrogen bond between the non-bonding n

electrons of the carbonyl oxygen and a proton of a water molecule.[90,91] The hydrogen bond lowers the energy of the n orbital relative to the energy in n-heptane, where there is no hydrogen bond, but does not affect the energy of the π^* orbital. This results in the electronic spectrum being shifted to higher energies. Similar behaviour has been observed in various organic halogen compounds[87] and is explained as being due to hydrogen bonding between the npπ electrons of the halogen and a proton of a water molecule.

The fact that the A spectra of the cyanogen halides are continuous under high resolution suggests that the upper state potential surface is repulsive and leads to dissociation of the molecule. This is supported by the fact that flash photolysis studies[63] of cyanogen bromide and cyanogen iodide have shown that when radiation is absorbed by the A systems of these molecules, they dissociate into a CN radical and a halogen atom. This is consistent with the promoted electron entering the 5σ orbital, which is anti-bonding between the halogen and carbon atoms. From the correlation rules given by Schuler,[96] it can be shown that a cyanogen halide molecule in the $A\,^1\Pi$ state correlates with a halogen atom in the ^2P state and a CN radical in the $X\,^2\Sigma^+$ ground state. The flash photolysis studies of cyanogen bromide and cyanogen iodide indicate that the molecules dissociate into a halogen atom in the ^2P state and a CN radical in either the $X\,^2\Sigma^+$ ground state or the low lying $A\,^2\Pi$ state. The results obtained from this study of the electronic spectra indicate that the CN radical is formed in its ground state.

Calculations by Moreau and Serre[88] on the halogenated acetylenes, which are iso-electronic with the cyanogen halides, indicate that for

an $np\sigma \leftarrow np\pi$ transition the oscillator strengths should increase in the order iodide, bromide, chloride. The results obtained in this investigation, which are summarized in Table 10.1, follow this order and thus provide support for this assignment.

In summary, the experimental evidence that is available supports the assignment of the A systems of the cyanogen halides to the transition $A\,^1\Pi \leftarrow X\,^1\Sigma^+$, with the upper state probably having the electron configuration in (10.2). It is not possible to obtain further evidence from vibrational or rotational analyses to support the assignment because the spectra are continuous.

10.3 Cyanogen Halide α Systems

10.3.1 Experimental Data

The experimental evidence which has been obtained for this region of absorption of the cyanogen halides is not as conclusive as that for the other regions of absorption in these molecules and so it is not possible to be as certain of the conclusions which are made about it.

The spectra of cyanogen iodide in n-heptane and aqueous solutions taken on the Cary spectrophotometer show absorption starting in the region 2100-2000 Å and extending to shorter wavelengths. Spectra of cyanogen iodide vapour taken on the off-plane Eagle vacuum spectrograph show absorption in the region 2000-1800 Å which is probably continuous. However, it was not possible to obtain good spectra with the 75 cm absorption cell that was used because the vapour pressure of cyanogen iodide is quite low at room temperature and the compound decomposes upon heating. There was also a problem with interference by the strong absorption of methyl iodide in this region. The methyl iodide was either present as a trace impurity in the samples or was produced by

the reaction of iodine atoms, formed by dissociation of cyanogen iodide upon absorption of radiation by the A system, with the grease used on the stopcock of the absorption cell. Independent confirmation that cyanogen iodide shows absorption in this region is given by the low resolution work of Yakovleva[57] who reports continuous absorption in the region 2000-1800 Å with maximum absorption at about 1890 Å and an oscillator strength of 2.9×10^{-3}.

Spectra of cyanogen bromide and cyanogen chloride taken on the vacuum spectrograph also show absorption in the region of 1800 Å. But, with these compounds as for cyanogen iodide, there was some methyl iodide impurity present which was very difficult to remove and absorbed very strongly in this region, thus obscuring to a large extent the absorption by cyanogen bromide and cyanogen chloride. In the case of cyanogen chloride there was also the problem that the A system lies in the region of 1800 Å and so prevented a positive identification of the α system.

10.3.2 Assignment of the α Systems

As discussed in Section 9.2, there are two possible explanations for a second low-lying excited electronic state of the cyanogen halides. One possibility is that this state arises from the electron configuration produced by promotion of one electron from the 1π molecular orbital to the 5σ molecular orbital; that is, the electron configuration and state symmetry are

$$(1\sigma)^2(2\sigma)^2(3\sigma)^2(4\sigma)^2(1\pi)^3(2\pi)^4(5\sigma) \qquad {}^1\Pi \qquad (10.3)$$

where only the singlet state is considered.

The excited state should remain linear in this case. The second possibility is that the excited state is one of those resulting from the electron configuration caused by promotion of one electron from the 2π molecular orbital to the 3π molecular orbital. If only singlet states are considered, then for a linear molecule the electron configuration and state symmetries are

$$(1\sigma)^2(2\sigma)^2(3\sigma)^2(4\sigma)^2(1\pi)^4(2\pi)^3(3\pi)^1 \quad {}^1\Sigma^+, {}^1\Sigma^-, {}^1\Delta \qquad (10.4)$$

whereas for a non-linear molecule the possible electron configurations and state symmetries are

$$(1a')^2(2a')^2(3a')^2(4a')^2(1a'')^2(5a')^2(2a'')^2(6a')^1(8a')^1 \qquad {}^1A' \qquad (10.5.a)$$

$$(2a'')^1(6a')^2(8a')^1 \qquad {}^1A'' \qquad (10.5.b)$$

$$(2a'')^2(6a')^1(3a'')^1 \qquad {}^1A'' \qquad (10.5.c)$$

$$(2a'')^1(6a')^2(3a'')^1 \qquad {}^1A' \qquad (10.5.d)$$

As discussed previously, Figure 9.2 indicates that (10.5.a) and (10.5.b) should correspond to stable non-linear excited states and (10.5.c) and (10.5.d) to stable linear excited states. Also, the non-linear excited states should lie at considerably lower energy than the linear excited states.

A fact that would support (10.3) being the excited state of the α systems of the cyanogen halides is that the spectra appear to be continuous as for the A systems. This would be more likely to be the case if the upper state involved the 5σ molecular orbital which is strongly anti-bonding. However, evidence that would favour the excited state being one of (10.5.a) or (10.5.b) comes from the analogy that can be made with the spectra observed by Romanet and Wojtkowiak[92] for various 1-alkynes and their 1-halogen derivatives in n-heptane solution which

are summarized in Table 10.3. The absorption of the 1-alkynes with λ_{max} at ~1865 Å is almost certainly caused by a $\pi^* \leftarrow \pi$ transition leading to a non-linear excited state as has been observed for acetylene.[93,94] For the 1-halo-1-alkynes two absorptions are observed; the first, whose λ_{max} depends upon the nature of the halogen atom, is observed at longer wavelengths and the second, whose λ_{max} is almost constant, is observed at shorter wavelengths. The absorptions at longer wavelengths can be assigned to an $np\sigma \leftarrow np\pi$ transition just as in the cyanogen halides, whereas the absorption systems at shorter wavelengths are likely the analogues of the $\pi^* \leftarrow \pi$ transitions observed for the 1-alkynes, although it is possible that they result from a $\sigma^* \leftarrow \pi$ transition, the upper state being analogous to (10.3).

The spectra of acetylene itself and the corresponding 1-halo-acetylenes are probably related in the same way as the spectra for the 1-alkynes and the 1-halo-1-alkynes. Because acetylene and the 1-halo-acetylenes are isoelectronic with hydrogen cyanide and the cyanogen halides, respectively, it is reasonable to expect that the second absorption system of the cyanogen halides would correspond to the first absorption system of hydrogen cyanide. The first absorption system of hydrogen cyanide[95] has been shown to be caused by a $\pi^* \leftarrow \pi$ transition resulting in a non-linear molecule in the excited state. Therefore, the absorption in the 1800 Å region for the cyanogen halides may be due to a $\pi^* \leftarrow \pi$ transition.

The upper electronic state responsible for the α systems of the cyanogen halides cannot be assigned unambiguously from the available experimental evidence. The electronic transition is either $^1\Pi \leftarrow X\,^1\Sigma^+$, the upper state being linear and having the electron configuration (10.3), or $^1A'$ or $^1A'' \leftarrow X\,^1\Sigma^+$, the upper state being

TABLE 10.3

ABSORPTION OF SOME 1-ALKYNES AND 1-HALO-1-ALKYNES

Compound*	λ_{max}, Å	ϵ_{max}	Oscillator Strength (Approximate)
RC≡CH	1865	450	9.7×10^{-3}
RC≡CI	2555	335	7.2
	1925	3000	65.
RC≡CBr	2195	525	11.3
	1890	750	16.2
RC≡CCl#	1940	950	20.5

* R = n-C_mH_{2m+1}, m=3,4,5,6.

very broad band

non-linear and having the electron configuration (10.5.a) or (10.5.b), respectively.

10.4 Cyanogen Halide B and C Systems

The B and C systems of the three cyanogen halides are considered together because, as will be shown later, they are closely related. These two systems are the first strong absorption systems observed for the cyanogen halides, a pressure of their vapours in the order of 0.01-0.1 mm Hg in a 15 cm path length being sufficient to produce strong absorption. The oscillator strengths for these electronic transitions are probably of the order of 10^{-2} -10^{-1}. Such relatively large values indicate that the transitions are allowed by the symmetry selection rules.

10.4.1 Cyanogen Iodide B and C Systems

The cyanogen iodide B and C systems each consist of a number of vibrational bands as shown in the microdensitometer traces of Figure 10.2. Examination of various bands in the third order of the off-plane Eagle vacuum spectrograph showed no signs of rotational structure, thus indicating either that the resolving power is insufficient or that the bands are predissociated. As will be shown later, it is more likely that the bands are predissociated.

The measured wavelengths, wavenumbers, and relative intensities of the vibrational bands are given for the B system in Table 10.4 and for the C system in Table 10.5. The precision in the wavelengths is about $\pm$0.1 Å (corresponding to about $\pm$5 cm^{-1}), the uncertainty being caused by the width of the bands and the lack of sharp features in them. The precision in the relative intensities is about $\pm$0.02 in

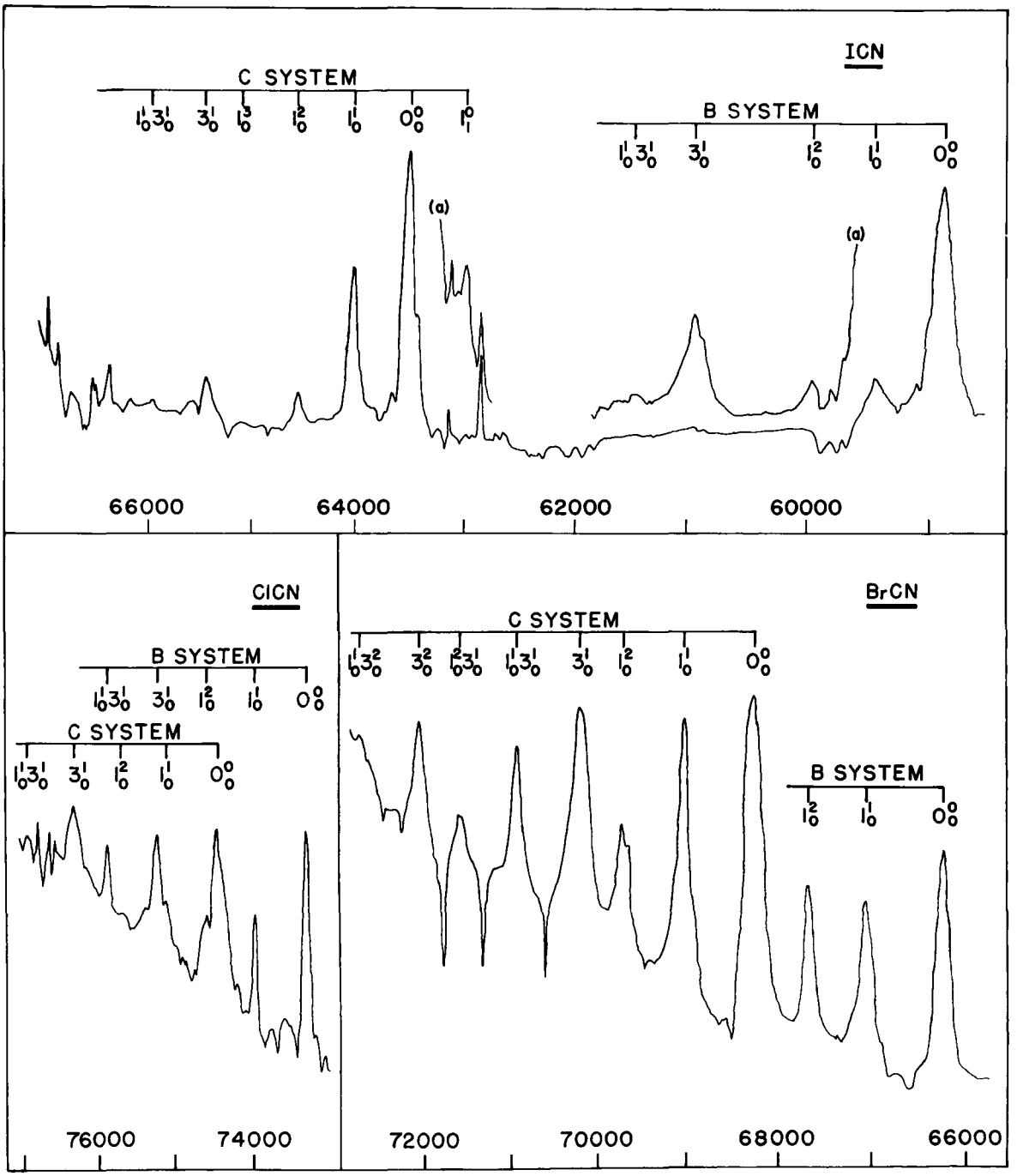

FIGURE 10.2

THE B AND C ABSORPTION SYSTEMS OF THE CYANOGEN HALIDES

The units on the abscissa are cm^{-1}. For cyanogen iodide the traces labelled (a) were obtained at higher pressures.

TABLE 10.4

ASSIGNMENT OF THE VIBRATIONAL BANDS FOR THE CYANOGEN IODIDE B SYSTEM

λ, Å	σ, cm^{-1}	Relative Intensity	Assignment
(1712.7)	(58389)	-----	1_1^0
1698.2	58887	1.000	0_0^0
1682.5	59434	0.306	1_0^1
1667.8	59960	(0.022)	1_0^2
1640.9	60945	0.057	3_0^1
1626.8	61472	(0.021)	$1_0^1 3_0^1$

TABLE 10.5

ASSIGNMENT OF THE VIBRATIONAL BANDS FOR THE CYANOGEN IODIDE C SYSTEM

λ, Å	σ, cm^{-1}	Relative Intensity	Assignment
1587.5	62991	-----	1_1^0
1575.5	63471	1.000	0_0^0
1562.6	63997	0.766	1_0^1
1549.6	64532	0.258	1_0^2
1536.8	65072	-----	1_0^3
1528.5	65424	0.255	3_0^1
1516.1	65959	(0.054)	$1_0^1 3_0^1$
(1504.5)	(66468)	-----	$1_0^2 3_0^1$

the relative units used in the tables, which are proportional to the absorbance as explained in Section 8.4. Values given in parentheses in Tables 10.4 and 10.5 are less certain than the others. Dashes indicate that no value was obtained experimentally.

The origin band of the C system of cyanogen iodide is about 1.2 times as intense as the origin band of the B system. Also, the C system has more vibrational bands, thus giving it a total integrated intensity which is about one and one-half times that of the B system.

There are no long progressions of vibrational bands and the intensity falls off rather rapidly to shorter wavelengths of the first strong band in each of the spectra. Therefore, it is apparent that the B and C systems of cyanogen iodide have linear excited states and that there is little change in the molecular dimensions upon electronic excitation since any gross change in geometry would result in extensive vibrational progressions in accordance with the Franck-Condon principle. When the molecule is linear in both the combining electronic states, the Herzberg-Teller selection rules state that only progressions in the totally symmetric vibrational modes can be excited strongly in the spectrum. Cyanogen iodide has three normal vibrational modes; two of these, ν_1 and ν_3, are totally symmetric and are largely localized in the I-C and C-N bonds, respectively, and the third, ν_2, is a doubly-degenerate bending vibration. The values of the three vibrational frequencies in the ground electronic state of cyanogen iodide are given in Table 10.10.

The observed vibrational bands of the B and C systems of cyanogen iodide can be explained satisfactorily in terms of two totally

symmetric vibrational modes and the analyses for the B and C systems are given in Tables 10.4 and 10.5, respectively, in the notation first described by Innes and Callomon.[100] The vibrational modes which are active in a given vibronic band are indicated by their numbers. The number of quanta of a vibrational mode which are excited in the upper and lower electronic states are indicated by superscripts and subscripts, respectively, following the number for that vibrational mode. The electronic origin band, for which no vibrational quanta are excited in either state, is denoted as 0_0^0.

Since it is possible to measure the relative intensities of several bands in each of the progressions of the two totally symmetric vibrations for the B and C systems of cyanogen iodide, the theory of Franck-Condon calculations discussed in Section 9.5 can be used to calculate the changes in the two bond lengths of the cyanogen iodide molecule upon electronic excitation. Equations 9.36 - 9.39 were used to calculate the absolute values of d_1 and d_3, the changes in the two totally symmetric normal coordinates, from the observed vibrational frequencies and relative intensities of the B system. The elements of the [L] matrix were calculated from the excited state vibrational frequencies and the atomic masses by the method described in Appendix III and substituted together with d_1 and d_3 in Equations 9.44 - 9.46 to calculate the changes in the bond lengths of the molecule.

The problem in the determination of the bond length changes is that the signs of d_1 and d_3 are not determined since the squares of the vibrational overlap integrals are used in the calculation. Because of this, there are four pairs of changes in bond lengths which are consistent with the observed intensity distribution. The four pairs

which have been calculated for the cyanogen iodide B system are listed as (a), (b), (c), and (d) in Table 10.6. The pairs (a) and (b) and the pairs (c) and (d) have the same absolute value because in going from (a) to (b) or from (c) to (d) the signs of both d_1 and d_3 are changed, whereas in going from (a) or (b) to (c) or (d) the sign of only one of d_1 and d_3 is changed.

The problem now is to determine which of the four possibilities corresponds to the actual changes occurring in the molecule. The best way to make the choice is by means of a rotational band contour analysis. Since the bond lengths in the ground state are accurately known (see Table 7.1), the excited state bond lengths for each of the four possibilities were obtained. These data were used with a computer program which calculates the energies and intensities for the possible transitions between the rotational levels of the linear molecule in the two combining vibronic states and then integrates the intensities and prints out the resulting band contour. The contours which were obtained for all four possible sets of excited state dimensions showed sharp heads. Since no sharp features were found in the observed spectra and the bands appeared to be predissociated, it was concluded that the vibronic bands must be predissociated and that no information could be obtained from the band contour calculations.

However, simplified Franck-Condon calculations enabled a choice to be made between the possible excited state geometries. This method has been used with good results by Craig[97] in the case of benzene and by several investigators[98] for carbonyl compounds. If a given normal vibration is localized to a large extent in one bond of a molecule, then it is a good approximation to set the change in the corresponding

normal coordinate equal to the change in that bond length. To check the degree of localization of the vibrational modes in the B excited state of cyanogen iodide, the potential energy distribution was calculated in the way described in Appendix IV. The potential energy distribution for each normal mode of vibration of a molecule gives the contribution to the potential energy from each of the force constants considered and is a measure of the localization of each normal mode in different parts of the molecule. The results given in Table 10.7 show that for the B state of cyanogen iodide ν_1' is 92% localized in the I-C bond and 8% in the C-N bond, while the opposite is true for ν_3'. Therefore, it would be expected that Franck-Condon calculations based on the assumption that the vibrations ν_1' and ν_3' are completely localized in the I-C and C-N bonds, respectively, will give results which are fairly close to the true values. The bond length changes that give the best agreement between the calculated and observed intensity distributions in the progressions in these vibrations are given as (e) of Table 10.6. These values are the moduli of the actual bond length changes since, as before, it is not possible to determine the signs of the changes from the relative intensities alone. The values from the simplified calculation agree fairly closely with the pairs of values (a) and (b) in Table 10.6 and so now the choice must be made between these two pairs of values.

The choice between the possible pairs of values (a) and (b) of Table 10.6 has been made on the basis of Clark's and Badger's rules.[99] These rules are empirical relations of bond length and vibrational frequency which have been developed for diatomic molecules. They do not give accurate values even for diatomic molecules and so in using

TABLE 10.6

POSSIBLE BOND LENGTH CHANGES FOR THE CYANOGEN IODIDE B SYSTEM (PRECISION IN mÅ given in parentheses)

Calculation	Δr(IC), Å	Δr(CN), Å
a	-0.051(2)	0.010(2)
b	0.051(2)	-0.010(2)
c	0.032(3)	0.023(2)
d	-0.032(3)	-0.023(2)
e	0.045	0.012
f	-0.086	0.019
g	-0.035	0.008

TABLE 10.7

POTENTIAL ENERGY DISTRIBUTION FOR THE CYANOGEN IODIDE B SYSTEM

Normal Mode	k_{12}(IC)	k_{23}(CN)
ν_1	0.92	0.08
ν_3	0.08	0.92

them for polyatomic molecules they will be less accurate still since it is necessary to treat each bond as a separate diatomic molecule. Clark's rule has been used here in the form

$$r_e'^{3}\,\omega_e' = r_e''^{3}\omega_e'' \qquad (10.6)$$

where r_e and ω_e are the bond length and vibrational frequency in a given electronic state and the upper and lower electronic states are indicated by single and double primes, respectively. Badger's rule has been used in the form

$$\omega_e'(r_e' - d_{ij})^3 = \omega_e''(r_e'' - d_{ij})^3 \qquad (10.7)$$

where r_e and ω_e are the same as above and d_{ij} is a constant which depends upon the rows of the periodic table to which the atoms i and j forming the bond belong. The values of d_{ij} which have been used here are summarized below.[118]

Row(atom i)	1	1	1	1
Row(atom j)	1	2	3	4
d_{ij}	0.68	0.94	1.06	1.18

The values of the bond length changes were calculated by Clark's and Badger's rules from the accurately known ground state bond lengths and the vibrational frequencies in the ground and excited states. The values calculated from Clark's and Badger's rules are given as (f) and (g), respectively, of Table 10.6. These support the bond length changes (a) obtained from the Franck-Condon calculations. The bond lengths in

the B state of cyanogen iodide are therefore found to be r(IC) = 1.94_3 Å and r(CN) = 1.16_9 Å.

The experimental data listed in Table 10.5 for the C system of cyanogen iodide can be used to calculate four possible pairs of changes in bond lengths upon excitation from the ground (X) state to the C state in exactly the same way as for the B system of cyanogen iodide. These are listed as (a), (b), (c), and (d) of Table 10.8. The potential energy distribution for the C excited state of cyanogen iodide, which is given in Table 10.9, shows that in the C state the vibrational modes ν_1' and ν_3' are localized to a large extent and so the changes in bond length calculated by the simplified Franck-Condon method, and given as (e) of Table 10.8, should be a good approximation to the absolute values of the true bond length changes. These indicate that the values of (a) or (b) are correct. The values of (a) are chosen as correct on the basis of the results obtained from Clark's and Badger's rules which are given as (f) and (g) of Table 10.8. Therefore, the bond lengths in the C state of cyanogen iodide are calculated to be r(IC) = 1.91_1 Å and r(CN) = 1.18_3 Å.

The vibrational frequencies and bond lengths for the X, B, and C states of cyanogen iodide are collected together in Table 10.10. In the ground state, the values of ν_2'' and ν_3'' are from the Raman spectrum[45] and the bond lengths are from the microwave spectra.[36] The value of 480 cm^{-1} for ν_1'' in the ground state has been obtained from the hot band 1_1^0 in the C system of cyanogen iodide; this value is also obtained from the infrared spectrum of cyanogen iodide in non-polar solvents.[119] The vibrational frequencies listed are probably accurate to about 10 cm^{-1}.

TABLE 10.8

POSSIBLE BOND LENGTH CHANGES FOR THE CYANOGEN IODIDE C SYSTEM (PRECISION IN mÅ GIVEN IN PARENTHESES)

Calculation	$\Delta r(IC)$, Å	$\Delta r(CN)$, Å
a	-0.083(3)	0.024(2)
b	0.083(3)	-0.024(2)
c	0.042(2)	0.045(3)
d	-0.042(2)	-0.045(3)
e	0.071	0.025
f	-0.060	0.041
g	-0.024	0.017

TABLE 10.9

POTENTIAL ENERGY DISTRIBUTION FOR THE CYANOGEN IODIDE C SYSTEM

Normal Mode	$k_{12}(IC)$	$k_{23}(CN)$
ν_1	0.91	0.09
ν_3	0.09	0.91

TABLE 10.10

VIBRATIONAL FREQUENCIES AND BOND LENGTHS FOR THE CYANOGEN IODIDE X, B, AND C STATES

State	ν_1, cm^{-1}	ν_2, cm^{-1}	ν_3, cm^{-1}	r(IC), Å	r(CN), Å
X	480	321	2158	1.994	1.159
B	547	---	2058	1.94_3	1.16_9
C	526	---	1953	1.91_1	1.18_3

The precision in the bond lengths calculated for the B and C systems of cyanogen iodide is about $\pm$0.005 Å. However, the accuracy is probably not as good as this figure suggests since the method of calculation involves several approximations, such as the use of harmonic oscillator wave functions and the neglect of the force constant between the halogen and nitrogen atoms. The bond length determined by Franck-Condon calculations[120] for the 1240 Å system of water differs by about 0.01 Å from the value obtained by a rotational analysis.[121] The errors in this investigation are probably of this order of magnitude also.

10.4.2 Cyanogen Bromide B and C Systems

A microdensitometer trace of the B and C systems of cyanogen bromide is given in Figure 10.2. The wavelengths, wavenumbers and relative intensities that have been measured for cyanogen bromide are listed in Table 10.11 for the B system and Table 10.12 for the C system. The precision in the wavelengths is about $\pm$0.15 Å (corresponding to about $\pm$7 cm^{-1}), and the precision in the relative intensities is about $\pm$0.04 of the relative units used, which are proportional to the absorbance. Again, the uncertainty in the wavelengths is a result of the lack of sharp features in the bands which could be used for measurement. Values given in parentheses are less certain than the others and dashes indicate that no value was obtained experimentally.

The B and C systems of cyanogen bromide have a smaller wavenumber separation than the B and C systems of cyanogen iodide, and there is overlapping of the two systems which prevents observation of much of the B system. The origin band of the C system is approximately one and one-half times as intense as the origin band of the B system and the C

TABLE 10.11

ASSIGNMENT OF THE VIBRATIONAL BANDS FOR THE CYANOGEN BROMIDE B SYSTEM

λ, Å	σ, cm^{-1}	Relative Intensity	Assignment
(1520.9)	(65750)	-----	1_1^0
1508.5	66290	1.000	0_0^0
1490.9	67076	0.665	1_0^1
1477.6	67680	0.650#	1_0^2
1464.3*	68290*	0.100*	3_0^1

overlapped by 1_1^0 of C system.

* assumed

TABLE 10.12

ASSIGNMENT OF THE VIBRATIONAL BANDS FOR THE CYANOGEN BROMIDE C SYSTEM

λ, Å	σ, cm^{-1}	Relative Intensity	Assignment
(1477.6)	(67680)	(0.433)#	1_1^0
1464.6	68278	1.000	0_0^0
1448.6	69030	0.757	1_0^1
(1435.0)	(69687)	0.302	1_0^2
1424.4	70204	0.495	3_0^1
1409.8	70933	0.307	$1_0^1 3_0^1$
1397.0	71583	0.081	$1_0^2 3_0^1$
1387.3	72081	0.194	3_0^2
1373.4	72811	(0.068)	$1_0^1 3_0^2$
1361.4	73453	-----	$1_0^2 3_0^2$

overlapped by 1_0^2 of B system.

system has more vibrational structure so that the total intensity of the C system is about twice that of the B system.

As was the case for cyanogen iodide, the vibrational intensity distribution and structure of the cyanogen bromide B and C systems shows that the molecule stays linear in the excited states of these transitions and that the molecular structure is little changed from that in the ground electronic state. The frequencies of the three normal vibrations of cyanogen bromide in the ground electronic state are given in Table 10.17. The value of 584 cm^{-1} given there for ν''_1 has been corrected for Fermi resonance,[51] the value observed in the infrared spectrum[50] being 575 cm^{-1}. The vibrational structure of the B and C systems can be explained by the assumption of two vibrational frequencies in the excited state of the same order of magnitude as ν''_1 and ν''_3 in the same way as for cyanogen iodide, and the analyses are given in Tables 10.11 and 10.12 for the B and C systems of cyanogen bromide, respectively. However, there are some problems that were not present in the cyanogen iodide spectra.

For the B system of cyanogen bromide, the analysis gives the values 786 and 604 cm^{-1} for the first and second quanta, respectively, of ν'_1 in the excited state. The drop from the first to the second interval is much too large to be attributed to errors in measurement or anharmonicity since the contribution due to each of these quantities is expected to be of the order of 10 cm^{-1} or less. The reason for the large difference between the two intervals must be that there is a strong Fermi resonance between the two vibrational levels in the upper electronic state described by the vibrational quantum numbers $(1,0^0,0)$ and $(0,2^0,0)$, where the vibrational levels are described by the set of

quantum numbers (v_1, v_2^{ℓ}, v_3), v_i being the number of quanta of the i^{th} normal vibration excited and the superscript ℓ being the vibrational angular momentum quantum number for the asymmetric bending vibration ν_2. This perturbation causes the level $(1,0^0,0)$ to be shifted up by a large amount and so makes the first interval greater than it would be in the absence of Fermi resonance. A Fermi resonance might also be expected between the levels $(2,0^0,0)$ and $(0,4^0,0)$. However, for this pair of levels it is likely that the zeroth order frequencies do not lie so close together because of the effects of anharmonicity, and therefore the perturbation is not so large. The effects of the Fermi resonance on the energy levels of ν_1' and ν_2' in the excited state are shown schematically in Figure 10.3. For a Fermi resonance as shown, the first vibrational interval is greater and the second vibrational interval is smaller than in the absence of the Fermi resonance. The zeroth order value for ν_1' in the B excited state, that is, the value that would be observed for ν_1' if there were no Fermi resonance, can be estimated to be about 700 cm^{-1} by taking the average of the two observed vibrational intervals. This would require the value of ν_2' in the B state to be about 350 cm^{-1}, which is not at all unreasonable since the value of ν_2'' in the ground state[52] is 342 cm^{-1}.

A problem with the assignment that has been given is that the band 1_0^2 of the B system at 67680 cm^{-1} appears to have about the same intensity as the band 1_0^1. This probably results partially from overlap of the band 1_0^2 of the B system by the hot band 1_1^0 of the C system. If the 67680 cm^{-1} band is assigned solely to the latter, a value of 598 cm^{-1} is obtained for ν_1'', which differs somewhat more than expected from the value of 575 cm^{-1} observed in the infrared.[50] The reason for this is

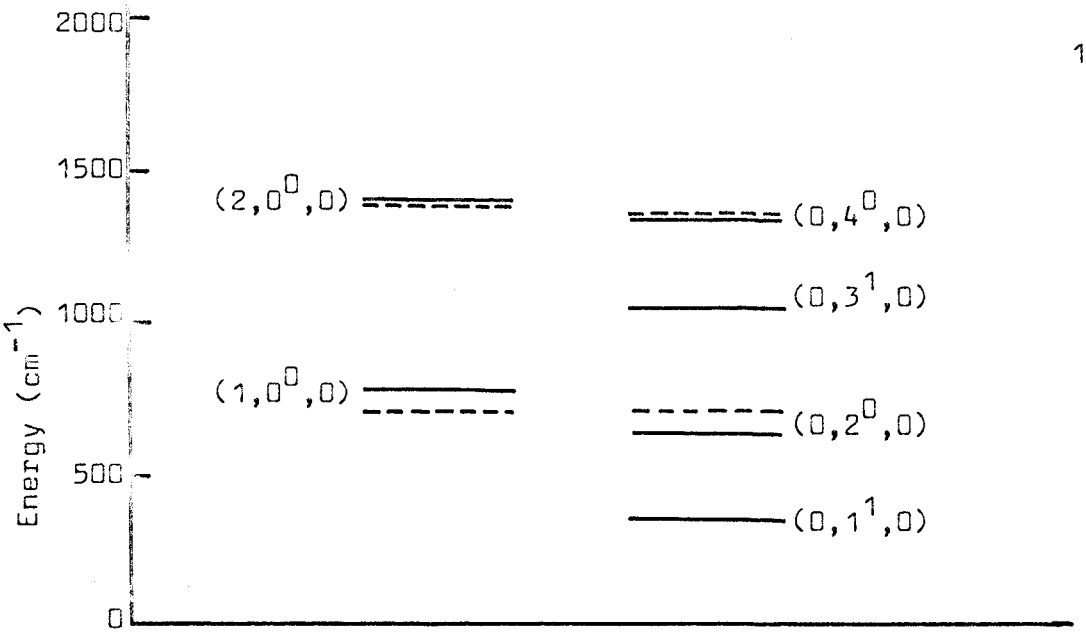

FIGURE 10.3

Fermi Resonance in the Cyanogen Bromide B and C Excited States. --- levels before Fermi resonance, —— levels after Fermi resonance.

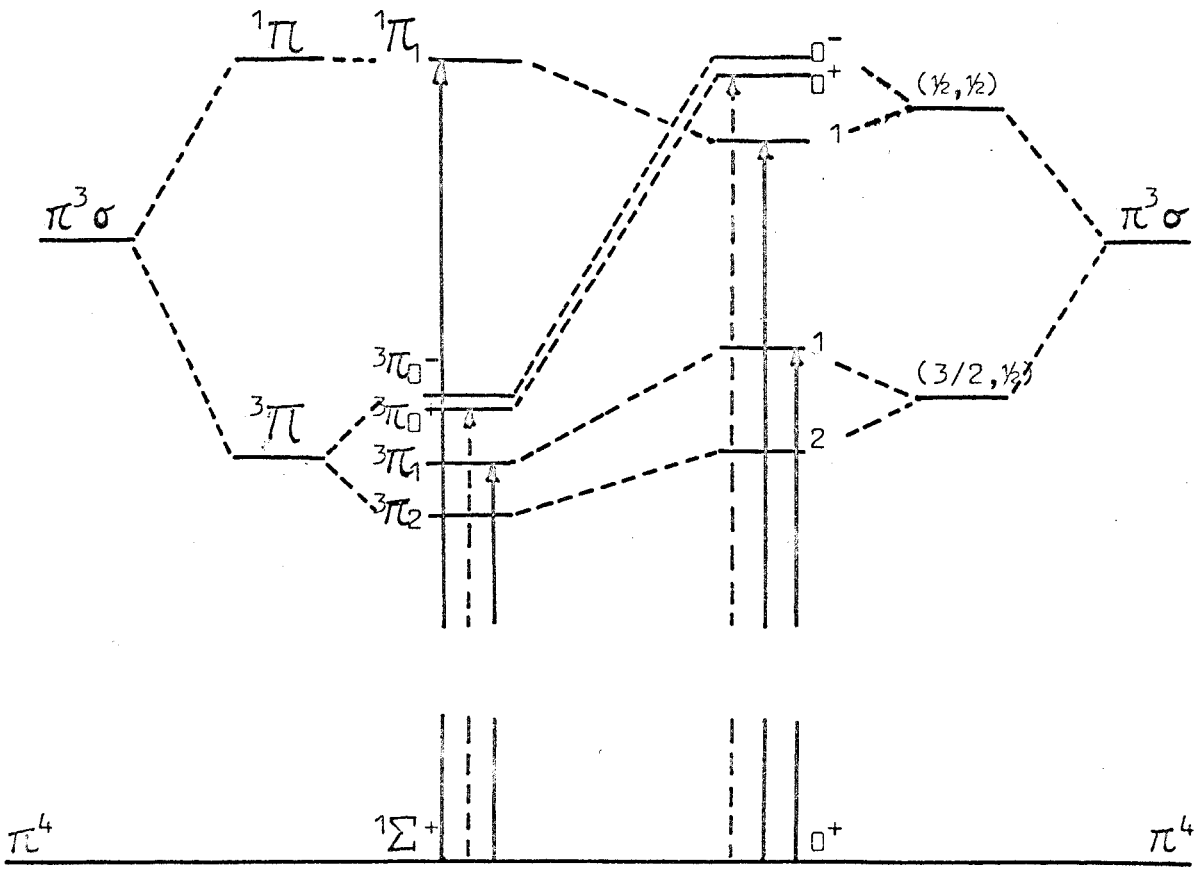

FIGURE 10.4

Correlation Diagram for (Λ,S) and (Ω_c,ω) Coupling of a ...$(\pi)^3(\sigma)$ Electron Configuration.

probably that the band 1_1^0 of the C system is considerably weaker than the band 1_0^2 of the B system and is buried beneath it. However, even with this overlapping of two bands, the band at 67680 cm^{-1} is still more intense relative to the band 1_0^1 at 67076 cm^{-1} than expected. Perhaps this is due to a weakening of the 1_0^1 band by the Fermi resonance discussed above.

The first quantum of ν_3' for the B system is expected to lie in the vicinity of the origin band for the C system, but there are no signs of it to be found in the spectrum. This is not too surprising since by analogy with the cyanogen iodide B system the first quantum of ν_3' should produce only a rather weak band whereas the origin band of the C system, which falls in the same region of the spectrum, is a very strong band which could prevent observation of any absorption due to the B system. The value of ν_3' for the B system of cyanogen bromide can be estimated to be about 2000 cm^{-1} from the fact that for the C system of cyanogen bromide ν_3' is 1926 cm^{-1}, and for cyanogen iodide and cyanogen chloride the values of ν_3' for the B system are greater than the values for the C system by about 100 and 50 cm^{-1}, respectively.

The C system of cyanogen bromide shows much more extensive vibrational structure than the B system. Two quanta of ν_3' are observed, the intervals being 1926 and 1877 cm^{-1}. The observed drop of about 50 cm^{-1} between quanta is reasonable for such a high frequency vibration. Progressions of two quanta of ν_1' are observed in combination with 0, 1, and 2 quanta of ν_3'. As is the case in the B system, there is a drop of 60 to 80 cm^{-1} from the first to the second interval of ν_1' in each case. Again, the most likely explanation of this is that a Fermi resonance is occurring between the levels $(1,0^0,v_3')$ and $(0,2^0,v_3')$ which

displaces the level $(1,0^0,v_3')$ up from its zeroth order position. Also as in the B system, it is likely that there is only a small perturbation between the levels $(2,0^0,v_3')$ and $(0,4^0,v_3')$ and so these levels are not shifted by much. The average of the two observed intervals for ν_1' gives an estimate of about 700 cm^{-1} for the zeroth order value of ν_1' in the C state; this requires a value of about 350 cm^{-1} for ν_2' which, as before, is not unreasonable.

The determination of the molecular structure of cyanogen bromide in the B and C states by the use of Franck-Condon calculations cannot be done with the same degree of confidence as for cyanogen iodide. The problem is that with Fermi resonance as postulated above there is a mixing of the wave functions of the two levels $(1,0^0,v_3')$ and $(0,2^0,v_3')$, as well as a shifting of the positions of the energy levels. This mixing of the wave functions will affect the calculated vibrational overlap integrals and thus make the bond length changes obtained incorrect. However, there is nothing that can be done to investigate this problem with the available experimental evidence. Therefore, the calculations were carried out in the same way as for cyanogen iodide and the results obtained are examined to see if they are reasonable.

For the cyanogen bromide B system, relative intensities were obtained experimentally only for the ν_1' progression. For the ν_3' progression a relative intensity of 0.1 was assumed for the band 3_0^1 so that the calculation could be carried out. This value for the relative intensity cannot be much in error since if the band were more intense it would probably be observed in the spectrum; and if it were less intense the effect on the results would be within the experimental

error as discussed later. The zeroth order values of 700 cm^{-1} for ν_1' and 584 cm^{-1} for ν_1'' have been used in the calculation since these are the harmonic values for the vibrational frequencies and the theory outlined assumes the harmonic oscillator approximation. The approximate value of 2000 cm^{-1} has been used for ν_3'. The mass of Br^{79}, which is slightly more abundant than Br^{81}, was used in the calculation.

The four possible pairs of bond length changes that were calculated are listed as (a), (b), (c), and (d) of Table 10.13. Since the potential energy distribution in Table 10.14 indicates that the excited state vibrations are localized to a large extent, the absolute values of the bond length changes calculated by the simplified Franck-Condon method should be close to the true values. These are listed as (e) of Table 10.13 and indicate that either the results of (a) or (b) are correct. As in the case of cyanogen iodide, the results of (a) have been chosen on the basis of the bond length changes calculated by Clark's and Badger's rules which are given as (f) and (g), respectively, of Table 10.13. The bond lengths obtained for the B state of cyanogen bromide are r(BrC) = 1.72 Å and r(CN) = 1.16 Å.

Franck-Condon calculations of the changes in the bond lengths for the C system of cyanogen bromide were carried out using the relative intensities of Table 10.12. The zeroth order values of 700 cm^{-1} for ν_1' and 584 cm^{-1} for ν_1'' and the mass of Br^{79} were used in the calculations as explained above. The four pairs of possible bond length changes consistent with the observed intensities are listed as (a), (b), (c), and (d) of Table 10.15. The absolute values of the bond length changes were calculated by the simplified Franck-Condon method and since the potential energy distribution indicates that the excited state

TABLE 10.13

POSSIBLE BOND LENGTH CHANGES FOR THE CYANOGEN BROMIDE B SYSTEM (PRECISION IN mÅ GIVEN IN PARENTHESES)

Calculation	Δr(BrC), Å	Δr(CN), Å
a	-0.067(5)	0.004(4)
b	0.067(5)	-0.004(4)
c	0.040(2)	0.038(5)
d	-0.040(2)	-0.038(5)
e	0.063	0.011
f	-0.106	0.037
g	-0.043	0.015

TABLE 10.14

POTENTIAL ENERGY DISTRIBUTION FOR THE CYANOGEN BROMIDE B SYSTEM

Normal Mode	k_{12}(BrC)	k_{23}(CN)
ν_1	0.83	0.17
ν_3	0.17	0.83

vibrations are quite localized, the results, given as (e) of Table 10.15, indicate that the values of (a) or (b) are the correct ones. On the basis of the values (f) and (g) obtained from Clark's and Badger's rules, respectively, the values of (a) have been chosen. The calculated bond lengths for the C state of cyanogen bromide are r(BrC) = 1.70_3 Å and r(CN) = 1.18_5 Å.

The vibrational frequencies and bond lengths for the X, B, and C states of cyanogen bromide are summarized in Table 10.17. The values given for ν_1 are the zeroth order values which were used in the calculation of the bond length changes. In the B and C states, the accuracy of the observed vibrational frequencies is better than 10 cm^{-1}, but it is not possible to give any estimates of the accuracy of the zeroth order vibrational frequencies.

The bond lengths for the B system are not accurate because of the assumptions that were made about the frequency ν_3' and the relative intensity of the 3_0^1 band. Nevertheless, it is quite certain that r(BrC) decreases and r(CN) increases, although the values are rather uncertain. The precision in the calculated bond lengths for the C system is about ±0.005 Å, but the accuracy is certainly not this good. The problem is that the amount of mixing of the wave functions because of the Fermi resonance cannot be determined. However, as will be discussed later, the bond length changes are of the order of magnitude expected and so are probably fairly close to the true values.

The separation of the origin bands of the B and C systems of cyanogen bromide is 1988 cm^{-1}. A possibility that has not been discounted yet is that the bands at 66290, 68278, 70204, and 72081 cm^{-1} are all

TABLE 10.15

POSSIBLE BOND LENGTH CHANGES FOR THE CYANOGEN BROMIDE C SYSTEM (PRECISION IN mÅ GIVEN IN PARENTHESES)

Calculation	$\Delta r(BrC)$, Å	$\Delta r(CN)$, Å
a	-0.086(5)	0.027(3)
b	0.086(5)	-0.027(3)
c	0.025(1)	0.067(5)
d	-0.025(1)	-0.067(5)
e	0.067	0.035
f	-0.106	0.051
g	-0.043	0.022

TABLE 10.16

POTENTIAL ENERGY DISTRIBUTION FOR THE CYANOGEN BROMIDE C SYSTEM

Normal Mode	$k_{12}(BrC)$	$k_{23}(CN)$
ν_1	0.81	0.19
ν_3	0.19	0.81

TABLE 10.17

VIBRATIONAL FREQUENCIES AND BOND LENGTHS FOR THE CYANOGEN BROMIDE X, B, and C STATES

State	ν_1, cm^{-1}	ν_2, cm^{-1}	ν_3, cm^{-1}	r(BrC), Å	r(CN), Å
X	584*	342	2198	1.789	1.158
B	700*	350#	2000#	1.72+	1.16+
C	700*	350#	1926	1.70_3	1.18_5

* zeroth order values (in absence of Fermi resonance)
\# estimated (see text)
\+ less accurate

members of a progression in ν_3' for one electronic transition. This would give vibrational intervals of 1988, 1926, and 1877 cm^{-1}. There are several reasons for not making such an assignment. The first is that by analogy with the hydrogen halides, the methyl halides, and the other cyanogen halides, two systems of comparable intensity whose origin bands are separated by 2000-3000 cm^{-1} are expected in the region where these bands are found. If these bands are all assigned as one electronic transition, then there is the problem of locating the other system, and there are no signs of another system, even very weak, in this region. Also, in this case the major progression would involve ν_3', which is localized mainly in the CN bond, and this is contrary to expectations as will be discussed later. Finally, the intensity distribution along this progression, if it is a progression, is rather irregular. Therefore, it is concluded that the assignment which has been given above must be correct.

10.4.3 Cyanogen Chloride B and C Systems

The vibrational bands which have been observed for the cyanogen chloride B and C systems are shown in the microdensitometer trace of Figure 10.2. The wavelengths, wavenumbers, and relative intensities of the vibrational bands are listed in Tables 10.18 and 10.19 for the B and C systems, respectively. The uncertainty in the measured wavelengths is about ± 0.1 Å (corresponding to ± 5 cm^{-1} approximately), this again being caused by the lack of sharpness of the bands. The precision in the measurement of the relative intensities is not as good as for cyanogen iodide and cyanogen bromide, being about ± 0.06 of the relative units used. The reasons for this are firstly that it is more difficult to obtain good spectra in the very high frequency region in which the

TABLE 10.18

ASSIGNMENT OF THE VIBRATIONAL BANDS FOR THE CYANOGEN CHLORIDE B SYSTEM

λ, Å	σ, cm^{-1}	Relative Intensity	Assignment
1363.7	73331	1.000	0_0^0
1351.7	73979	0.483	1_0^1
1340.2	74618	0.251*	1_0^2
1329.3	75227	0.371	3_0^1
1317.9	75879	0.195	$1_0^1 3_0^1$
(1307.4)	(76491)	-----	$1_0^2 3_0^1$

* overlapped by 0_0^0(C)

TABLE 10.19

ASSIGNMENT OF THE VIBRATIONAL BANDS FOR THE CYANOGEN CHLORIDE C SYSTEM

λ, Å	σ, cm^{-1}	Relative Intensity	Assignment
1342.9	74468	1.000	0_0^0
1331.4	75109	0.349	1_0^1
1320.0	75758	0.076	1_0^2
1310.5	76308	0.456	3_0^1
(1299.8)	(76935)	-----	$1_0^1 3_0^1$

B and C systems of cyanogen chloride lie, and secondly that the B and C systems overlap to quite a large extent and cause some uncertainty in the measurements. In contrast to what is observed for cyanogen iodide and cyanogen bromide, the B system of cyanogen chloride is more intense than the C system, the ratio of their spectral intensities being about one and one-half to one.

The observed overall vibrational structure indicates that cyanogen chloride stays linear and undergoes little change in dimensions in both the B and C excited states. The three vibrational frequencies of cyanogen chloride in the ground electronic state are given in Table 10.24. There is a Fermi resonance between the levels $(1,0^0,0)$ and $(0,2^0,0)$ in the ground state; the observed value for ν_1'' is 714 cm^{-1} and the calculated zeroth order value is 744.2 cm^{-1}. Both the B and C systems of cyanogen chloride can be analyzed in terms of progressions in two totally symmetric vibrations in the upper state and the analyses are indicated in Tables 10.18 and 10.19, respectively.

In the Franck-Condon calculations of the changes in the bond lengths of cyanogen chloride, the mass of Cl^{35}, which is the more abundant isotope, has been used. Also, the zeroth order (harmonic) value of ν_1'' has been used instead of the value observed in the vibrational spectrum. Aside from these changes, the method of calculation was the same as for cyanogen iodide.

The four possible pairs of bond length changes calculated for the B system of cyanogen chloride are given as (a), (b), (c), and (d) of Table 10.20. Because the potential energy distribution given in Table 10.21 indicates that the vibrations are quite localized, the absolute values of the changes in the bond lengths calculated by the

TABLE 10.20

POSSIBLE BOND LENGTH CHANGES FOR THE CYANOGEN CHLORIDE B SYSTEM (PRECISION IN mÅ GIVEN IN PARENTHESES)

Calculation	Δr(ClC), Å	Δr(CN), Å
a	-0.074(5)	0.031(3)
b	0.074(5)	-0.031(3)
c	0.023(2)	0.051(3)
d	-0.023(2)	-0.051(3)
e	0.054	0.032
f	0.077	0.061
g	0.032	0.025

TABLE 10.21

POTENTIAL ENERGY DISTRIBUTION FOR THE CYANOGEN CHLORIDE B SYSTEM

Normal Mode	k_{12}(ClC)	k_{23}(CN)
ν_1	0.89	0.11
ν_3	0.11	0.89

simplified Franck-Condon method and listed as (e) in Table 10.20 should be close to the true values. Unfortunately, there is not a very good agreement between the changes (e) and any of the preceding values, particularly for the C-Cl bond length. Cyanogen chloride differs from cyanogen bromide and cyanogen iodide in that both ν_1 and ν_3 decrease upon excitation. Correspondingly, Clark's and Badger's rules predict that both bond lengths increase, as shown in (f) and (g), respectively, of Table 10.20. This favours the results of (c) in the Franck-Condon calculations. Although an unambiguous choice cannot be made here, it is highly unlikely that the appreciable drop in both ν_1 and ν_3 is compatible with bond shortening upon excitation. So (c) is chosen as showing the correct change, giving the bond lengths for the B state of cyanogen chloride as r(ClC) = 1.65_4 Å and r(CN) = 1.21_0 Å.

The possible bond length changes for the C system of cyanogen chloride were calculated in the same way as for the B system and are given as (a), (b), (c), and (d) of Table 10.22. The values obtained from the simplified Franck-Condon calculations are given as (e) and those obtained from Clark's and Badger's rules are given as (f) and (g), respectively, of Table 10.22. The problems of determining the correct bond length changes are the same as encountered for the B state of cyanogen chloride, the choice being between (a) and (c) again. As above, the changes (c) of Table 10.22 are chosen to be correct and the bond lengths for the C state of cyanogen chloride are found to be r(ClC) = 1.64_4 Å and r(CN) = 1.21_3 Å.

The vibrational frequencies and bond lengths for the X, B, and C states of cyanogen chloride are summarized in Table 10.24. The value

TABLE 10.22

POSSIBLE BOND LENGTH CHANGES FOR THE CYANOGEN CHLORIDE C SYSTEM (PRECISION IN mÅ GIVEN IN PARENTHESES)

Calculation	$\Delta r(ClC)$, Å	$\Delta r(CN)$, Å
a	-0.069(5)	0.037(3)
b	0.069(5)	-0.037(3)
c	0.013(2)	0.054(4)
d	-0.013(2)	-0.054(4)
e	0.046	0.035
f	0.083	0.075
g	0.035	0.031

TABLE 10.23

POTENTIAL ENERGY DISTRIBUTION FOR THE CYANOGEN CHLORIDE C SYSTEM

Normal Mode	$k_{12}(ClC)$	$k_{23}(CN)$
ν_1	0.88	0.12
ν_3	0.12	0.88

given for ν_1'' in the X state is the zeroth order value, the observed value being 714 cm^{-1} because of the Fermi resonance. The excited state vibrational frequencies are accurate to about 10 cm^{-1}. The accuracy in the calculated bond length changes is probably only about $\pm$0.01-0.02 Å because the relative intensities of the vibronic bands could not be measured as accurately as for the other compounds since it was more difficult to obtain good spectra and the two electronic systems overlap extensively. Two alternatives for the bond lengths in the B and C states of cyanogen chloride are given in Table 10.24. The bond lengths given first are those obtained using the changes (c), whereas the other bond lengths are obtained using the changes (a). The drop in both ν_1 and ν_3 upon electronic excitation favours the former set of bond lengths, but the results obtained for cyanogen iodide and cyanogen bromide favour the latter. Although it is not possible to be certain, it seems likely that cyanogen chloride differs from cyanogen iodide and cyanogen bromide in that both bond lengths increase upon excitation.

10.4.4 Assignment of the Cyanogen Halide B and C Systems

At the beginning of this section, it was stated that the reason for considering the B and C systems of the cyanogen halides together is that they are very closely related. The close relationship that was referred to is the fact that one electron configuration, produced by the promotion of one electron from the ground state electron configuration, gives rise to both electronic states. This will now be discussed in more detail.

The B and C systems are the first strong vibrationally discrete absorption spectra observed for the cyanogen halides in going towards

TABLE 10.24

VIBRATIONAL FREQUENCIES AND BOND LENGTHS FOR THE CYANOGEN CHLORIDE X, B, AND C STATES

State	ν_1, cm^{-1}	ν_2, cm^{-1}	ν_3, cm^{-1}	r(ClC), Å	r(CN), Å
X	744.2*	378.4	2215.6	1.631	1.159
B	648	-----	1896	1.65_4#	1.21_0#
				1.55_8+	1.19_0+
C	641	-----	1840	1.64_4#	1.21_3#
				1.56_2+	1.19_6+

* zeroth order value (in absence of Fermi resonance)

\# calculated using the changes (c)

\+ calculated using the changes (a)

higher frequencies and are undoubtedly the analogues of the B and C systems observed for other halogen containing molecules such as the hydrogen halides and the methyl halides. The intensities of these two absorption systems in the three types of compounds are all very similar, a pressure-path length of 10^{-3} -10^{-2} cm-atmosphere being required to observe them. Also, the term values, that is, the wavenumber difference between the ionization potential and the vibrationless level of the electronic state, for the B states of the compounds containing the same halogen atom are very similar as can be seen from Table 10.25. The other data which are given in Table 10.25 show that the separation of the origin bands and the relative intensities of the B and C systems for compounds containing the same halogen are also very similar.

The data which are given in the previous paragraph all suggest that the electronic transitions are localized to a large extent in the region of the halogen atom. The molecular orbital from which the electron is promoted in these transitions is assigned as the 2π molecular orbital which is formed mainly from the π-type (p_x and p_y) atomic orbitals of the halogen atom and is localized on this atom to a large extent, although there is quite definitely some conjugation with the π electrons of the CN part of the molecule as will be discussed later in this section.

Rydberg transitions, that is, transitions in which the promoted electron enters a molecular orbital which is formed from extravalence shell atomic orbitals, are expected to lie at high energies, giving absorption in the vacuum ultraviolet. Also, the electron which is

TABLE 10.25

COMPARISON OF DATA ON THE B AND C SYSTEMS OF THE HYDROGEN HALIDES, METHYL HALIDES, AND CYANOGEN HALIDES

Compound	First Ionization Potential	$\sigma_{0_{0(B)}^{0}}$, cm^{-1}	$\sigma_{0_{0(C)}^{0}}$, cm^{-1}	$\Delta\sigma_{BC}$, cm^{-1}	T_B, cm^{-1}	Intensity(C)/Intensity(B)
I	84340					
HI	83723	56750	62320	5570	26973	~1/1
CH_3I	76930	49710	54625	4915	27220	5/4
ICN	88563	58887	63471	4584	29676	3/2
Br	95522					
HBr	93725	67084	70542	3455	26641	2/1
CH_3Br	85020	56030	59100	3070	28990	~1/1
BrCN	96387	66290	68278	1988	30097	2/1
Cl	104962					
HCl	102759	75134	77480	2345	27625	10/1(?)
CH_3Cl	90500	62300	63500	1200	28200	< 1/1
ClCN	100742	73331	74468	1137	27411	3/4

excited in a Rydberg transition is often a "lone pair" electron and the term value for an electronic energy level in a molecule is quite often very close to the term value for the analogous level in the free atom. A comparison of the term values for the vibrationless levels of the cyanogen halide B states with the term values for various levels of the corresponding halogen atoms shows that there is fairly close agreement with the term values of the levels $np^4(n+1)s\ ^4P_{5/2}$, where n = 3, 4, and 5 for chlorine, bromine, and iodine, respectively. This agreement, shown in Table 10.26, suggests that the upper molecular orbital to which the excited electron is promoted is constructed mainly from the (n+1)s atomic orbital of the halogen atom. Since a s atomic orbital can be a component of only a σ-type molecular orbital for a linear molecule, the upper orbital for these states must be of σ symmetry. Although this molecular orbital, which is denoted σ_X here, is probably formed mainly from the (n+1)s atomic orbital of the halogen atom, there is likely some contribution to it from the $3s\sigma$ and $3p\sigma$ atomic orbitals of the carbon and nitrogen atoms.

That the B and C states of the cyanogen halides arise from the electron configuration formed by promotion of one electron from the 2π to the σ_X molecular orbital is supported by the fact that an analogous assignment has been made for the B and C states of the hydrogen halides and methyl halides.[101] And in these cases, it is known that the upper molecular orbital must have $\sigma(a_1)$ symmetry since the rotational structure observed in the vibronic bands is of perpendicular type. Unfortunately, this kind of evidence is not available for the cyanogen halides because the bands are predissociated.

TABLE 10.26

COMPARISON OF SOME TERM VALUES OF THE HALOGEN ATOMS AND THE CYANOGEN HALIDES

Halogen	Term Value, cm^{-1} X $np^4(n+1)s\ ^4P_{5/2}$	Term Value, cm^{-1} XCN $O_0^0(B)$
I	29707	29676
Br	32092	30097
Cl	33008	27411

TABLE 10.27

SPIN-ORBIT COUPLING CONSTANTS OF THE HALOGEN ATOMS AND THE HYDROGEN HALIDE AND METHYL HALIDE MONOPOSITIVE MOLECULAR IONS

Halogen	$\lambda(X)$, cm^{-1}	$A(HX^+)$, cm^{-1}	$A(CH_3X^+)$, cm^{-1}
I	5069	5407	5060
Br	2457	2653	2540
Cl	587	644	680

It still has not been explained how the single electron configuration gives rise to both the B and C electronic states. There are various types of coupling of angular momenta which can occur in molecules just as in atoms. The analogue of (L,S) coupling in atoms is (Λ,S) coupling in linear molecules. In this coupling scheme, the components of orbital angular momentum about the internuclear axis for each electron couple together to give a total component of orbital angular momentum about the internuclear axis $\Lambda\hbar$ and the spin angular momenta for each electron couple together to give a total spin angular momentum $S\hbar$. The component of orbital angular momentum about the internuclear axis $\Lambda\hbar$ and the total spin angular momentum $S\hbar$ then interact by spin-orbit coupling. The total spin angular momentum $S\hbar$ has components about the internuclear axis $\Sigma\hbar$ (Σ = S, S-1, ..., -S) and the energy of the components caused by the spin-orbit coupling is described by the equation

$$T_e = T_o + \mathcal{A}\Lambda\Sigma \qquad (10.8)$$

where T_e is the energy (in cm^{-1}) of a component including spin-orbit coupling, T_o is the energy of the state neglecting spin-orbit coupling, and $\mathcal{A}$ is a spin-orbit coupling constant which is constant for a given Λ. If the closed shells are omitted, then the electron configuration and the resulting molecular states for the case here are those given below.

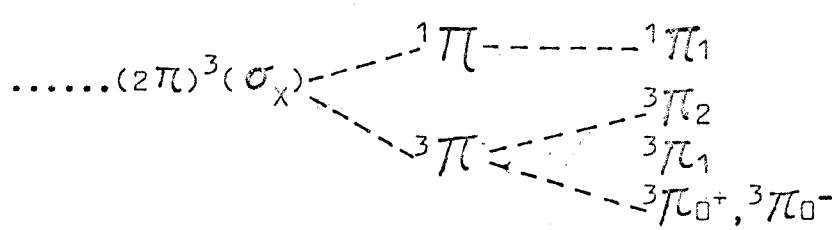

(10.9)

Inter-electronic repulsion causes the main splitting between the $^1\pi$ and $^3\pi$ states, with the latter at lower energy. Spin-orbit coupling between $\Lambda\hbar$ and $S\hbar$ may then cause further small splitting in the case of the triplet state. The subscripts on the symmetry species for the electronic states are the quantum numbers Ω for the component of the total angular momentum about the internuclear axis $\Omega\hbar$. Ω is defined by the equation

$$\Omega = \left| \Lambda + \Sigma \right| \qquad (10.10)$$

Another type of coupling of angular momenta which can occur for linear molecules is (Ω_c, ω) coupling which is analogous to (J, j) coupling in atoms. In this type of coupling, the electrons in the molecular core, composed of all electrons except the one which is promoted, are strongly coupled together in (Λ, S) coupling and give a component of total angular momentum about the internuclear axis $\Omega_c\hbar$. The total angular momentum $\omega\hbar$ of the promoted electron is then coupled to $\Omega_c\hbar$. If filled molecular orbitals are omitted, the electron configuration and resulting states for the molecular core in this case are

$$\ldots\ldots(2\pi)^3 \begin{cases} \text{-----} \; ^2\Pi_{1/2} \\ \text{-----} \; ^2\Pi_{3/2} \end{cases} \qquad (10.11)$$

From Equation 10.8, the separation of the $^2\Pi_{1/2}$ and $^2\Pi_{3/2}$ states is equal to A, the spin-orbit coupling constant for the monopositive molecular ion; the $^2\Pi_{3/2}$ state lies at lower energy since the 2π molecular orbital is more than half filled. The total angular momentum of the promoted electron, which is $\frac{1}{2}\hbar$ since it is in a σ molecular

orbital, couples with the component of total angular momentum about the internuclear axis of the molecular core electrons, which is either $\frac{1}{2}\hbar$ or $(3/2)\hbar$ depending upon the component considered, to cause a further small splitting. This is shown below where the resulting states of the molecule are labelled by their Ω value, that is, the quantum number for their component of total angular momentum about the internuclear axis, since in this coupling scheme it is the only good quantum number.

$$\left[\ldots\ldots(2\pi)^3 \;\; {}^2\Pi_{1/2}\right](\sigma_X) \lessdot \begin{matrix} \nearrow 1 \\ \searrow 0^+,\ 0^- \end{matrix} \qquad (10.12)$$

$$\left[\ldots\ldots(2\pi)^3 \;\; {}^2\Pi_{3/2}\right](\sigma_X) \lessdot \begin{matrix} \nearrow 2 \\ \searrow 1 \end{matrix}$$

It is possible to correlate these two coupling limits by varying the strength with which the promoted electron is coupled to the internuclear axis since Ω is a good quantum number in both coupling cases; the correlation is shown in Figure 10.4.

In (Ω_c, ω) coupling, Ω is the only good quantum number and the selection rule for electronic transitions is

$$\Delta\Omega = 0, \pm 1 \qquad \text{and} \qquad 0^+ \not\leftrightarrow 0^- \qquad (10.13)$$

Since the ground electronic state of the cyanogen halides has $\Omega = 0$, there should be three electronic transitions to the states formed by the electron configuration (10.12) as shown on the right hand side of Figure 10.4. Transitions with $\Delta\Omega = 1$ are expected to be more intense than those with $\Delta\Omega = 0$. Therefore, two of the electronic transitions, shown by solid lines in Figure 10.4, should be observed with about the

same intensity and should be separated by an amount approximately equal to the spin-orbit coupling constant of the molecular ion.

In (Λ,S) coupling, the selection rules for electronic transitions are

$$\Delta\Lambda = 0, \pm 1 \qquad \text{and} \qquad \Delta S = 0 \tag{10.14}$$

although the selection rule on S is less rigorous for molecules with heavy atoms because of the larger spin-orbit coupling for them. Since the ground electronic state of the cyanogen halides is $^1\Sigma^+$, there should be three electronic transitions to the states formed by the electron configuration (10.9), as shown on the left hand side of Figure 10.4. Two of these transitions, shown by solid lines in the figure, should be more intense than the third. The separation of these two systems should be greater than the spin-orbit coupling constant of the molecular ion and the transition to higher energy should be more intense than the other.

The spin-orbit coupling constants for the iodine, bromine, and chlorine atoms and for the hydrogen halide and methyl halide monopositive molecular ions are given in Table 10.27. Since the constants are approximately the same for each halogen in the three cases, it is likely that the spin-orbit coupling constants for the cyanogen halide molecular ions should be about the same as those of the corresponding halogen atom, although according to Mulliken[101] they may be somewhat reduced. The reason for this is that the 2π molecular orbital is not simply a $np\pi$ atomic orbital on the halogen atom, but instead has the form

$$2\pi = - c'_{21}\pi_X + c'_{22}\pi_C + c'_{23}\pi_N \tag{10.15}$$

where c'_{22} and c'_{23} are considerably smaller than c'_{21}. Mulliken states that the value of the spin-orbit coupling constant of the molecular ion is reduced from that of the free atom by this π bonding in proportion to $|c'_{21}|^2$, which is less than unity.

The wavenumber separation and the approximate relative intensities of the B and C systems of the cyanogen halides are listed in Table 10.25. These data show that the coupling in cyanogen iodide and cyanogen bromide is fairly close to (Ω_c, ω) coupling. The intensities of the B and C systems are about equal although in both cases the C system is slightly more intense, thus indicating that the coupling is not completely of (Ω_c, ω) type. For both molecules, the separation of the B and C systems is about 500 cm^{-1} less than the spin-orbit coupling constant of the free halogen atom; this can be ascribed to the effect of π bonding described above.

The separation of the B and C systems of cyanogen chloride is considerably greater than the spin-orbit coupling constant of chlorine, but is about the same as observed for methyl chloride.[102] This would indicate that for cyanogen chloride the coupling is more towards (Λ, S) coupling. However, there is a difficulty with this suggestion in that the B system is more intense than the C system which is contrary to expectations for (Λ, S) coupling, although the same thing seems to be true for methyl chloride.[102] It is possible that there is some perturbation on these systems similar to that postulated by Schaufele and Goodman[89] to account for the fact that in vinyl iodide the B system is also more intense than the C system although the separation of the two systems would indicate that the intensities should be almost equal, with the C system perhaps slightly more intense.

The B and C systems of the cyanogen halides have been assigned as the first members of a Rydberg series in which an electron is promoted from the 2π molecular orbital localized mainly on the halogen to the σ_X orbital which is also localized mainly on the halogen. From the nature of the transition, it would be expected that the dimensions of the molecule in the excited states are little different from those in the ground electronic state and that the major change which does occur is in the halogen-carbon bond length. The excited state molecular dimensions which have been obtained by a quantitative application of the Franck-Condon principle agree well with these expectations in the cases of cyanogen iodide and cyanogen bromide. In the case of cyanogen chloride, the calculated changes in bond lengths are small; but for the most probable changes in bond lengths the change in the C-N bond is greater than in the Cl-C bond. The difference in the bond length changes between cyanogen chloride on the one hand and cyanogen bromide and cyanogen iodide on the other must be the result of a change in the form of the molecular orbitals between them. This is not too surprising since it is known that the amount of conjugation of the halogen π electrons with the CN π electrons in the ground state is greatest for cyanogen chloride.[114]

It has been mentioned before that the bands of the B and C systems for the cyanogen halides all appear to be predissociated. The state which is responsible for this perturbation may be the A $^1\pi$ which, as discussed in Section 10.2, appears to have a repulsive potential surface. Such a cause for predissociation has been suggested in the B and C systems of trifluoromethyl iodide.[105]

10.5 Shorter Wavelength Absorption of the Cyanogen Halides

In this section, the absorption spectra of the cyanogen halides which have been observed in the region between the C system and the short wavelength limit of the spectrograph (about 1250-1300 Å) are discussed. The spectra which have been observed are all due to Rydberg transitions to excited states which in general lie well below the first ionization potentials of the molecules. These transitions are localized to a large extent on the halogen atom with the promoted electron entering essentially an extravalence shell orbital of the halogen atom. Therefore, the orbitals containing the promoted electron in these excited states are labelled in the way described in Section 9.6; that is, they are labelled $n\ell\Gamma_i$ where n is the principal quantum number and ℓ is the orbital angular momentum quantum number for the basis atomic orbital and Γ_i is the irreducible representation under the molecular point group.

10.5.1 Shorter Wavelength Absorption of Cyanogen Iodide

The largest number of absorption regions has been found for cyanogen iodide as shown in Figure 10.1. The additional systems observed are mostly vibrationally discrete. The wavelengths, wavenumbers, and approximate relative intensities of the observed bands are listed in Table 10.28. The measurements for some bands are not too accurate because of the overlapping of bands and the interference due to emission lines of the Lyman source.

Complex structure is observed in the 1480-1440 Å region. This is the strongest absorption region in the spectrum and consists of a number of bands surperimposed on what appears to be an absorption

TABLE 10.28

SHORTER WAVELENGTH ABSORPTION OF CYANOGEN IODIDE

λ, Å	σ, cm^{-1}	Intensity	Assignment of the Excited State
1480.2	67559	ms	
1476.6	67723	m	
1470.8	67991	vs	D'...$(2\pi)^3(6p\sigma)\ ^3\Pi$
1467.2	68156	s	
1461.9	68404	vs	
1455.8	68692	s	
1453.3	68811	w	
1450.3	68951	vs	D ...$(2\pi)^3(6p\pi)\ ^1\Sigma^+$
1447.3	69092	s	
1441.1	69392	m	
1410.0	70922	m	
(1405.6)	(71146)	m	
(1391.4)	(71868)	m	
1383.6	72277	ms	
1376.5	72650	s	E'...$(2\pi)^3(6p\sigma)\ ^1\Pi$
1372.1	72881	ms	
1367.7	73114	m	
1362.5	73396	m	
1358.2	73629	w	E ...$(2\pi)^3(6p\pi)\ ^3\Sigma^+$
1349.2	74115	w	
1333.7	74979	m	
1331.3	75117	s	...$(2\pi)^3(7s\sigma)\ ^3\Pi$

cont'd

λ, Å	σ, cm^{-1}	Intensity	Assignment of the Excited State
1327.7	75317	ms	
1322.5	75613	m	
(1299.6)	(76947)	m	
(1289.5)	(77548)	m	$\ldots(2\pi)^3(7p\sigma)\ ^3\Pi$
(1284.2)	(77870)	w	
(1257.1)	(79549)	w	$\ldots(2\pi)^3(7s\sigma)\ ^1\Pi$

continuum. Another region of absorption, which is somewhat less intense but qualitatively similar in appearance to the 1480-1440 Å absorption, is observed between 1385 and 1350 Å. It is possible to identify pairs of bands, one in each of the regions 1480-1440 Å and 1385-1350 Å, which are separated by about 4700 cm^{-1}. These are listed in Table 10.29. The observation of pairs of bands with this separation suggests that these two regions contain members of a Rydberg series which are split by spin-orbit coupling in the same way as the B and C systems of cyanogen iodide.

The strong band labelled D at 68951 cm^{-1} has a term value of 19612 cm^{-1} which is quite close to that of 19434 cm^{-1} for the $5p^4 6p\ ^4P_{5/2}$ level of the free iodine atom. This suggests that the band D results from a Rydberg transition to an electronic state resulting from the electron configuration in which an electron has been promoted from the 2π molecular orbital to a molecular orbital which is formed mainly from the 6p atomic orbital of iodine. But in a linear molecule, p atomic orbitals split into $p\sigma$ and $p\pi$ components. Promotion of an electron from the 2π to the $6p\pi$ molecular orbital gives the following electron configuration and electronic states.

$$\ldots\ldots(2\pi)^3\,(6p\pi) \begin{cases} {}^3\Sigma^+,\ {}^3\Sigma^-,\ {}^3\Delta \\ {}^1\Sigma^+,\ {}^1\Sigma^-,\ {}^1\Delta \end{cases} \qquad (10.16)$$

Strong transitions from the ground electronic state are allowed only to the Σ^+ states. The $^1\Sigma^+$ and $^3\Sigma^+$ states are probably separated by spin-orbit coupling as are the B and C states so that they should be

TABLE 10.29

SOME PAIRS OF BANDS OF CYANOGEN IODIDE

	σ, cm^{-1}		σ, cm^{-1}	$\Delta\sigma$, cm^{-1}
	67559		72277	4718
D'	67991	E'	72650	4659
	68156		72881	4725
	68404		73114	4710
	68692		73396	4704
D	68951	E	73629	4678
	69392		74115	4723

TABLE 10.30

SHORTER WAVELENGTH ABSORPTION OF CYANOGEN BROMIDE

λ, Å	σ, cm^{-1}	Intensity	Assignment of the Excited State
(1346.5)	(74269)	m	
(1339.2)	(74671)	ms	
(1333.3)	(75001)	ms	
(1328.9)	(75249)	m	
1314.1	76099	s	D'...$(2\pi)^3(5p\sigma)\ ^3\pi$
1288.5	77611	w	
1284.4	77856	s	
1280.8	78078	s	E'...$(2\pi)^3(5p\sigma)\ ^1\pi$
1275.2	78422	m	
(1253.8)	(79759)	w	

about 4600 cm^{-1} apart, and according to Recknagel[104] the $^3\Sigma^+$ state should be at higher energy. The band D is assigned as the transition to the $^1\Sigma^+$ state and the band labelled E at 73629 cm^{-1}, which is separated by 4678 cm^{-1} from the band D and is weaker than it, is assigned as the transition to the $^3\Sigma^+$ state.

Promotion of an electron from the 2π to the $6p\sigma$ molecular orbital gives the electron configuration and electronic states

$$.....(2\pi)^3\,(6p\sigma) \begin{cases} \text{---} \; ^1\pi \\ \text{- - -} \; ^3\pi \end{cases} \qquad (10.17)$$

These two states are probably split by spin-orbit coupling, with the $^3\pi$ state lying at lower energy just as for the B and C states. Transitions to the $^3\pi$ and $^1\pi$ states are probably responsible for the band D' at 67991 cm^{-1} and the band E' at 72650 cm^{-1}, respectively. There are several reasons for this choice. They are the only pair of bands which have a separation close to that of the bands D and E as can be seen from Table 10.29, and they have about the same intensity, as do the B and C systems which also result from a $...(\pi)^3\,(\sigma)$ configuration. This gives a splitting of 960 cm^{-1} between the states formed from the $6p\sigma$ and $6p\pi$ molecular orbitals derived from the iodine 6p atomic orbital. This seems to be a reasonable value since in water[103] the separation of the Rydberg states $^1A_1$ and $^1B_1$, which result from electron configurations produced by promotion of an electron to two of the molecular orbitals formed by the splitting of the degeneracy of the 3p atomic orbitals of the oxygen atom in water, are separated by about 1500 cm^{-1}.

This still leaves a number of bands in each of the two regions

1480-1440 Å and 1385-1350 Å unaccounted for. It is possible that some of the bands are vibrational bands associated with the D', D, E', and E bands. However, it is difficult to find many bands with the expected vibrational intervals or the correct relative intensities for this explanation to hold. It is possible that transitions to electronic states resulting from electronic configurations in which an electron has been promoted to molecular orbitals which are formed mainly from the 5d atomic orbital of iodine lie in this region. Because of the lowered symmetry, the 5d atomic orbital should be split into one $5d\sigma$, one $5d\pi$, and one $5d\delta$ component.

In the previous section, the B and C systems of cyanogen iodide were assigned to a transition which requires promotion of an electron from the 2π molecular orbital to a molecular orbital σ_X, the latter formed primarily from the $6s\sigma$ orbital of the iodine atom. Bands which have been observed at 75117 and 79549 cm^{-1} are assigned as the analogues of the B and C origin bands, respectively, with the upper orbital now being $7s\sigma$. If the origin band of the B system at 58887 cm^{-1} and the band at 75117 cm^{-1} are used to determine the constants in the Rydberg Equation 9.47, the value obtained for the first ionization potential of cyanogen iodide is 87719 cm^{-1} and the quantum defect is 4.04_9. This value of the ionization potential agrees well with that of 88560 cm^{-1} obtained from electron impact studies,[62] especially when it is remembered that lower members of molecular Rydberg series do not generally fit Equation 9.47 too well. The value of 4.04_9 obtained for the quantum defect agrees quite well with the value of 3.99_4 obtained for the ns Rydberg series of the iodine atom and so confirms the assignment as an $ns\sigma$ Rydberg series localized on the iodine atom of the molecule.

The band D' at 67991 cm^{-1} has been assigned as the transition to the lower energy $^3\Pi$ state resulting from promotion of an electron from the 2π to the $6p\sigma$ molecular orbital. It is likely that the band at 77548 cm^{-1} is an analogous band resulting from the transition to the $^3\Pi$ state resulting from the electron configuration produced by promotion of an electron from the 2π to the $7p\sigma$ molecular orbital. Use of these two bands with the Rydberg equation gives a value of 87041 cm^{-1} for the first ionization potential and a quantum defect of 3.60_0. The value of the ionization potential is somewhat lower than that obtained from electron impact,[62] but this is probably due to the fact that the band at 77548 cm^{-1} could not be measured too accurately because of the presence of emission lines in this region. The quantum defect is quite close to the value of 3.58_9 obtained from the np Rydberg series of iodine and thus confirms the assignment made.

From the Rydberg transitions which have been observed, it is possible to confirm the value obtained for the first ionization potential of cyanogen iodide from electron impact studies. This ionization potential corresponds to formation of the monopositive molecular ion in its lowest electronic state which is $^2\Pi_{3/2}$ (see (10.11)). Because the transitions observed for the cyanogen iodide molecule appear to have (Ω_c,ω) coupling, the spin-orbit coupling constant of the molecular ion can be estimated to be about 4600-4700 cm^{-1}. Therefore, the low lying $^2\Pi_{1/2}$ state of the molecular ion should be about this amount above the ground state of the ion and the second ionization potential of cyanogen iodide should be about 4600 cm^{-1} (approximately 0.57 eV) greater than the first ionization potential.

The Rydberg levels leading to the $^2\Pi_{3/2}$ and $^2\Pi_{1/2}$ states of the cyanogen iodide monopositive molecular ion are shown schematically in Figure 10.5. Because spectra could not be observed at wavelengths shorter than 1250 Å, it is not possible to be completely sure about the assignment of the Rydberg levels although the available evidence supports the assignments given. Also given in the Figure are the pairs of levels listed in Table 10.29 which have not been accounted for. It is suggested that some of these pairs of levels may arise from transitions to states resulting from electron promotion to molecular orbitals formed mainly from the iodine 5d atomic orbital.

10.5.2 Shorter Wavelength Absorption of Cyanogen Bromide

The wavelengths, wavenumbers, and approximate relative intensities of the absorption bands of cyanogen bromide which have been observed between the C system and the short wavelength limit of the spectrograph are listed in Table 10.30. The accuracy of the measurements is not very high in most cases because of interferance by emission and absorption lines of the Lyman source.

A rather broad band D' at 76099 cm^{-1} is the most intense in this region and has a term value of 20288 cm^{-1} which is close to that of 20856 cm^{-1} for the $4p^4\ 5p\ ^4P_{5/2}$ level of the free bromine atom. Therefore, it is likely that this band results from a transition to an excited state formed by promotion of an electron from the 2π molecular orbital of cyanogen bromide to a molecular orbital formed from the 5p atomic orbital of bromine. The separation of the B and C origin bands in cyanogen bromide is 1988 cm^{-1}. The band E' at 78078 cm^{-1}, which is separated from the band D' by 1979 cm^{-1}, is likely the transition to

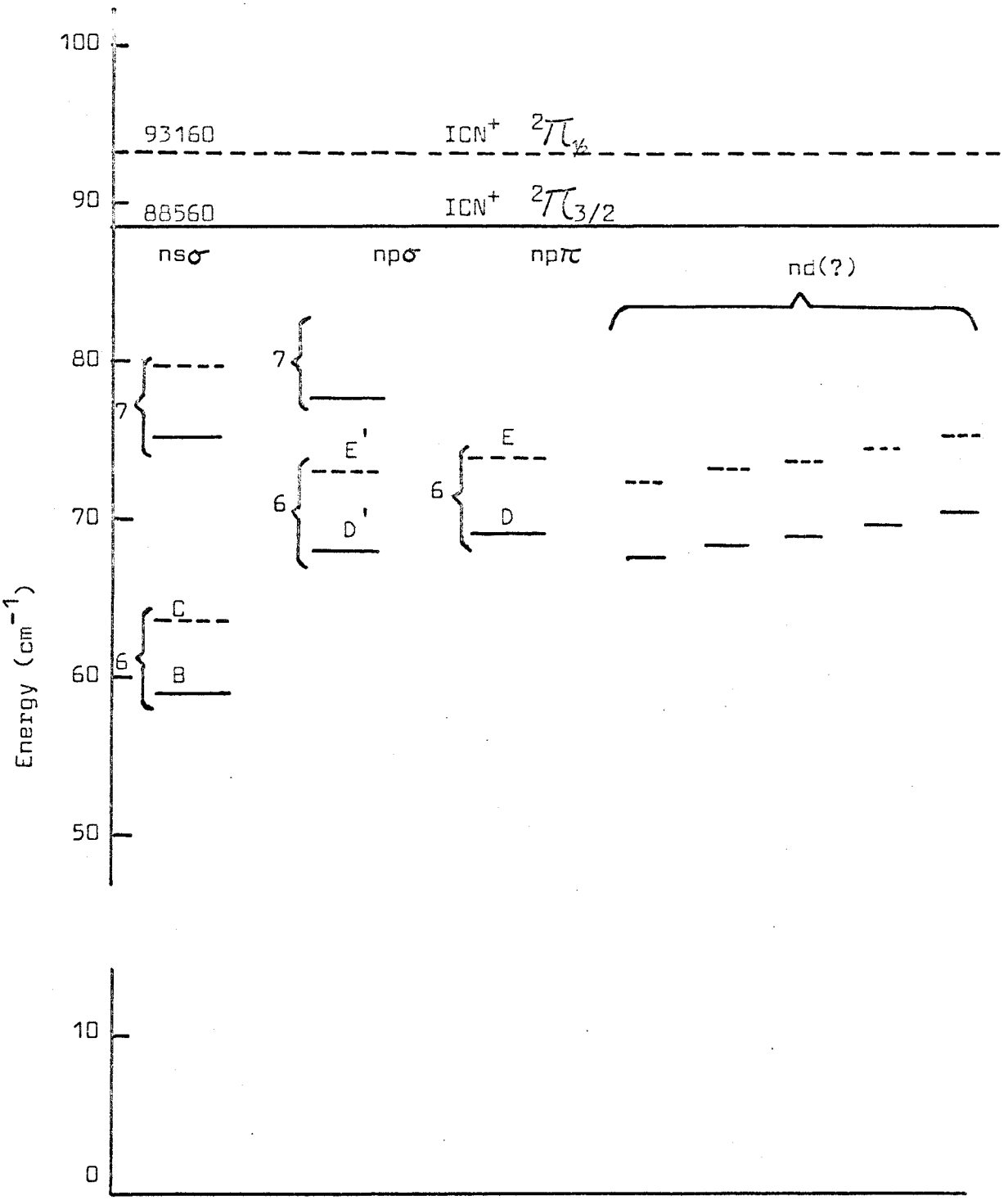

FIGURE 10.5
SOME RYDBERG LEVELS OF CYANOGEN IODIDE

the other state arising from the same electron configuration. Since the bands D' and E' are of about the same intensity, the electron configuration is probably

$$\ldots\ldots(2\pi)^3\,(5p\sigma) \begin{cases} \nearrow\ {}^1\pi \\ \searrow\ {}^3\pi \end{cases} \qquad (10.18)$$

The absorption in the region 1350-1325 Å is rather diffuse and the wavelengths given are for a few of the maxima observed. It is not possible to say what is causing this absorption, but it may be the analogue of the absorption in cyanogen iodide which seems to underlie the absorption in the 1480-1440 Å region.

No other Rydberg series members have been observed so that an estimate of the ionization potential cannot be made by use of the Rydberg equation. However, the term values for the observed systems indicate that the ionization potential measured by electron impact[62] is correct. From the analysis of the B and C systems of cyanogen bromide, it is possible to estimate that the spin-orbit coupling constant for the cyanogen bromide molecular ion is slightly less than 2000 cm^{-1}. Therefore, the second ionization potential for cyanogen bromide (to the $^2\pi_{1/2}$ state of the molecular ion) is about 2000 cm^{-1} (0.25 eV) greater than the first ionization potential.

10.6 Summary of Results

The electronic absorption spectra of cyanogen iodide, cyanogen bromide, and cyanogen chloride in the vapour phase have been studied down to about 1250 Å with a high resolution vacuum spectrograph. Spectra due to both intravalence and Rydberg transitions have been

observed.

The two regions of absorption lying at lowest energy for each of the molecules are caused by intravalence transitions. The first of these is assigned as an $A^1\Pi \leftarrow X^1\Sigma^+$ transition and leads to dissociation of the molecule into a halogen atom in the ^2P state and a CN radical in the $X^2\Sigma^+$ state. The second region of absorption, labelled α, is due either to a $^1\Pi \leftarrow X^1\Sigma^+$ transition leading to a linear molecule in the excited state or to a $^1A''$ or $^1A' \leftarrow X^1\Sigma^+$ transition leading to a non-linear molecule in the excited state.

Rydberg transitions are responsible for the spectra observed at higher frequencies. The first two Rydberg systems are assigned as $B^3\Pi \leftarrow X^1\Sigma^+$ and $C^1\Pi \leftarrow X^1\Sigma^+$. Vibrational analyses have been made for these two systems and the molecular structure in the excited states has been determined by a quantitative application of the Franck-Condon principle.

A number of regions of absorption observed at higher frequencies for cyanogen iodide and cyanogen bromide are also assigned as Rydberg transitions, but it has not been possible to make any extensive analyses in these cases. The values of the first ionization potentials of the cyanogen halides have been confirmed and estimates of the spin-orbit coupling constant of the molecular ion and the second ionization potentials of the molecules have been made for cyanogen iodide and cyanogen bromide.

BIBLIOGRAPHY

1. J. C. Boyce, Rev. Mod. Phys. 13, 1 (1941).
2. P. G. Wilkinson and D. W. Angel, J. Opt. Soc. Am. 52, 1120 (1962).
3. P. G. Wilkinson, J. Mol. Spectry. 6, 1 (1961).
4. V. Schumann, Ber. Wien. Akad. 102, IIa, 625 (1893).
5. T. Lyman, Astrophys. J., 23, 181 (1906).
6. G. R. Harrison, Rev. Sci. Inst. 2, 600 (1931) and 4, 651 (1933).
7. P. G. Wilkinson, J. Mol. Spectry. 1, 288 (1957).
8. P. G. Wilkinson and E. T. Byram, Appl. Opt. 4, 581 (1965).
9. J. E. Parkin and K. K. Innes, J. Mol. Spectry. 15, 407 (1965).
10. A. E. Douglas and J. G. Potter, Appl. Opt. 1, 727 (1962).
11. H. A. Rowland, Phil. Mag. 13, 469 (1882).
12. H. A. Rowland, Phil. Mag. 16, 197 and 210 (1883).
13. A. Eagle, Astrophys. J. 31, 120 (1910) and Proc. Roy. Soc. (London) 23, 233 (1911).
14. H. G. Beutler, J. Opt. Soc. Am. 35, 311 (1945).
15. T. Namioka, J. Opt. Soc. Am. 49, 446 (1959).
16. F. A. Jenkins and H. E. White, Fundamentals of Optics, McGraw-Hill Book Co. Inc. (1957), p. 7.
17. G. W. King, J. Sci. Inst. 37, 439 (1960).
18. F. S. Johnson, K. Watanabe and R. Tousey, J. Opt. Soc. Am. 41, 702 (1951).
19. G. H. Dieke and S. P. Cunningham, J. Opt. Soc. Am. 42, 187 (1952).
20. Gerhard Herzberg, Spectra of Diatomic Molecules, Princeton, New Jersey: D. Van Nostrand Company, Inc. (1950), p. 402 ff.
21. R. E. Huffman, Y. Tanaka, and J. C. Larrabee, Appl. Opt. 2, 617 (1963).
22. R. G. Newburgh, L. Heroux, and H. E. Hinteregger, Appl. Opt. 1, 733 (1962).

23. R. E. Worley, Rev. Sci. Inst. 13, 67 (1942).

24. W. R. S. Garton, J. Sci. Inst. 30, 119 (1953) and 36, 11 (1959).

25. A. E. Douglas and G. Herzberg, J. Opt. Soc. Am. 47, 625 (1957).

26. J. Curry and G. Herzberg, Ann. Physik 19, 800 (1934).

27. Reference 16, p. 23.

28. Reference 16, p.51.

29. Reference 16, p. 46

30. R. A. Sawyer, Experimental Spectroscopy, Dover Publications Inc., New York (1963). pp. 110, 162.

31. M. Born and J. R. Oppenheimer, Ann. Physik. 84, 457 (1927).

32. Henry Eyring, John Walter and George E. Kimball, "Quantum Chemistry", New York: John Wiley and Sons, Inc. (1960), p. 190 ff.

33. E. B. Wilson, Jr., J. C. Decius and P. C. Cross, "Molecular Vibrations", New York: McGraw-Hill Book Co. Inc. (1955) p. 283.

34. Reference 32, p. 107 ff.

35. F. S. Fawcett and R. D. Lipscomb, J. Amer. Chem. Soc. 82, 1509 (1960) and 86, 2576 (1964).

36. J. K. Tyler and J. Sheridan, Trans. Faraday Soc. 59, 2661 (1963).

37. E. E. Aynsley, R. E. Dodd and R. Little, Proc. Chem. Soc. 265 (1959).

38. R. E. Dodd and R. Little, Spectrochim. Acta 16, 1083 (1960).

39. A. D. Walsh, J. Chem Soc. 2266 (1953).

40. C. H. Townes, A. N. Holden and F. R. Merrit, Phys. Rev. 71, 64 (1947) and 74, 1113 (1948).

41. A. G. Smith, H. Ring, W. V. Smith and W. Gordy, Phys. Rev. 74, 370 (1948).

42. S. J. Tetenbaum, Phys. Rev. 86, 440 (1952).

43. C. A. Burrus and W. Gordy, Phys. Rev. 101, 599 (1956).

44. W. J. Lafferty, D. R. Lide and R. A. Toth, J. Chem. Phys. 43, 2063 (1965).

45. W. West and M. Farnsworth, J. Chem. Phys. 1, 402 (1933).

46. J. Wagner, Z. fur Physikal. Chem. B48, 309 (1941) and A193, 55 (1943).

47. W. G. Penney and G. B. B. M. Sutherland, Proc. Roy. Soc. (Lond.) A 156, 654 (1936).

48. W. S. Richardson and E. B. Wilson, Jr., J. Chem. Phys. 18, 155 (1950).

49. E. R. Nixon and P. C. Cross, J. Chem. Phys. 18, 1316 (1950).

50. W. C. Freitag and E. R. Nixon, J. Chem. Phys. 24, 109 (1956).

51. A. G. Maki and C. T. Gott, J. Chem. Phys. 36, 2282 (1962).

52. A. G. Maki, J. Chem. Phys. 38, 1261 (1963).

53. R. M. Badger and Sho-Chow Woo, J. Amer. Chem. Soc. 53, 2572 (1931).

54. R. B. Mooney and H. G. Reid, Nature 128, 271 (1931) and Proc. Roy. Soc. (Edin.) 52, 152 (1931).

55. D. E. Gillam, Trans. Faraday. Soc. 29, 1132 (1933).

56. W. C. Price and A. D. Walsh, Trans. Faraday. Soc. 41, 381 (1945).

57. A. V. Yakovleva, Izvest. Akad. Nauk. S. S. R., Ser. Fiz. 14, 517 (1950). See also CA 45 - 3239b.

58. J. Y. Beach and A. Turkevich, J. Amer. Chem. Soc. 61, 299 (1939).

59. J. A. Ketelaar and J. W. Zwartsenberg, Rec. Trav. Chim. 58, 449 (1939).

60. S. Geller and A. L. Schawlow, J. Chem. Phys. 23, 779 (1955).

61. R. B. Heiart and G. B. Carpenter, Acta Crysta. 9, 889 (1956).

62. J. T. Herron and V. H. Dibeler, J. Amer. Chem. Soc. 82, 1555 (1960).

63. N. Basco, J. E. Nicholas, R. G. W. Norrish and W. H. J. Vickers, Proc. Roy. Soc. (Lond.) A272, 147 (1963).

64. J. A. A. Ketelaar and S. Kruyer, Rec. Trav. Chim. Des Pays-Bas 62, 550 (1943).

65. P. G. Wilkinson, J. Opt. Soc. Am. 45, 862 (1955).

66. K. W. Meissner, R. D. VanVeld, and P. G. Wilkinson, J. Opt. Soc. Am. 48, 1001 (1958).

67. P. G. Wilkinson and K. L. Andrew, J. Opt. Soc. Am. 53, 710 (1963).

68. G. W. Robinson, "Electronic Spectra", in "Methods of Experimental Physics", Volume 3 Molecular Physics, edited by Dudley Williams: New York: Academic Press (1962) p. 243 - 244.

69. Walter Kauzman, "Quantum Chemistry", New York: Academic Press. (1957). p. 581.

70. George R. Harrison, Richard C. Lord, and John R. Loofbourow, "Practical Spectroscopy", New York: Prentice-Hall Inc. (1948) Chapter 13.

71. Gerald W. King, "Spectroscopy and Molecular Structure", New York: Holt, Rinehart and Winston, Inc. (1964) p. 275.

72. A. D. Walsh, J. Chem. Soc. 2260 (1953).

73. Gerhard Herzberg, "Infra-red and Raman Spectra of Polyatomic Molecules", Princeton, New Jersey: D. Van Nostrand Co. Inc. (1945). p. 210.

74. G. Herzberg and E. Teller, Z. Physik. Chem., B21, 410 (1933).

75. J. Franck, Trans. Faraday Soc. 21, 536 (1925).

76. E. U. Condon, Phys. Rev. 32, 858 (1928).

77. J. B. Coon, R. E. Dewames and C. M. Loyd, J. Mol. Spectry. 8, 285 (1962).

78. Reference 68, p. 245.

79. Reference 71, p. 339.

80. F. Duschinsky, Acta Physicochim. U. R. S. S. VII, 551 (1937).

81. Reference 73, pp. 173-174.

82. Reference 71, p. 316.

83. J. L. Hencher, Ph. D. Thesis, (McMaster University, 1964), p. 141.

84. Gerhard Herzberg, "Atomic Spectra and Atomic Structure", New York: Dover Publications (1944), p. 197.

85. A. D. Walsh, J. Phys. Radium 15, 501 (1954).

86. R. S. Mulliken, J. Chem. Phys. 8, 382 (1940).

87. K. Kimura and S. Nagakura, Spectrochim. Acta 17, 166 (1961).

88. C. Moreau and J. Serre, Theoret. Chim. Acta 2, 40 (1964).

89. R. F. Schaufele and L. Goodman, Trans. Faraday Soc. 61, 20 (1965).

90. G. J. Brealey and M. Kasha, J. Amer. Chem. Soc. 77, 4462 (1955).

91. V. G. Krishna and L. Goodman, J. Amer. Chem. Soc. 83, 2042 (1961).

92. R. Romanet and B. Wojtkowiak, Comptes Rendus 250, 2865 and 3305 (1960).

93. C. K. Ingold and G. W. King, J. Chem. Soc. 2702 (1953).

94. K. K. Innes, J. Chem. Phys. 22, 863 (1954).

95. G. Herzberg and K. K. Innes, Can. J. Phys. 35, 842 (1957).

96. K. E. Schuler, J. Chem. Phys. 21, 624 (1953).

97. D. P. Craig, J. Chem. Soc. 2146 (1950).

98. J. A. Howe & J. H. Goldstein, J. Amer. Chem. Soc. 80, 4846 (1958).
T. Anno & A. Sado, J. Chem. Phys. 32, 1611 (1960).
K. Inuzuka, Bull. Chem. Soc. Jap. 33, 678 (1960).

99. Reference 20, p. 457.

100. J. H. Callomon and K. K. Innes, J. Mol. Spectry. 10, 166 (1963).

101. R. S. Mulliken, Phys. Rev. 61, 277 (1942).

102. G. Herzberg and B. Scheibe, Z. Physik. Chem. B7, 390 (1930).

103. J. W. C. Johns, Can. J. Phys. 41, 209 (1963).

104. A. Recknagel, Zeit. f. Physik 87, 397 (1934).

105. L. H. Sutcliffe and A. D. Walsh, Trans. Faraday Soc. 57, 873 (1961).

106. Reference 71, p. 293.

107. J. Kraitchman, Amer. J. Phys. 21, 17 (1953).

108. D. R. Herschbach and V. W. Laurie, J. Chem. Phys. 37, 1668 and 1687 (1962).

109. L. A. Jones "Measurement of Radiant Energy with Photographic Materials in "Measurement of Radiant Energy" edited by W. E. Forsyth: New York: McGraw-Hill Book Company, Inc. (1937). Chapter VIII, p. 246.

110. Reference 73, p. 215.

111. Reference 73, p. 210.

112. R. S. Mulliken, Rev. Mod. Phys. 14, 204 (1942).

113. E. L. Wagner, J. Chem. Phys. 43, 2728 (1965).

114. C. H. Townes and B. P. Dailey, J. Chem. Phys. 17, 788 (1949).

115. J. Hinze and H. H. Jaffe, J. Amer. Chem. Soc. 84, 540 (1962).
J. Hinze, M. A. Whitehead and H. H. Jaffe, J. Amer. Chem. Soc. 85, 148 (1963).
J. E. Huheey, J. Phys. Chem. 69, 3284 (1965).

116. Reference 71, p. 232.

117. Reference 71, p. 130.

118. Linus Pauling, "The Nature of the Chemical Bond", Ithaca, New York: Cornell University Press (1960). p. 231.

119. R. Dahl, T. Gramstad, and P. Klaeboe, Acta Chem. Scand. 19, 2248 (1965).

120. S. Ball, J. Mol. Spectry. 16, 205 (1965).

121. J. W. C. Johns, Can. J. Phys. 41, 209 (1963).

A P P E N D I X

APPENDIX I

EQUATIONS FROM CHAPTER 2

The full form of the equation for the light path function F (Equation 2.1) discussed in Chapter 2 is given in this Appendix. The equations resulting from the differentiation of F with respect to ω and λ (Equations 2.2 and 2.3, respectively) are also given.

The following equation gives the full expression for the light path function F.

$$F = AP + BP + \frac{\omega m}{d}\lambda$$

$$= r\left\{1 + \frac{z^2}{r^2}\right\}^{\frac{1}{2}} + r'\left\{1 + \frac{z'^2}{r'^2}\right\}^{\frac{1}{2}}$$

$$+\omega\left[\frac{m\lambda}{d} - \left\{1 + \frac{z^2}{r^2}\right\}^{-\frac{1}{2}}\sin\alpha - \left\{1 + \frac{z'^2}{r'^2}\right\}^{-\frac{1}{2}}\sin\beta\right]$$

$$- \ell\left[\frac{z}{r}\left\{1 + \frac{z^2}{r^2}\right\}^{-\frac{1}{2}} + \frac{z'}{r'}\left\{1 + \frac{z'^2}{r'^2}\right\}^{-\frac{1}{2}}\right]$$

$$+\tfrac{1}{2}\omega^2 \sum_{n=0}^{\infty} \omega^n \left[\left\{\frac{\sin\alpha}{r}\right\}^n\left\{\frac{\cos^2\alpha}{r} - \frac{\cos\alpha}{R}\right\} + \left\{\frac{\sin\beta}{r'}\right\}^n\left\{\frac{\cos^2\beta}{r'} - \frac{\cos\beta}{R}\right\}\right]$$

$$+\tfrac{1}{2}\ell^2\left\{\frac{1}{r} - \frac{\cos\alpha}{R} + \frac{1}{r'} - \frac{\cos\beta}{R}\right\}$$

$$+\left[\tfrac{1}{2}\ell^2\omega\left\{\frac{\sin\alpha}{r}\left\{\frac{1}{r} - \frac{\cos\alpha}{R}\right\} + \frac{\sin\beta}{r'}\left\{\frac{1}{r'} - \frac{\cos\beta}{R}\right\}\right\}\right.$$

$$\left. - \ell\omega\left\{\frac{z\sin\alpha}{r^2} + \frac{z'\sin\beta}{r'^2}\right\}\right.$$

$$- \frac{\omega^2}{8}\left[\frac{1}{r}\left\{\frac{\cos^2\alpha}{r} - \frac{\cos\alpha}{R}\right\}\left\{\tfrac{1}{2}\omega^2\left\{\frac{\cos^2\alpha}{r} - \frac{\cos\alpha}{R}\right\} + \ell^2\left\{\frac{1}{r} - \frac{\cos\alpha}{R}\right\}\right.\right.$$

$$\left.\left. + \frac{z^2}{r} - \frac{2z\ell}{r}\right\}\sum_{n=0}^{\infty}(n+1)(n+2)\left\{\frac{\omega\sin\alpha}{r}\right\}^n\right.$$

$$+\frac{1}{r}\left\{\frac{\cos^2\beta}{r'}-\frac{\cos\beta}{R}\right\}\left[\tfrac{1}{2}\omega^2\left\{\frac{\cos^2\beta}{r'}-\frac{\cos\beta}{R}\right\}+\ell^2\left\{\frac{1}{r'}-\frac{\cos\beta}{R}\right\}\right.$$

$$\left.+\frac{z'^2}{r'}-\frac{2z'\ell}{r'}\right\}\sum_{n=0}^{\infty}(n+1)(n+2)\left\{\frac{\omega\sin\beta}{r'}\right\}^n\Bigg]$$

$$+\left[\tfrac{1}{2}\ell^2\omega^2\left\{\frac{\sin^2\alpha}{r^2}\left\{\frac{1}{r}-\frac{\cos\alpha}{R}\right\}+\frac{\sin^2\beta}{r'^2}\left\{\frac{1}{r'}-\frac{\cos\beta}{R}\right\}\right\}\right.$$

$$-\ell\omega^2\left\{z\frac{\sin^2\alpha}{r^3}+\frac{z'\sin^2\beta}{r'^3}\right\}+\tfrac{1}{2}\omega^2\left\{\frac{z^2\sin^2\alpha}{r^3}+\frac{z'^2\sin^2\beta}{r'^3}\right\}$$

$$\left.+\frac{(\omega^2+\ell^2)^2}{8R^2}\left\{\frac{1}{r}-\frac{\cos\alpha}{R}+\frac{1}{r'}-\frac{\cos\beta}{R}\right\}\right]$$

$$-\frac{\ell^2}{8}\left[\frac{1}{r}\left\{\ell\left\{\frac{1}{r}-\frac{\cos\alpha}{R}\right\}-\frac{2z}{r}\right\}^2+\frac{2z^2}{r^2}\left\{\frac{1}{r}-\frac{\cos\alpha}{R}\right\}\right.$$

$$+\frac{1}{r'}\left\{\ell\left\{\frac{1}{r'}-\frac{\cos\beta}{R}\right\}-\frac{2z'}{r'}\right\}^2+\frac{2z'^2}{r'^2}\left\{\frac{1}{r'}-\frac{\cos\beta}{R}\right\}$$

$$+O\left\{\frac{\omega^5}{R^4}\right\} \qquad \text{(A.1.1)}$$

Differentiation of Equation A.1.1 with respect to w gives the following equation.

$$\frac{\partial F}{\partial \omega}=0=\left[\frac{m\lambda}{d}-\left\{1+\frac{z^2}{r^2}\right\}^{-\frac{1}{2}}\sin\alpha-\left\{1+\frac{z'^2}{r'^2}\right\}^{-\frac{1}{2}}\sin\beta\right]$$

$$+\tfrac{1}{2}\sum_{n=0}^{\infty}(n+2)\omega^{n+1}\left[\left\{\frac{\sin\alpha}{r}\right\}^n\left\{\frac{\cos^2\alpha}{r}-\frac{\cos\alpha}{R}\right\}+\left\{\frac{\sin\beta}{r'}\right\}^n\left\{\frac{\cos^2\beta}{r'}-\frac{\cos\beta}{R}\right\}\right]$$

$$+\left[\tfrac{1}{2}\ell^2\left\{\frac{\sin\alpha}{r}\left\{\frac{1}{r}-\frac{\cos\alpha}{R}\right\}+\frac{\sin\beta}{r'}\left\{\frac{1}{r'}-\frac{\cos\beta}{R}\right\}\right\}-\ell\left\{\frac{z\sin\alpha}{r^2}+\frac{z'\sin\beta}{r'^2}\right\}\right]$$

$$-\frac{1}{16r}\left\{\frac{\cos^2\alpha}{r}-\frac{\cos\alpha}{R}\right\}\left[\left\{\frac{\cos^2\alpha}{r}-\frac{\cos\alpha}{R}\right\}\sum_{n=0}^{\infty}(n+1)(n+2)(n+4)\omega^{n+3}\left\{\frac{\sin}{r}\right\}^n\right.$$

$$+ 2\left\{\ell^2\left(\frac{1}{r} - \frac{\cos\alpha}{R}\right) + \frac{z^2}{r} - \frac{2z\ell}{r}\right\} \sum_{n=0}^{\infty} (n+1)(n+2)^2\omega^{n+1}\left(\frac{\sin\alpha}{r}\right)^n$$

$$- \frac{1}{16r'}\left(\frac{\cos^2\beta}{r'} - \frac{\cos\beta}{R}\right)\left[\left(\frac{\cos^2\beta}{r'} - \frac{\cos\beta}{R}\right)\sum_{n=0}^{\infty}(n+1)(n+2)(n+4)\omega^{n+3}\left(\frac{\sin\beta}{r'}\right)^n\right.$$

$$+2\left\{\ell^2\left(\frac{1}{r'} - \frac{\cos\beta}{R}\right) + \frac{z'^2}{r'} - \frac{2z'\ell}{r'}\right\}\sum_{n=0}^{\infty}(n+1)(n+2)^2\omega^{n+1}\left(\frac{\sin\beta}{r'}\right)^n$$

$$+\omega\left[\ell^2\left\{\frac{\sin^2\alpha}{r^2}\left(\frac{1}{r} - \frac{\cos\alpha}{R}\right) + \frac{\sin^2\beta}{r'^2}\left(\frac{1}{r'} - \frac{\cos\beta}{R}\right)\right\} - 2\ell\left(\frac{z\sin^2\alpha}{r^3} + \frac{z'\sin^2\beta}{r'^3}\right)\right.$$

$$\left.+ \frac{z^2\sin^2\alpha}{r^3} + \frac{z'^2\sin^2\beta}{r'^3} + \frac{\omega^2+\ell^2}{2R^2}\left(\frac{1}{r} - \frac{\cos\alpha}{R} + \frac{1}{r'} - \frac{\cos\beta}{R}\right)\right]$$

$$+ O\left(\omega^4/R^4\right) \qquad (A.1.2)$$

The following equation gives the derivative of the light path function F with respect to .

$$\frac{\partial F}{\partial \ell} = 0 = -\left[\frac{z}{r}\left(1 + \frac{z^2}{r^2}\right)^{-1/2} + \frac{z''}{r'}\left(1 + \frac{z'^2}{r'^2}\right)^{-1/2}\right] + \ell\left(\frac{1}{r} - \frac{\cos\alpha}{R} + \frac{1}{r'} - \frac{\cos\beta}{R}\right)$$

$$+\omega\left[\ell\left\{\frac{\sin\alpha}{r}\left(\frac{1}{r} - \frac{\cos\alpha}{R}\right) + \frac{\sin\beta}{r'}\left(\frac{1}{r'} - \frac{\cos\beta}{R}\right)\right\} - \left(\frac{z\sin\alpha}{r^2} + \frac{z'\sin\beta}{r'^2}\right)\right.$$

$$-\frac{\omega^2}{4}\left[\frac{1}{r}\left(\frac{\cos^2\alpha}{r} - \frac{\cos\alpha}{R}\right)\left\{\ell\left(\frac{1}{r} - \frac{\cos\alpha}{R}\right) - \frac{z}{r}\right\}\sum_{n=0}^{\infty}(n+1)(n+2)\left(\frac{\omega\sin\alpha}{r}\right)^n\right.$$

$$+ \frac{1}{r'}\left(\frac{\cos^2\beta}{r'} - \frac{\cos\beta}{R}\right)\left\{\ell\left(\frac{1}{r'} - \frac{\cos\beta}{R}\right) - \frac{z'}{r'}\right\}\sum_{n=0}^{\infty}(n+1)(n+2)\left(\frac{\omega\sin\beta}{r'}\right)^n$$

$$+\left[\ell\omega^2\left\{\frac{\sin^2\alpha}{r^2}\left(\frac{1}{r} - \frac{\cos\alpha}{R}\right) + \frac{\sin^2\beta}{r'^2}\left(\frac{1}{r'} - \frac{\cos\beta}{R}\right)\right\} - \omega^2\left(\frac{z\sin^2\alpha}{r^3} + \frac{z'\sin^2\beta}{r'^3}\right)\right.$$

$$\left.+ \ell\left(\frac{\omega^2+\ell^2}{2R^2}\right)\left(\frac{1}{r} - \frac{\cos\alpha}{R} + \frac{1}{r'} - \frac{\cos\beta}{R}\right)\right]$$

$$- \frac{\ell}{2}\left[\frac{1}{r}\left\{\ell\left(\frac{1}{r} - \frac{\cos\alpha}{R}\right) - \frac{2z}{r}\right\}\left\{\ell\left(\frac{1}{r} - \frac{\cos\alpha}{R}\right) - \frac{z}{r}\right\} + \frac{z^2}{r^2}\left(\frac{1}{r} - \frac{\cos\alpha}{R}\right)\right.$$

$$\left. + \frac{1}{r'}\left\{\ell\left(\frac{1}{r'} - \frac{\cos\beta}{R}\right) - \frac{2z'}{r'}\right\}\left\{\ell\left(\frac{1}{r'} - \frac{\cos\beta}{R}\right) - \frac{z'}{r'}\right\} + \frac{z'^2}{r'^2}\left(\frac{1}{r'} - \frac{\cos\beta}{R}\right)\right.$$

$$+ O\left(\frac{\omega^4}{R^4}\right) \qquad \text{(A.1.3)}$$

APPENDIX II

MOLECULAR ORBITALS OF THE CYANOGEN HALIDES

A.2.1 Basic Principles

For descriptive purposes, the electronic wave function ψ_e is usually expressed as a product of one electron molecular orbitals. In turn, the molecular orbitals are usually constructed as linear combinations of atomic orbitals centred on the various nuclei of the molecule (LCAO/MO approximation). Mathematically, a molecular orbital ϕ_i is expressed in the form

$$\phi_i = \sum_p c_{ip}\chi_p \qquad (A.2.1)$$

where χ_p is an atomic orbital and c_{ip} is a constant coefficient. The molecular orbitals are usually constructed to be bases for irreducible representations of the molecular point group since this allows much useful information about the symmetries of electronic states and selection rules to be obtained in a simple manner.

Only valence shell atomic orbitals are used here to construct molecular orbitals. The atomic orbitals used are the 2s and 2p of carbon, the 2s and 2p of nitrogen, and ns and np of the halogen, n being equal to 3, 4, and 5 for chlorine, bromine, and iodine, respectively. The valence shell d atomic orbitals of the halogens have not been included for several reasons. The d orbitals would not be expected to have a major effect on the molecular binding since they lie at relatively high energies and would not participate in molecular orbital

formation to a large extent. Also, the d atomic orbitals are on an end atom of the cyanogen halides and would not have a large effect on the variation of the binding energy of the molecular orbitals as the valence angle changes. Inclusion of the d orbitals should not alter the qualitative conclusions based on symmetry arguments, which are most important in this discussion.

There are $2\ell+1$ atomic orbitals with orbital angular momentum quantum number ℓ, and in a free atom they are degenerate. The maximum necessary degeneracy that can exist for the molecular point groups of interest here is two-fold. Therefore, the degeneracy of atomic orbitals with $\ell > 0$ is reduced under these point groups. Table 9.3 gives the irreducible representations for which s, p, and d atomic orbitals form bases under the $C_{\infty v}$ and C_s point groups.

In constructing a molecular orbital which is a basis for a given irreducible representation, only those atomic orbitals which also form bases for this irreducible representation need be included since the irreducible representations of a point group are orthogonal to each other. For both the linear and bent cyanogen halides, the coefficients c_{ip} of the atomic orbitals in a given molecular orbital are not determined by symmetry; and no quantitative calculations have been done to determine their values. Therefore, only approximate semi-localized molecular orbitals are considered here for the linear and non-linear cyanogen halides.

A.2.2. Linear Cyanogen Halides

For the linear cyanogen halides, Cartesian axes are taken on each nucleus so that the z axes are along the internuclear axis and

positive in the direction from the halogen to the nitrogen atom. In this discussion, the convention of using lower case letters to designate the symmetry of individual molecular orbitals and upper case letters to designate the symmetry of molecular electronic wave functions is followed. The molecular orbitals of a given irreducible representation are numbered in order of increasing energy, that is, in order of decreasing binding energy. The atomic orbitals are written in the following way. For nitrogen, for example, the 2s atomic orbital is written s_N and the $2p_x$, $2p_y$, and $2p_z$ atomic orbitals are written x_N, y_N, and z_N, respectively.

In both the linear and non-linear molecules, the valence shell s atomic orbitals of nitrogen and the halogen are assumed to be unaffected by molecule formation, that is, they remain as atomic orbitals in the molecule. This is a good assumption for qualitative considerations. The two lowest energy molecular orbitals for the linear molecule are therefore

$$1\sigma = s_N \qquad \text{(A.2.2)}$$

$$2\sigma = s_X \qquad \text{(A.2.3)}$$

The sigma-bonding framework for the linear molecule is formed from the four atomic orbitals z_X, s_C, z_C, and z_N which belong to the σ irreducible representation and can be combined to give four σ molecular orbitals. The carbon atom is assumed to be sp hybridized, so that the four molecular orbitals can be expressed in the localized forms given below, where all mixing coefficients c_{ip} are taken to be positive.

$$3\sigma = c_{32}(s_C+z_C) - c_{34}z_N \qquad (c_{32} \simeq c_{34}) \qquad (A.2.4)$$

$$4\sigma = c_{41}z_X+c_{42}(s_C-z_C) \qquad (c_{41} \simeq c_{42}) \qquad (A.2.5)$$

$$5\sigma = - c_{51}z_X+c_{52}(s_C-z_C) \qquad (c_{51} \simeq c_{52}) \qquad (A.2.6)$$

$$6\sigma = c_{62}(s_C+z_C) + c_{64}z_N \qquad (c_{62} \simeq c_{64}) \qquad (A.2.7)$$

The molecular orbitals 3σ and 4σ are strongly bonding in the C-N and X-C regions, respectively, whereas 5σ and 6σ are strongly anti-bonding in the X-C and C-N regions, respectively. 3σ and 4σ lie quite low in energy since the electrons in them form the sigma-bonding framework of the molecules. 5σ and 6σ lie much higher in energy since they are the anti-bonding sigma orbitals corresponding to 4σ and 3σ, respectively.

The p_x and p_y atomic orbitals on each atom together provide a basis for the π irreducible representation of the $C_{\infty v}$ point group and are written together in the form π_N for the p_x and p_y atomic orbitals of nitrogen for example. Three molecular orbitals are formed from the three π-type atomic orbitals; each of these molecular orbitals is doubly-degenerate and accomodates four electrons.

The lowest energy π molecular orbital is formed by combining the three π-type atomic orbitals in phase so that there are no nodes passing through the internuclear axis.

$$1\pi = c'_{11}\pi_X+c'_{12}\pi_C+c'_{13}\pi_N \qquad (c'_{11} \ll c'_{12} \simeq c'_{13}) \qquad (A.2.8)$$

The other two π molecular orbitals each have one node passing through the internuclear axis, the pair of atoms between which the node lies being determined by the relative electronegativities of the atoms.

For all three cyanogen halides, the halogen is more electronegative than the carbon and nitrogen,[115] so that the 2π molecular orbital is written

$$2\pi = - c'_{21}\pi_X + c'_{22}\pi_C + c'_{23}\pi_N \qquad (c'_{21} \gg c'_{22} \simeq c'_{23}) \quad (A.2.9)$$

and the 3π molecular orbital is written

$$3\pi = c'_{31}\pi_X + c'_{32}\pi_C - c'_{33}\pi_N \qquad (c'_{31} \ll c'_{32} \simeq c'_{33}) \quad (A.2.10)$$

The relative magnitudes of the mixing coefficients for the three π molecular orbitals have been chosen partly on the basis of molecular orbital calculations made for the π electrons of cyanogen bromide,[113] and partly from the results of this investigation which are given in Chapter 10. Since the cyanogen halides have sixteen valence electrons, from Figure 9.2 the highest energy filled molecular orbital is 2π. The 2π molecular orbital must be largely localized on the halogen atom because the lowest ionization potentials of the cyanogen halides, which involve excitation of an electron from this orbital, are very close to those of the corresponding halogen atoms, as discussed in Chapter 10. Microwave studies have shown that r"(CN) for the cyanogen halides is only about 0.004 Å greater than in hydrogen cyanide,[36] thus indicating that the C-N bond in the cyanogen halides is essentially a normal triple bond. Therefore, the molecular orbital 1π, which is the only other filled π molecular orbital in the ground state, must be localized to a large degree in the C-N bond and the coefficients have the relative magnitudes given in (A.2.8). The 3π molecular orbital is probably also localized in the region of the C-N bond, the coefficients of the atomic orbitals in it having the relative magnitudes shown.

The actual values of the coefficients c_{ip} vary between the three cyanogen halides since the amount of conjugation of the halogen "lone pair" electrons with the C-N "triple bond" is not expected to be the same for all three halogen atoms. Evidence from the microwave spectra[36,114] shows that the amount of conjugation decreases in the order cyanogen chloride, cyanogen bromide, cyanogen iodide. The electronic spectra observed in this work also support this result.

The molecular orbitals for the linear cyanogen halides are shown schematically on the right hand side of Figure 9.1. The localization of the π molecular orbitals discussed above is indicated in this figure by cross-hatching in the region of localization. The relative energies of the molecular orbitals, which are shown very qualitatively on the right hand side of Figure 9.2, have been estimated from the results obtained experimentally and theoretically for other triatomic molecules and from the results obtained in this investigation of the cyanogen halides. The first six molecular orbitals lie in the energy order found for most triatomics. 1σ and 2σ lie at lowest energy since they remain as atomic orbitals. 3σ and 4σ both lie at relatively low energies also since they form the sigma-bonding framework of the molecule; the former probably lies at lower energy than the latter. 1π and 2π are the next two molecular orbitals in order of increasing energy. They both lie rather higher in energy than 3σ and 4σ, but the energy difference between them is probably not too large.

The next two molecular orbitals in order of increasing energy are 5σ and 3π. This order is contrary to what is predicted for most triatomics, but is clearly indicated from the results of the electronic

spectra obtained here and discussed in Chapter 10. 5σ lies about 5-7 eV higher in energy than 2π , and 3π must lie higher in energy than 5σ , although the energy difference is not known. 6σ lies highest in energy of the molecular orbitals formed here.

A.2.3 Non-Linear Cyanogen Halides

The specific case where the angle formed by the nuclei is 90° is considered. Cartesian axes are oriented on each nucleus so that the y axis is parallel to the X-C bond, the z axis is parallel to the C-N bond, and the x axis is perpendicular to the plane of the molecule. The non-linear cyanogen halides belong to the C_s point group and Table 9.3 shows that the s atomic orbital on each atom has a' symmetry and two of the p atomic orbitals (p_y and p_z) have a' symmetry where as the third (p_x) has a" symmetry.

As for the linear nuclear configuration, the s atomic orbitals of nitrogen and the halogen remain as atomic orbitals so that the two lowest energy molecular orbitals are

$$1a' = s_N \qquad (A.2.11)$$

$$2a' = s_X \qquad (A.2.12)$$

Since the valence angle is 90°, the sigma-bonding framework of the molecule is formed by direct overlap of the p atomic orbitals y_X, y_C, z_C, and z_N, so there should be four sigma-type molecular orbitals. These are

$$3a' = b_{31}z_C - b_{32}z_N \qquad (b_{31} \simeq b_{32}) \qquad (A.2.13)$$

$$4a' = -b_{41}y_X + b_{42}y_C \qquad (b_{41} \simeq b_{42}) \qquad (A.2.14)$$

$$7a' = b_{71}y_X + b_{72}y_C \qquad (b_{71} \simeq b_{72}) \qquad (A.2.15)$$

$$9a' = b_{91}z_C + b_{92}z_N \qquad (b_{91} \simeq b_{92}) \qquad (A.2.16)$$

3a' and 4a' are bonding, whereas 9a' and 7a' are anti-bonding, in the C-N and X-C bonds, respectively.

There are three p atomic orbitals, one on each atom, which have a" symmetry and these are combined to give the following molecular orbitals.

$$1a'' = b''_{11}x_X + b''_{12}x_C + b''_{13}x_N \qquad (b''_{11} \ll b''_{12} \simeq b''_{13}) \qquad (A.2.17)$$

$$2a'' = -b''_{21}x_X + b''_{22}x_C + b''_{23}x_N \qquad (b''_{21} \gg b''_{22} \simeq b''_{23}) \qquad (A.2.18)$$

$$3a'' = b''_{31}x_X + b''_{32}x_C - b''_{33}x_N \qquad (b''_{31} \ll b''_{32} \simeq b''_{33}) \qquad (A.2.19)$$

Two p atomic orbitals of a' symmetry, one each on the halogen and nitrogen atoms, and the s atomic orbital of a' symmetry on the carbon atom have not been used yet. The s atomic orbital of carbon is assumed not to hybridize or mix with other orbitals and so gives the molecular orbital

$$8a' = s_C \qquad (A.2.20)$$

Combination of z_X and y_N gives the two molecular orbitals

$$5a' = b_{51}z_X + b_{52}y_N \qquad (b_{51} \ll b_{52}) \qquad (A.2.21)$$

$$6a' = -b_{61}z_X + b_{62}y_N \qquad (b_{61} \gg b_{62}) \qquad (A.2.22)$$

This gives a total of twelve molecular orbitals as required from the number of atomic orbitals started with. These molecular orbitals are shown schematically on the left hand side of Figure 9.1.

The order of increasing energy of the molecular orbitals for the non-linear cyanogen halides has been obtained by correlation with the molecular orbitals of the linear cyanogen halides as described in Section 9.2 and is shown on the left hand side of Figure 9.2. Again, the energy order is probably correct, but the intervals are only very qualitative and vary between the different cyanogen halides.

APPENDIX III

CALCULATION OF THE [L] MATRIX

In order to use Franck-Condon calculations to obtain changes in molecular structure upon electronic excitation, it is necessary to relate changes in normal coordinates to changes in bond lengths and bond angles. It was shown in Section 9.5 how changes d_i in totally symmetric normal coordinates can be obtained and that these are related to mass-weighted Cartesian displacement coordinates η_i by the [L] matrix.

$$\begin{bmatrix} \eta_1 \\ \eta_2 \\ \eta_3 \end{bmatrix} = \begin{bmatrix} \ell_{11} & \ell_{13} \\ \ell_{21} & \ell_{23} \\ \ell_{31} & \ell_{33} \end{bmatrix} \begin{bmatrix} d_1 \\ d_3 \end{bmatrix} \qquad \text{(A.3.1)}$$

It will now be shown how the elements of the [L] matrix are calculated.[82]

Since only the two totally symmetric stretching vibrations of the cyanogen halides are of interest here, the model used for the calculations can be taken to be a linear triatomic molecule restricted to motion in one dimension. This model is shown in Figure A.3.1, where atom 1

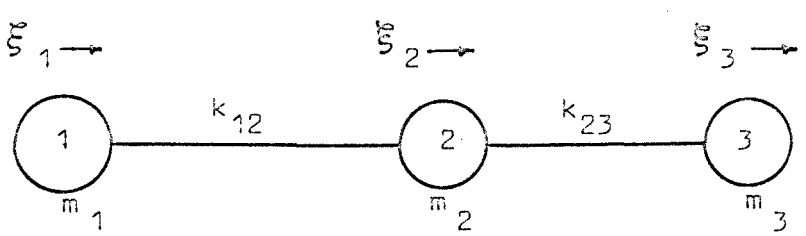

FIGURE A.3.1.

is the halogen atom, atom 2 is the carbon atom and atom 3 is the nitrogen atom. For atom i, m_i is the mass and ξ_i is its one dimensional Cartesian displacement coordinate giving the displacement of the atom from its equilibrium position. ξ_i is related to the mass-weighted Cartesian displacement coordinate η_i by the equation

$$\eta_i = m_i^{1/2} \xi_i \qquad (A.3.2)$$

The stretching force constant between atoms 1 and 2 is denoted k_{12} and that between atoms 2 and 3 as k_{23}. The interaction between atoms 1 and 3 is assumed to be negligibly small.

From the definitions above, the kinetic energy T and the potential energy V (in harmonic oscillator approximation) are

$$\begin{aligned} 2T &= m_1 \dot{\xi}_1^2 + m_2 \dot{\xi}_2^2 + m_3 \dot{\xi}_3^2 = \dot{\eta}_1^2 + \dot{\eta}_2^2 + \dot{\eta}_3^2 \\ &= \sum_{i=1}^{3} \dot{\eta}_i^2 \end{aligned} \qquad (A.3.3)$$

$$\begin{aligned} 2V &= k_{12}(\xi_2 - \xi_1)^2 + k_{23}(\xi_3 - \xi_2)^2 \\ &= k_{12}\xi_1^2 + (k_{12}+k_{23})\xi_2^2 + k_{23}\xi_3^2 - 2k_{12}\xi_1\xi_2 - 2k_{23}\xi_2\xi_3 \\ &= \frac{k_{12}}{m_1}\eta_1^2 + \frac{k_{12}+k_{23}}{m_2}\eta_2^2 + \frac{k_{23}}{m_3}\eta_3^2 - \frac{2k_{12}}{(m_1m_2)^{1/2}}\eta_1\eta_2 - \frac{2k_{23}}{(m_2m_3)^{1/2}}\eta_2\eta_3 \\ &= \sum_{i=1}^{3} \sum_{j \le i} b_{ij}\eta_i\eta_j \end{aligned} \qquad (A.3.4)$$

If the Lagrangian function $\mathcal{L}$, defined by the equation

$$\mathcal{L} = T - V \qquad (A.3.5)$$

is substituted in the equations of motion

$$\frac{d}{dt} \cdot \frac{\partial \mathcal{L}}{\partial \dot{\eta}_i} - \frac{\partial \mathcal{L}}{\partial \eta_i} = 0 \qquad (i=1,2,3) \qquad (A.3.6)$$

then a set of three secular equations may be obtained.

$$\ddot{\eta}_i + \sum_{j \neq i} b_{ij} \eta_j = 0 \qquad (i=1,2,3) \qquad (A.3.7)$$

The solutions for these equations are of the form

$$\eta_i = \eta_i^0 \sin (t\sqrt{\lambda} + \delta) \qquad (A.3.8)$$

where η_i^0, λ, and δ are constants and t is time. Use of these solutions gives the secular equations in the form

$$\sum_{j \neq i} b_{ij} \eta_j^0 + (b_{ii} - \lambda)\eta_i^0 = 0 \qquad (i=1,2,3) \qquad (A.3.9)$$

These secular equations have a solution only if the secular determinant

$$\left| b_{ij} - \lambda \delta_{ij} \right| = 0 \qquad (A.3.10)$$

is satisfied. The λ are the roots of the secular determinant and are related to the vibrational frequencies ν (in cm^{-1}) by

$$\lambda_i = 4\pi^2 c^2 \nu_i^2 \qquad (A.3.11)$$

and δ_{ij} is the Kronecker delta, being equal to 1 for i = j, and 0 for $i \neq j$.

The secular determinant for the totally symmetric vibrations

of the cyanogen halides is

$$\begin{vmatrix} \frac{k_{12}}{m_1} - \lambda & -\frac{k_{12}}{(m_1 m_2)^{\frac{1}{2}}} & 0 \\ -\frac{k_{12}}{(m_1 m_2)^{\frac{1}{2}}} & \frac{k_{12}+k_{23}}{m_2} - \lambda & -\frac{k_{23}}{(m_2 m_3)^{\frac{1}{2}}} \\ 0 & -\frac{k_{23}}{(m_2 m_3)^{\frac{1}{2}}} & \frac{k_{23}}{m_3} - \lambda \end{vmatrix} = 0 \qquad (A.3.12)$$

This equation expands to give a cubic equation in λ. One of the roots is $\lambda = 0$, which corresponds to the normal coordinate for translation of the molecule in one dimension and is not considered further here. The other two roots, which are labelled λ_1 and λ_3 to conform with convention, are given by the equations

$$\lambda_1 + \lambda_3 = \frac{k_{12}}{m_1} + \frac{k_{12}+k_{23}}{m_2} + \frac{k_{23}}{m_3} \qquad (A.3.13)$$

$$\lambda_1 \lambda_3 = \frac{k_{12}k_{23}}{m_1 m_2 m_3} (m_1+m_2+m_3) \qquad (A.3.14)$$

Substitution of a given λ_k in the secular equations of Equation A.3.9 gives three equations which can be solved for the relative values of the η_{jk}^{o}. If ℓ_{jk} is defined by

$$\ell_{jk} = K_k \eta_{jk}^{o} \qquad (A.3.15)$$

where K_k is a constant for a given λ_k, and it is required that

$$\sum_j \ell_{jk}^{2} = 1 \qquad (A.3.16)$$

then it is possible to solve for the ℓ_{jk} and obtain the following equations.

$$\ell_{1k} = \left[1 + \left\{\frac{\frac{k_{12}}{m_1} - \lambda_k}{\frac{k_{12}}{(m_1 m_2)^{1/2}}}\right\}^2 + \left\{\left[\left(\frac{k_{12}+k_{23}}{m_2} - \lambda_k\right)\left(\frac{k_{12}}{m_1} - \lambda_k\right) - \frac{k_{12}^2}{m_1 m_2}\right]\left[\frac{(m_1 m_2^2 m_3)^{1/2}}{k_{12} k_{23}}\right]\right\}^2\right]^{-1/2} \quad \text{(A.3.17)}$$

$$\ell_{2k} = \left[\frac{\frac{k_{12}}{m_1} - \lambda_k}{\frac{k_{12}}{(m_1 m_2)^{1/2}}}\right] \ell_{1k} \quad \text{(A.3.18)}$$

$$\ell_{3k} = \left[\left(\frac{k_{12}+k_{23}}{m_2} - \lambda_k\right)\left(\frac{k_{12}}{m_1} - \lambda_k\right) - \frac{k_{12}^2}{m_1 m_2}\right]\left[\frac{(m_1 m_2^2 m_3)^{1/2}}{k_{12} k_{23}}\right] \ell_{1k} \quad \text{(A.3.19)}$$

These ℓ_{jk} are the elements of the [L] matrix.

As mentioned before, this [L] matrix is a modification of the usual [L] matrix since the normal coordinate for translation is ignored, thus removing one column from the [L] matrix and making it non-square.

APPENDIX IV

CALCULATION OF THE POTENTIAL ENERGY DISTRIBUTION

The total vibrational potential energy of a molecule is made up from contributions by all the normal vibrations of the molecule. The potential energy distribution breaks the total potential energy up in such a way as to show the dependence of each normal vibration on the force constants considered in the molecule. That is, the potential energy distribution shows the various contributions to each normal vibration and thus can be used to investigate the degree of localization of any normal vibration of a molecule. This is of interest when simplified Franck-Condon calculations, in which not all the totally symmetric normal vibrations are considered together, are being carried out.

The elements of the potential energy distribution matrix $[V_\lambda^\varphi]$ are defined by the equation[83]

$$(V_\lambda^\varphi)_{\ell k} = \frac{1}{\lambda_\ell} J_{\ell k}^\varphi \varphi_k \qquad (A.4.1)$$

where λ_ℓ is related to the ℓ^{th} vibrational frequency ν_ℓ by Equation A.3.11, $J_{\ell k}^\varphi$ is an element of the Jacobian matrix $[J^\varphi]$ and is defined by

$$J_{\ell k}^\varphi = \frac{\partial \lambda_\ell}{\partial \varphi_k} \qquad (A.4.2)$$

and φ_k is the k^{th} force constant. For each vibrational frequency the elements of $[V_\lambda^\varphi]$ are required to be normalized, that is,

$$\frac{1}{\lambda_\ell} \sum_{k=1}^{n_\varphi} J^{\varphi}_{\ell k} \varphi_k = 1 \qquad (A.4.3)$$

where n_φ is the number of force constants.

If the totally symmetric internal coordinates of the cyanogen halides are defined by the equations

$$S_1 = \xi_2 - \xi_1 \qquad (A.4.4)$$

$$S_3 = \xi_3 - \xi_2 \qquad (A.4.5)$$

and a column matrix $[S]$ is formed from S_1 and S_3, then the relations previously shown between ξ_i and η_i, and between $[\eta]$ and $[Q]$ can be used to show that

$$[S] = [H][Q] \qquad (A.4.6)$$

where

$$[H] = \begin{bmatrix} h_{11} & h_{12} \\ h_{21} & h_{22} \end{bmatrix} = \begin{bmatrix} -m_1^{-\frac{1}{2}} l_{11} + m_2^{-\frac{1}{2}} l_{21}, & -m_1^{-\frac{1}{2}} l_{13} + m_2^{-\frac{1}{2}} l_{23} \\ -m_2^{-\frac{1}{2}} l_{21} + m_3^{-\frac{1}{2}} l_{31}, & -m_2^{-\frac{1}{2}} l_{23} + m_3^{-\frac{1}{2}} l_{33} \end{bmatrix} \qquad (A.4.7)$$

and l_{ij} is an element of the $[L]$ matrix and m_i is the mass of atom i.

For the totally symmetric normal vibrations of the cyanogen halides, it can be shown that

$$J^{\varphi}_{\ell k} = h^2_{k\ell} \qquad (A.4.8)$$

Since the vibrational frequencies and atomic masses are known, and the force constants and $[L]$ matrix elements can be calculated as shown in Appendix III, the potential energy distribution matrix $[V^{\varphi}_{\lambda}]$ can be calculated readily.